EUROPEAN ORGANIZATION FOR NUCLEAR RESEARCH

CERN-PH-EP/2008-016
14 October 2008

Search for Charged Higgs Bosons in e^+e^- Collisions at $\sqrt{s} = 189 - 209$ GeV

The OPAL Collaboration

Abstract

A search is made for charged Higgs bosons predicted by Two-Higgs-Doublet extensions of the Standard Model (2HDM) using electron-positron collision data collected by the OPAL experiment at $\sqrt{s} = 189 - 209$ GeV, corresponding to an integrated luminosity of approximately 600 pb^{-1}. Charged Higgs bosons are assumed to be pair-produced and to decay into $q\bar{q}$, $\tau\nu_\tau$ or $AW^{\pm *}$. No signal is observed. Model-independent limits on the charged Higgs-boson production cross section are derived by combining these results with previous searches at lower energies. Excluded areas on the $[m_{H^\pm}, BR(H^\pm \to \tau\nu_\tau)]$ plane are presented assuming $BR(H^\pm \to \tau\nu_\tau) + BR(H^\pm \to q\bar{q}) = 1$. Under the above assumption, motivated by general 2HDM type II models, charged Higgs bosons are excluded up to a mass of 76.6 GeV at 95% confidence level, independent of the branching ratio $BR(H^\pm \to \tau\nu_\tau)$. A scan of the 2HDM type I model parameter space is performed and limits on the Higgs-boson masses $m_{H^\pm}$ and m_A are presented for different choices of $\tan\beta$.

Submitted to Eur. Phys. J. C

The OPAL Collaboration

G. Abbiendi[2], C. Ainsley[5], P.F. Åkesson[7], G. Alexander[21], G. Anagnostou[1], K.J. Anderson[8], S. Asai[22], D. Axen[26], I. Bailey[25], E. Barberio[7,p], T. Barillari[31], R.J. Barlow[15], R.J. Batley[5], P. Bechtle[24], T. Behnke[24], K.W. Bell[19], P.J. Bell[1], G. Bella[21], A. Bellerive[6], G. Benelli[4], S. Bethke[31], O. Biebel[30], O. Boeriu[9], P. Bock[10], M. Boutemeur[30], S. Braibant[2], R.M. Brown[19], H.J. Burckhart[7], S. Campana[4], P. Capiluppi[2], R.K. Carnegie[6], A.A. Carter[12], J.R. Carter[5], C.Y. Chang[16], D.G. Charlton[1], C. Ciocca[2], A. Csilling[28], M. Cuffiani[2], S. Dado[20], M. Dallavalle[2], A. De Roeck[7], E.A. De Wolf[7,s], K. Desch[24], B. Dienes[29], J. Dubbert[30], E. Duchovni[23], G. Duckeck[30], I.P. Duerdoth[15], E. Etzion[21], F. Fabbri[2], P. Ferrari[7], F. Fiedler[30], I. Fleck[9], M. Ford[15], A. Frey[7], P. Gagnon[11], J.W. Gary[4], C. Geich-Gimbel[3], G. Giacomelli[2], P. Giacomelli[2], M. Giunta[4], J. Goldberg[20], E. Gross[23], J. Grunhaus[21], M. Gruwé[7], A. Gupta[8], C. Hajdu[28], M. Hamann[24], G.G. Hanson[4], A. Harel[20], M. Hauschild[7], C.M. Hawkes[1], R. Hawkings[7], G. Herten[9], R.D. Heuer[24], J.C. Hill[5], D. Horváth[28,c], P. Igo-Kemenes[10], K. Ishii[22], H. Jeremie[17], P. Jovanovic[1], T.R. Junk[6,i], J. Kanzaki[22,u], D. Karlen[25], K. Kawagoe[22], T. Kawamoto[22], R.K. Keeler[25], R.G. Kellogg[16], B.W. Kennedy[19], S. Kluth[31], T. Kobayashi[22], M. Kobel[3,t], S. Komamiya[22], T. Krämer[24], A. Krasznahorkay Jr.[29,e], P. Krieger[6,l], J. von Krogh[10], T. Kuhl[24], M. Kupper[23], G.D. Lafferty[15], H. Landsman[20], D. Lanske[13], D. Lellouch[23], J. Letts[o], L. Levinson[23], J. Lillich[9], S.L. Lloyd[12], F.K. Loebinger[15], J. Lu[26,b], A. Ludwig[3,t], J. Ludwig[9], W. Mader[3,t], S. Marcellini[2], A.J. Martin[12], T. Mashimo[22], P. Mättig[m], J. McKenna[26], R.A. McPherson[25], F. Meijers[7], W. Menges[24], F.S. Merritt[8], H. Mes[6,a], N. Meyer[24], A. Michelini[2], S. Mihara[22], G. Mikenberg[23], D.J. Miller[14], W. Mohr[9], T. Mori[22], A. Mutter[9], K. Nagai[12], I. Nakamura[22,v], H. Nanjo[22], H.A. Neal[32], S.W. O'Neale[1,*], A. Oh[7], A. Okpara[10], M.J. Oreglia[8], S. Orito[22,*], C. Pahl[31], G. Pásztor[4,g], J.R. Pater[15], J.E. Pilcher[8], J. Pinfold[27], D.E. Plane[7], O. Pooth[13], M. Przybycień[7,n], A. Quadt[31], K. Rabbertz[7,r], C. Rembser[7], P. Renkel[23], J.M. Roney[25], A.M. Rossi[2], Y. Rozen[20], K. Runge[9], K. Sachs[6], T. Saeki[22], E.K.G. Sarkisyan[7,j], A.D. Schaile[30], O. Schaile[30], P. Scharff-Hansen[7], J. Schieck[31], T. Schörner-Sadenius[7,z], M. Schröder[7], M. Schumacher[3], R. Seuster[13,f], T.G. Shears[7,h], B.C. Shen[4], P. Sherwood[14], A. Skuja[16], A.M. Smith[7], R. Sobie[25], S. Söldner-Rembold[15], F. Spano[8,x], A. Stahl[13], D. Strom[18], R. Ströhmer[30], S. Tarem[20], M. Tasevsky[7,d], R. Teuscher[8], M.A. Thomson[5], E. Torrence[18], D. Toya[22], I. Trigger[7,w], Z. Trócsányi[29,e], E. Tsur[21], M.F. Turner-Watson[1], I. Ueda[22], B. Ujvári[29,e], C.F. Vollmer[30], P. Vannerem[9], R. Vértesi[29,e], M. Verzocchi[16], H. Voss[7,q], J. Vossebeld[7,h], C.P. Ward[5], D.R. Ward[5], P.M. Watkins[1], A.T. Watson[1], N.K. Watson[1], P.S. Wells[7], T. Wengler[7], N. Wermes[3], G.W. Wilson[15,k], J.A. Wilson[1], G. Wolf[23], T.R. Wyatt[15], S. Yamashita[22], D. Zer-Zion[4], L. Zivkovic[20]

[1]School of Physics and Astronomy, University of Birmingham, Birmingham B15 2TT, UK
[2]Dipartimento di Fisica dell' Università di Bologna and INFN, I-40126 Bologna, Italy
[3]Physikalisches Institut, Universität Bonn, D-53115 Bonn, Germany
[4]Department of Physics, University of California, Riverside CA 92521, USA
[5]Cavendish Laboratory, Cambridge CB3 0HE, UK
[6]Ottawa-Carleton Institute for Physics, Department of Physics, Carleton University, Ottawa, Ontario K1S 5B6, Canada

[7]CERN, European Organisation for Nuclear Research, CH-1211 Geneva 23, Switzerland
[8]Enrico Fermi Institute and Department of Physics, University of Chicago, Chicago IL 60637, USA
[9]Fakultät für Physik, Albert-Ludwigs-Universität Freiburg, D-79104 Freiburg, Germany
[10]Physikalisches Institut, Universität Heidelberg, D-69120 Heidelberg, Germany
[11]Indiana University, Department of Physics, Bloomington IN 47405, USA
[12]Queen Mary and Westfield College, University of London, London E1 4NS, UK
[13]Technische Hochschule Aachen, III Physikalisches Institut, Sommerfeldstrasse 26-28, D-52056 Aachen, Germany
[14]University College London, London WC1E 6BT, UK
[15]School of Physics and Astronomy, Schuster Laboratory, The University of Manchester M13 9PL, UK
[16]Department of Physics, University of Maryland, College Park, MD 20742, USA
[17]Laboratoire de Physique Nucléaire, Université de Montréal, Montréal, Québec H3C 3J7, Canada
[18]University of Oregon, Department of Physics, Eugene OR 97403, USA
[19]Rutherford Appleton Laboratory, Chilton, Didcot, Oxfordshire OX11 0QX, UK
[20]Department of Physics, Technion-Israel Institute of Technology, Haifa 32000, Israel
[21]Department of Physics and Astronomy, Tel Aviv University, Tel Aviv 69978, Israel
[22]International Centre for Elementary Particle Physics and Department of Physics, University of Tokyo, Tokyo 113-0033, and Kobe University, Kobe 657-8501, Japan
[23]Particle Physics Department, Weizmann Institute of Science, Rehovot 76100, Israel
[24]Universität Hamburg/DESY, Institut für Experimentalphysik, Notkestrasse 85, D-22607 Hamburg, Germany
[25]University of Victoria, Department of Physics, P O Box 3055, Victoria BC V8W 3P6, Canada
[26]University of British Columbia, Department of Physics, Vancouver BC V6T 1Z1, Canada
[27]University of Alberta, Department of Physics, Edmonton AB T6G 2J1, Canada
[28]Research Institute for Particle and Nuclear Physics, H-1525 Budapest, P O Box 49, Hungary
[29]Institute of Nuclear Research, H-4001 Debrecen, P O Box 51, Hungary
[30]Ludwig-Maximilians-Universität München, Sektion Physik, Am Coulombwall 1, D-85748 Garching, Germany
[31]Max-Planck-Institute für Physik, Föhringer Ring 6, D-80805 München, Germany
[32]Yale University, Department of Physics, New Haven, CT 06520, USA

[a] and at TRIUMF, Vancouver, Canada V6T 2A3
[b] now at University of Alberta
[c] and Institute of Nuclear Research, Debrecen, Hungary
[d] now at Institute of Physics, Academy of Sciences of the Czech Republic 18221 Prague, Czech Republic
[e] and Department of Experimental Physics, University of Debrecen, Hungary
[f] and MPI München
[g] and Research Institute for Particle and Nuclear Physics, Budapest, Hungary
[h] now at University of Liverpool, Dept of Physics, Liverpool L69 3BX, U.K.
[i] now at Dept. Physics, University of Illinois at Urbana-Champaign, U.S.A.

[j] now at University of Texas at Arlington, Department of Physics, Arlington TX, 76019, U.S.A.
[k] now at University of Kansas, Dept of Physics and Astronomy, Lawrence, KS 66045, U.S.A.
[l] now at University of Toronto, Dept of Physics, Toronto, Canada
[m] current address Bergische Universität, Wuppertal, Germany
[n] now at University of Mining and Metallurgy, Cracow, Poland
[o] now at University of California, San Diego, U.S.A.
[p] now at The University of Melbourne, Victoria, Australia
[q] now at IPHE Université de Lausanne, CH-1015 Lausanne, Switzerland
[r] now at IEKP Universität Karlsruhe, Germany
[s] now at University of Antwerpen, Physics Department,B-2610 Antwerpen, Belgium; supported by Interuniversity Attraction Poles Programme – Belgian Science Policy
[t] now at Technische Universität, Dresden, Germany
[u] and High Energy Accelerator Research Organisation (KEK), Tsukuba, Ibaraki, Japan
[v] now at University of Pennsylvania, Philadelphia, Pennsylvania, USA
[w] now at TRIUMF, Vancouver, Canada
[x] now at Columbia University
[y] now at CERN
[z] now at DESY
[*] Deceased

1 Introduction

In the Standard Model (SM) [1], the electroweak symmetry is broken via the Higgs mechanism [2] generating the masses of elementary particles. This requires the introduction of a complex scalar Higgs-field doublet and implies the existence of a single neutral scalar particle, the Higgs boson. While the SM accurately describes the interactions between elementary particles, it leaves several fundamental questions unanswered. Therefore, it is of great interest to study extended models.

The minimal extension of the SM Higgs sector required, for example, by supersymmetric models contains two Higgs-field doublets [3] resulting in five Higgs bosons: two charged ($H^{\pm}$) and three neutral. If CP-conservation is assumed, the three neutral Higgs bosons are CP-eigenstates: h and H are CP-even and A is CP-odd. Two-Higgs-Doublet Models (2HDMs) are classified according to the Higgs-fermion coupling structure. In type I models (2HDM(I)) [4], all quarks and leptons couple to the same Higgs doublet, while in type II models (2HDM(II)) [5], down-type fermions couple to the first Higgs doublet, and up-type fermions to the second.

Charged Higgs bosons are expected to be pair-produced in the process $e^+e^- \to H^+H^-$ at LEP, the reaction $e^+e^- \to H^{\pm}W^{\mp}$ having a much lower cross section [6]. In 2HDMs, the tree-level cross section [7] for pair production is completely determined by the charged Higgs-boson mass and known SM parameters.

The $H^{\pm}$ branching ratios are model-dependent. In most of the 2HDM(II) parameter space, charged Higgs bosons decay into the heaviest kinematically allowed fermions, namely $\tau\nu_\tau$ and quark pairs[1]. The situation changes in 2HDM(I), where the decay $H^{\pm} \to AW^{\pm *}$ can become

[1] Throughout this paper charge conjugation is implied. For simplicity, the notation $\tau\nu_\tau$ stands for $\tau^+\nu_\tau$ and $\tau^-\bar{\nu}_\tau$ and $q\bar{q}$ for a quark and anti-quark of any flavor.

dominant if the ratio of the vacuum expectation values of the two Higgs-field doublets $\tan\beta \gtrapprox 1$ and the A boson is sufficiently light [8].

In this paper we search for charged Higgs bosons decaying into $q\bar{q}$, $\tau\nu_\tau$ and $AW^{\pm *}$ using the data collected by the OPAL Collaboration in 1998−2000. The results are interpreted within general 2HDM(II) assuming $BR(H^\pm \to \tau\nu_\tau) + BR(H^\pm \to q\bar{q}) = 1$ for the branching ratios and in 2HDM(I) taking into account decays of charged Higgs bosons via $AW^{\pm *}$, as well. Our result is not confined to $q\bar{q}$=$\{c\bar{s}, \bar{c}s\}$ although that is the dominant hadronic decay channel in most of the parameter space.

The previously published OPAL lower limit on the charged Higgs-boson mass, under the assumption of $BR(H^\pm \to \tau\nu_\tau) + BR(H^\pm \to q\bar{q}) = 1$, is $m_{H^\pm} > 59.5$ GeV at 95% confidence level (CL) using data collected at $\sqrt{s} \leq 183$ GeV [9, 10]. Lower bounds of $74.4 - 79.3$ GeV have been reported by the other LEP collaborations [11–13] based on the full LEP2 data set. The DELPHI Collaboration also performed a search for $H^\pm \to AW^{\pm *}$ decay and constrained the charged Higgs-boson mass in 2HDM(I) [12] to be $m_{H^\pm} \geq 76.7$ GeV at 95%CL.

2 Experimental considerations

The OPAL detector is described in [14]. The events are reconstructed from charged-particle tracks and energy deposits (*clusters*) in the electromagnetic and hadron calorimeters. The tracks and clusters must pass a set of quality requirements similar to those used in previous OPAL Higgs-boson searches [15]. In calculating the total visible energies and momenta of events and individual jets, corrections are applied to prevent double-counting of energy in the case of tracks and associated clusters [15].

The data analyzed in this paper were collected in 1998−2000 at center-of-mass energies of $189 - 209$ GeV as given in Table 1. Due to different requirements on the operational state of the OPAL subdetectors, the integrated luminosity of about 600 pb^{-1} differs slightly among search channels.

Year	1998	1999				2000
E_{cm} (GeV)	186−190	190−194	194−198	198−201	201−203	200−209
$<E_{cm}>$ (GeV)	188.6	191.6	195.5	199.5	201.9	206.0
E_{cm}^{MC} (GeV)	189	192	196	200	202	206
$\int \mathcal{L}dt$ (pb^{-1}) (2τ)	183.5	29.3	76.4	76.6	45.5	212.6
$\int \mathcal{L}dt$ (pb^{-1}) ($2j + \tau$, $4j$)	179.6	29.3	76.3	75.9	36.6	217.4
$\int \mathcal{L}dt$ (pb^{-1}) ($8j$, $6j + \ell$, $4j + \tau$)	175.0	28.9	74.8	77.2	36.1	211.1

Table 1: *Data-taking year, center-of-mass energy bins, luminosity-weighted average center-of-mass energies, the energies of signal and background Monte Carlo simulations, and integrated luminosities of the data. The data correspond to total integrated luminosities of 623.9* pb^{-1} *for the two-tau, 615.1* pb^{-1} *for the two-jet plus tau and the four-jet channels and 603.1* pb^{-1} *for the* $H^\pm \to AW^{\pm *}$ *selections.*

In this paper the following final states are sought:
- $H^+H^- \to \tau^+\nu_\tau\tau^-\bar{\nu}_\tau$ (*two-tau final state,* 2τ),
- $H^+H^- \to q\bar{q}\tau\nu_\tau$ (*two-jet plus tau final state,* $2j + \tau$),
- $H^+H^- \to q\bar{q}q\bar{q}$ (*four-jet final state,* $4j$),
- $H^+H^- \to AW^{+*}AW^{-*} \to b\bar{b}q\bar{q}b\bar{b}q\bar{q}$ (*eight-jet final state,* $8j$),

- $H^+H^- \to AW^{+*}AW^{-*} \to b\bar{b}q\bar{q}b\bar{b}\ell\nu_\ell$ (*six-jet plus lepton final state,* $6j + \ell$),
- $H^+H^- \to AW^{\pm *}\tau\nu_\tau \to b\bar{b}q\bar{q}\tau\nu_\tau$ (*four-jet plus tau final state,* $4j + \tau$).

The signal detection efficiencies and accepted background cross sections are estimated using a variety of Monte Carlo samples. The HZHA generator [16] is used to simulate H^+H^- production at fixed values of the charged Higgs-boson mass in steps of $1 - 5$ GeV from the kinematic limit down to 50 GeV for fermionic decays and 40 GeV for bosonic decays.

The background processes are simulated primarily by the following event generators: PYTHIA [17] and KK2F [18] ($Z/\gamma^* \to q\bar{q}(\gamma)$), grc4f [19] (four-fermion processes, 4f), BHWIDE [20] and TEEGG [21] ($e^+e^-(\gamma)$), KORALZ [22] and KK2F ($\mu^+\mu^-(\gamma)$ and $\tau^+\tau^-(\gamma)$), PHOJET [23], HERWIG [24], Vermaseren [25] (hadronic and leptonic two-photon processes).

The generated partons, both for the signal and the SM Monte Carlo simulations, are hadronized using JETSET [17], with parameters described in [26]. For systematic studies, cluster fragmentation implemented in HERWIG for the process $Z/\gamma^* \to q\bar{q}(\gamma)$ is used. The predictions of 4f processes are cross-checked using EXCALIBUR [27], KoralW [28] and KandY [29].

The obtained Monte Carlo samples are processed through a full simulation of the OPAL detector [30]. The event selection is described below.

3 Search for four-fermion final states

In most of the parameter space of 2HDM(II) and with a sufficiently heavy A boson in 2HDM(I), the fermionic decays of the charged Higgs boson dominate and lead to four-fermion final states. The most important decay mode is typically $H^\pm \to \tau\nu_\tau$, with the hadronic mode $H^\pm \to q\bar{q}$ reaching about 40% branching ratio at maximum.

The search for the fully leptonic final state $H^+H^- \to \tau^+\nu_\tau\tau^-\bar{\nu}_\tau$ is described in [31]. The searches for the $H^+H^- \to q\bar{q}\tau\nu_\tau$ and the $H^+H^- \to q\bar{q}q\bar{q}$ events are optimized using Monte Carlo simulation of $H^+ \to c\bar{s}$ decays. The sensitivities to other quark flavors are similar and the possible differences are taken into account as systematic uncertainties. Therefore, our results are valid for any hadronic decay of the charged Higgs boson.

Four-fermion final states originating from H^+H^- production would have very similar kinematic properties to W^+W^- production, which therefore constitutes an irreducible background to our searches, especially when $m_{H^\pm}$ is close to $m_{W^\pm}$. To suppress this difficult SM background, a mass-dependent likelihood selection (similar to the technique described in [32]) is introduced. For each charged Higgs-boson mass tested ($m_{\rm test}$), a specific analysis optimized for a reference mass ($m_{\rm ref}$) close to the hypothesized value is used.

We have chosen a set of reference charged Higgs-boson masses at which signal samples are generated. Around these reference points, mass regions (labeled by $m_{\rm ref}$) are defined with the borders centered between the neighboring points. For each individual mass region, at each center-of-mass energy, we create a separate likelihood selection with the signal histograms built using events generated at $m_{\rm ref}$. The background histograms are composed of the SM processes and are identical for all mass regions.

When testing the hypothesis of a signal with mass $m_{\rm test}$, the background and data rate and discriminant (i.e. the reconstructed Higgs-boson mass) distribution depend on the mass region to which $m_{\rm test}$ belongs. The signal quantities depend on the value of $m_{\rm test}$ itself and are determined as follows. The signal rate and discriminant distribution are computed, with the likelihood selection optimized for $m_{\rm ref}$, for three simulated signal samples with masses $m_{\rm low}$,

$m_{\rm ref}$ and $m_{\rm high}$. Here, $m_{\rm low}$ and $m_{\rm high}$ are the closest mass points to $m_{\rm ref}$ at which signal Monte Carlo samples are generated, with $m_{\rm low} < m_{\rm ref} < m_{\rm high}$. The signal rate and discriminant distribution for $m_{\rm test}$ are then calculated by linear interpolation from the quantities for $m_{\rm low}$ and $m_{\rm ref}$ if $m_{\rm test} < m_{\rm ref}$, or for $m_{\rm ref}$ and $m_{\rm high}$ if $m_{\rm test} > m_{\rm ref}$.

When building the likelihood function three event classes are considered: signal, four-fermion background and two-fermion background. The likelihood output gives the probability that a given event belongs to the signal rather than to one of the two background sources.

3.1 The two-jet plus tau final state

The analysis closely follows our published one at $\sqrt{s}$ = 183 GeV [10]. It proceeds in two steps. First, events consistent with the final state topology of an isolated tau lepton, a pair of hadronic jets and sizable missing energy are preselected and are then processed by a likelihood selection. The sensitivity of the likelihood selection is improved by building mass-dependent discriminant functions as explained above.

Events are selected if their likelihood output ($\mathcal{L}$) is greater than a cut value chosen to maximize the sensitivity of the selection at each simulated charged Higgs-boson mass. Apart from the neighborhood of the $\mathrm{W^+W^-}$ peak, the optimal cut does not depend significantly on the simulated mass and is chosen to be $\mathcal{L} > 0.85$. Around the $\mathrm{W^+W^-}$ peak, it is gradually reduced to 0.6 at the lowest.

At the end of the selection, 331 events are selected in the data sample with 316.9 $\pm$ 3.2 (stat.) $\pm$38.4 (syst.) events expected from SM processes for a test mass of $m_{\mathrm{H^\pm}}$=75 GeV. The sources of systematic uncertainties are discussed below. Four-fermion processes account for more than 99% of the SM background and result in a large peak in the reconstructed mass centered at the $\mathrm{W^\pm}$ mass (with a second peak at the Z mass for test masses of $m_{\mathrm{H^\pm}} > 85$ GeV). The signal detection efficiencies for the various LEP energies are between 25% and 53% for any charged Higgs-boson mass.

The likelihood output and reconstructed di-jet mass distributions for simulated Higgs-boson masses of 60 GeV and 75 GeV are presented in Figures 1(a-d). The reconstructed Higgs-boson mass resolution is $2.0 - 2.5$ GeV [10]. Figure 2(a) gives the mass dependence of the expected number of background and signal events and compares them to the observed number of events at each test mass.

The systematic uncertainties are estimated for several choices of the charged Higgs-boson mass from 50 GeV to 90 GeV at center-of-mass energies of $\sqrt{s}$=189 GeV, 200 GeV and 206 GeV to cover the full LEP2 range. The following sources of uncertainties are considered: limited number of generated Monte Carlo events, statistical and systematic uncertainty on the luminosity measurement, modeling of kinematic variables in the pre- and likelihood selections, tau lepton identification, dependence of the signal detection efficiency on final-state quark flavor, signal selection efficiency interpolation between generated Monte Carlo points, background hadronization model, and four-fermion background model. The contributions from the different sources are summarized in Table 2.

In the limit calculation, the efficiency and background estimates of the $2\mathrm{j} + \tau$ channel are reduced by $0.8-1.7\%$ (depending on the center-of-mass energy) in order to account for accidental vetoes due to accelerator-related backgrounds in the forward detectors.

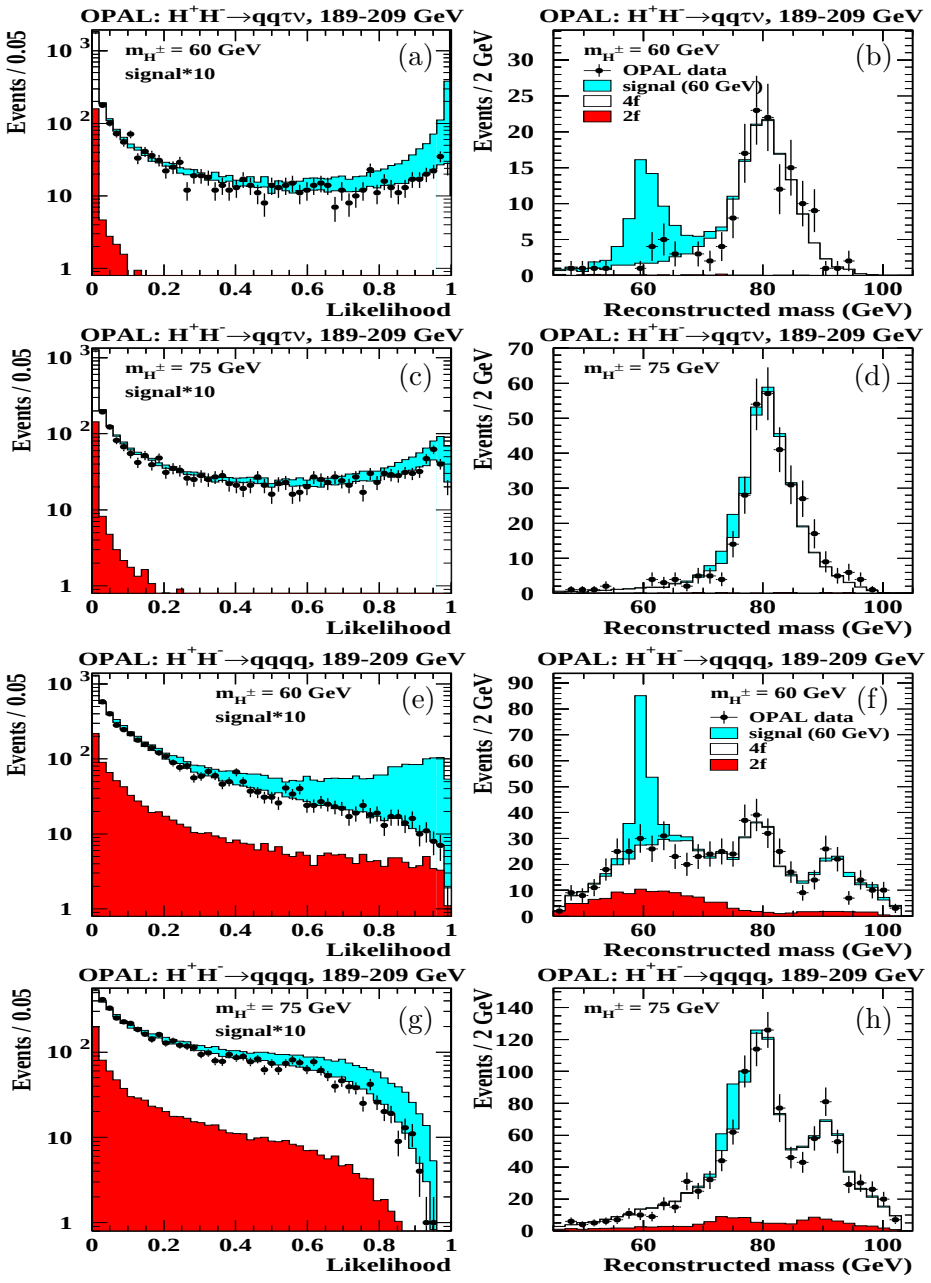

Figure 1: *Likelihood output and reconstructed di-jet mass distributions for the (a-d)* $2\mathrm{j}+\tau$ *and (e-h)* $4\mathrm{j}$ *channels. The distributions are summed up for all center-of-mass energies and correspond to 60 GeV and 75 GeV simulated charged Higgs-boson masses. All Monte Carlo distributions are normalized to the integrated luminosity of the data. When plotting the likelihood output, the signal expectation is scaled up by a factor of 10 for better visibility. A hadronic branching ratio of 0.5 is assumed for the* $2\mathrm{j}+\tau$ *signal, and 1.0 for the* $4\mathrm{j}$ *signal. The reconstructed mass distributions are shown after the likelihood selection.*

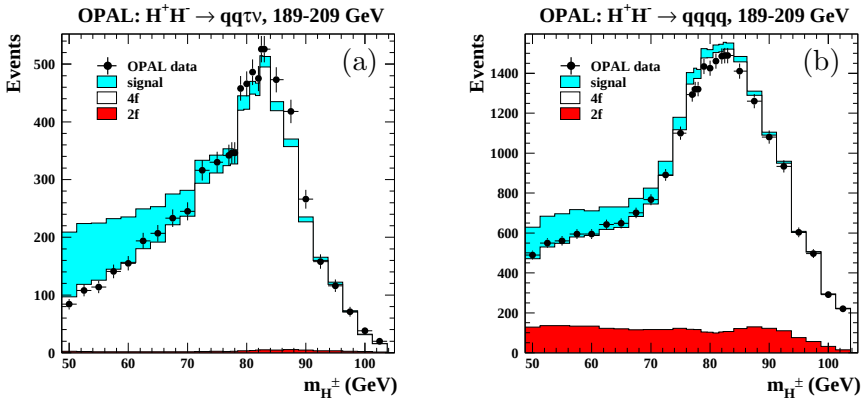

Figure 2: *The number of observed data, expected background and signal events for the (a)* $2\mathrm{j}+\tau$ *and (b)* 4j *channels. The numbers are summed up for all center-of-mass energies and shown as a function of the reference charged Higgs-boson mass. A hadronic branching ratio of 0.5 is assumed for the* $2\mathrm{j}+\tau$ *signal, and 1.0 for the* 4j *signal. Each bin corresponds to a different likelihood selection optimized for the mass at which the dot is centered. Since the same background simulations are used to form the reference histograms and the same data enter the selection, the neighboring points are strongly correlated.*

Source	$2\mathrm{j}+\tau$		4j	
	signal	background	signal	background
MC statistics	3.1−4.6	1.4−4.3	1.6−2.4	0.9−1.9
luminosity	0.3	0.3	0.3	0.3
preselection	1.5−4.7	1.8−7.6	0.3−1.1	0.5−2.2
likelihood selection	0.9−6.5	5.8−22.7	0.7−2.4	2.1−7.5
tau identification	3.0	3.0	N.A.	N.A.
quark flavor	2.7−3.8	N.A.	1.2−6.4	N.A.
interpolation	0.2−0.4	N.A.	0.7−3.7	N.A.
hadronization model	N.A.	1.0−2.7	N.A.	0.7−4.1
4f background model	N.A.	0.3−3.3	N.A.	1.7−3.7

Table 2: *Relative systematic uncertainties on the expected background and signal rates for the* $2\mathrm{j}+\tau$ *and* 4j *final states. The numbers are given in % and depend on the centre-of-mass energy and the reference charged Higgs-boson mass. N.A. stands for not applicable.*

3.2 The four-jet final state

The event selection follows our published analysis at $\sqrt{s}$=183 GeV [10]: first, well-separated four-jet events with large visible energy are preselected; then a set of variables is combined using a likelihood technique. To improve the discriminating power of the likelihood selection, a new reference variable is introduced: the logarithm of the matrix element probability for W^+W^- production averaged over all possible jet-parton assignments computed by EXCALIBUR [27]. Moreover, we introduce mass-dependent likelihood functions as explained above. As the optimal cut value on the likelihood output is not that sensitive to the charged Higgs-boson mass in this search channel, we use the condition $\mathcal{L} > 0.45$ at all center-of-mass energies and for all test masses.

There is a good agreement between the observed data and the SM Monte Carlo expectations at all stages of the selection. After all cuts, 1100 events are selected in the data, while 1117.8 $\pm$ 5.9 (stat.) $\pm$74.4 (syst.) events are expected from SM processes for a test mass of $m_{H^\pm}$=75 GeV. The four-fermion processes account for about 90% of the expected background and result in a large peak centered at the $W^\pm$ mass and a smaller one at the Z boson mass. The signal detection efficiencies are between 41% and 59% for any test mass and center-of-mass energy.

Typical likelihood output and reconstructed di-jet mass distributions of the selected events together with the SM background expectation and signal shapes for simulated charged Higgs-boson masses of 60 GeV and 75 GeV are plotted in Figures 1(e-h). The Higgs-boson mass can be reconstructed with a resolution of $1 - 1.5$ GeV [10]. Figure 2(b) shows the mass dependence of the expected number of background and signal events and compares them to the observed number of events at each test mass. Systematic uncertainties are estimated in the same manner as for the $2j + \tau$ search and are given in Table 2.

4 Search for $AW^{+*}AW^{-*}$ events

In a large part of the 2HDM(I) parameter space, the branching ratio of $H^\pm \to AW^{\pm *}$ dominates. The possible decay modes of the A boson and the $W^{\pm *}$ lead to many possible $H^+H^- \to AW^{+*}AW^{-*}$ event topologies. Above $m_A \approx 12$ GeV, the A boson decays predominantly into a $b\bar{b}$ pair, and thus its detection is based on b-flavor identification. Two possibilities, covering 90% of the decays of two $W^{\pm *}$, are considered: quark pairs from both $W^{\pm *}$ bosons or a quark pair from one and a leptonic final state from the other. The event topologies are therefore "eight jets" or "six jets and a lepton with missing energy", with four jets containing b-flavor in both cases.

The background comes from several Standard Model processes. ZZ and W^+W^- production can result in multi-jet events. While ZZ events can contain true b-flavored jets, W^+W^- events are selected as candidates when c-flavored jets fake b-jets. Radiative QCD corrections to $e^+e^- \to q\bar{q}$ also give a significant contribution to the expected background.

Due to the complexity of the eight-parton final state, it is more efficient to use general event properties and variables designed specifically to discriminate against the main background than a full reconstruction of the event. As a consequence, no attempt is made to reconstruct the charged Higgs-boson mass.

The analysis proceeds in two steps. First a preselection is applied to select b-tagged multi-jet events compatible with the signal hypothesis. Then a likelihood selection (with three event classes: signal, four-fermion background and two-fermion background) is applied.

The preselection of multi-jet events uses the same variables as the search for the hadronic final state in [10] with optimized cut positions. However, it introduces a very powerful new criterion, especially against the W^+W^- background, on a combined b-tagging variable ($\mathcal{B}_{\rm evt}$) requiring the consistency of the event with the presence of b-quark jets.

The neural network method used for b-tagging in the OPAL SM Higgs-boson search [15] is used to calculate on a jet-by-jet basis the discriminating variables $f^i_{\rm c/b}$ and $f^i_{\rm uds/b}$. These are constructed for each jet i as the ratios of probabilities for the jet to be c- or uds-like versus the probability to be b-like. The inputs to the neural network include information about the presence of secondary vertices in a jet, the jet shape, and the presence of leptons with large transverse momentum. The Monte Carlo description of the neural network output was checked with LEP1 data with a jet energy of about 46 GeV. The main background in this search at LEP2 comes from four-fermion processes, in which the mean jet energy is about 50 GeV, very close to the LEP1 jet energy; therefore, an adequate modeling of the data is expected with an event reconstruction assuming four jets.

The $AW^{+*}AW^{-*}$ signal topology depends on the Higgs-boson masses. At $m_{\rm A}{\approx}12$ GeV or $m_{\rm A}{\approx}m_{\rm H^\pm}$, the available energy in the A or $W^{\pm *}$ system is too low to form two clean, collimated jets. At high $m_{\rm H^\pm}$, the boost of the A and $W^{\pm *}$ bosons is small in the laboratory frame and the original eight partons cannot be identified. At low $m_{\rm H^\pm}$, the A and $W^{\pm *}$ bosons might have a boost, but it is still not possible to resolve correctly the two partons from their decay. From these considerations, one can conclude that it is not useful to require eight (or even six) jets in the event, as these jets will not correspond to the original partons. Consequently, to get the best possible modeling of the data, four jets are reconstructed with the Durham jet-finding algorithm [33] before the b-tagger is run.

The flavor-discriminating variables are combined for the four reconstructed jets by

$$\mathcal{B}_{\rm evt} = \frac{1}{1 + \alpha \cdot \prod_i f^i_{\rm c/b} + \beta \cdot \prod_i f^i_{\rm uds/b}} \tag{1}$$

The index i runs over the reconstructed jets ($i = 1, ...4$) and the parameters α and β are numerical coefficients whose optimal values depend on the flavor composition of the signal and background final states. However, since the expected sensitivity of the search is only slightly dependent on the values of α and β, they are fixed at $\alpha = 0.1$ and $\beta = 0.7$. Events are retained if $\mathcal{B}_{\rm evt} > 0.4$.

The preselections of the two event topologies (8j and $6j + \ell$) are very similar. However, in the $6j + \ell$ channel, no kinematic fit is made to the $W^+W^-{\to}q\bar{q}q\bar{q}$ hypothesis and, therefore, no cuts are made on the fit probabilities. No lepton identification is applied; instead the search is based on indirect detection of the associated neutrino by measuring the missing energy.

After the preselection the observed data show an excess over the predicted Monte Carlo background. This can partly be explained by the apparent difference between the gluon splitting rate into $c\bar{c}$ and $b\bar{b}$ pairs in the data and in the background Monte Carlo simulation. The measured rates are $g_{c\bar{c}} = 3.2 \pm 0.21 \pm 0.38\%$ [34] and $g_{b\bar{b}} = 0.307 \pm 0.053 \pm 0.097\%$ [35] from the LEP1 OPAL data. The gluon splitting rates in the Monte Carlo are extracted from $e^+e^-{\to}ZZ{\to}\ell^+\ell^-q\bar{q}$ events and are found to be $g^{\rm MC}_{c\bar{c}} = 1.33 \pm 0.06\%$ and $g^{\rm MC}_{b\bar{b}} = 0.116 \pm 0.0167\%$, averaged over all center-of-mass energies. This mismodeling can be compensated by reweighting the SM Monte Carlo events with gluon splitting to heavy quarks by universal reweighting factors [36] and at the same time deweighting the non-split events to keep the

total numbers of W^+W^-, ZZ and two-fermion background events fixed at generator level. The reweighting factor is 2.41 for $g \to c\bar{c}$ and 2.65 for $g \to b\bar{b}$. This correction results in a background enhancement factor of 1.08 to 1.1 after the preselection, depending on the search channel and the center-of-mass energy, but it does not affect the shape of the background distributions. The numbers of preselected events after the reweighting are given in Table 3.

LEP energy (year)		preselection 8j	preselection 6j + ℓ	exclusive 8j	exclusive 6j + ℓ	overlap
189 GeV	data	238	358	3	24	5
(1998)	background	231.2±2.9	342.2±3.6	2.1±0.3	24.4±1.0	6.3±0.5
192 − 202 GeV	data	297	310	16	16	17
(1999)	background	270.4±2.9	285.0±3.0	13.3±0.7	10.4±0.6	13.4±0.7
200 − 209 GeV	data	265	281	9	8	15
(2000)	background	252.5±3.7	270.5±5.0	13.0±0.9	9.3±0.8	12.9±0.9

Table 3: *Observed data and expected SM background events for each year in the* $AW^{+*}AW^{-*}$ *searches. The* 8j *and* 6j + ℓ *event samples after the preselection step (2nd and 3rd columns) are highly overlapping. After the likelihood selection, the overlapping events are removed from the* 8j *and* 6j + ℓ *samples and form a separate search channel (last three columns). The uncertainty on the background prediction due to the limited number of simulated events is given. The Monte Carlo reweighting to the measured gluon splitting rates is included.*

As a final selection, likelihood functions are built to identify signal events. The reference distributions depend on the LEP energy, but they are constructed to be independent of the considered $(m_{H^\pm}, m_A)$ combination. To this end, we form the signal reference distributions by averaging all simulated H^+H^- samples in the $(m_{H^\pm}, m_A)$ mass range of interest.

Since the selections at $\sqrt{s} = 192 - 209$ GeV are aimed at charged Higgs-boson masses around the expected sensitivity reach of about 80−90 GeV, all masses up to the kinematic limit are included. On the other hand, at $\sqrt{s}$=189 GeV only charged Higgs-boson masses up to 50 GeV are included since the selections at this energy are optimized to reach down to as low as a charged Higgs-boson mass of 40 GeV where the LEP1 exclusion limit lies. The input variables for the 8j final state are: the Durham jet-resolution parameters[2] $\log_{10} y_{34}$ and $\log_{10} y_{56}$, the oblateness [37] event shape variable, the opening angle of the widest jet defined by the size of the cone containing 68% of the total jet energy, the charge-signed cosine of the production angle in the $W^+W^- \to q\bar{q}q\bar{q}$ hypothesis, and the b-tagging variable $\mathcal{B}_{evt}$. At $\sqrt{s}$=189 GeV, $\log_{10} y_{23}$, $\log_{10} y_{45}$, $\log_{10} y_{67}$, and the maximum jet energy are also used. Moreover, the sphericity [38] event shape variable has more discriminating power and thus replaces oblateness. Although the y_{ij} variables are somewhat correlated, they contain additional information: their differences reflect the kinematics of the initial partons.

The input variables for the 6j + ℓ selection are: $\log_{10} y_{34}$, $\log_{10} y_{56}$, the oblateness, the missing energy of the event, and $\mathcal{B}_{evt}$. At $\sqrt{s}$=189 GeV, $\log_{10} y_{23}$, the maximum jet energy and the sphericity are also included.

Events are selected if they pass a lower cut on the likelihood output. This final cut does not remove (especially in the year 1999 data) all the excess events observed after the

[2]Throughout this paper y_{ij} denotes the parameter of the Durham jet finder at which the event classification changes from i-jet to j-jet, where $j = i + 1$.

preselection. The distributions of the critical selection variables, y_{34}, y_{56} and $\mathcal{B}_{\rm evt}$, are plotted on Figure 3 both in background-enriched data samples and after the preselection. To prepare these background-enriched data samples, the preselection cuts on y_{34} and $\mathcal{B}_{\rm evt}$ are dropped, except for the study of the y_{56} variable where we keep the cut on y_{34} in order to select multi-jet events. The resulting samples are completely dominated by background processes. We find systematic differences between the data samples and the equivalent background Monte Carlo simulations at both stages. The observed excess cannot be attributed to a Higgs-boson signal whose contribution is expected to be at most 0.5% in the background-enriched data samples. The interpretation of the excess in terms of a systematic uncertainty on the background prediction will be discussed later.

The non-signal nature of the excess is also demonstrated by Figure 4, which shows the distributions of the likelihood output. The positions of the likelihood cut are indicated by vertical lines.

Because the 8j and the 6j + ℓ selections have several discriminating variables in common, a major overlap between these selections exists. To assure that every event is counted only once, the two samples are redistributed into three: (*i*) events exclusively classified as 8j candidates, (*ii*) events exclusively classified as 6j + ℓ candidates and (*iii*) events accepted by both selections. If an event falls into class (*iii*), the larger likelihood output of the two selections is kept for further processing. The final results using the above classification are quoted in Table 3.

This modified channel definition not only removes the overlap but also increases the efficiency for detecting signal events by considering the cross-channel efficiencies (e.g. the efficiency to select $\rm H^+H^-\to b\bar{b}q\bar{q}b\bar{b}q\bar{q}$ signal by the exclusive 6j + ℓ selection can be as high as 18%, though it is typically only a few %). The efficiencies are determined independently for all simulated $(m_{\rm H^\pm}, m_{\rm A})$ combinations and interpolated to arbitrary $(m_{\rm H^\pm}, m_{\rm A})$ by two-dimensional spline interpolation. The behavior of the selection efficiencies depends strongly on the targeted charged Higgs-boson mass range and also varies with the mass difference $\Delta m = m_{\rm H^\pm} - m_{\rm A}$. In most cases the overlap channel has the highest efficiency. At $\sqrt{s}$=189 GeV and $m_{\rm H^\pm}$=45 GeV, it reaches 32% for the $\rm b\bar{b}q\bar{q}b\bar{b}\ell\nu_\ell$ and 44% for the $\rm H^+H^-\to b\bar{b}q\bar{q}b\bar{b}q\bar{q}$ signal close to the $m_{\rm H^\pm}$=$m_{\rm A}$ diagonal. At $\sqrt{s}$=206 GeV and $m_{\rm H^\pm}$=90 GeV, the overlap efficiency can be as high as 62% for the $\rm b\bar{b}q\bar{q}b\bar{b}\ell\nu_\ell$ and 71% for the $\rm H^+H^-\to b\bar{b}q\bar{q}b\bar{b}q\bar{q}$ signal. The exclusive 6j + ℓ selection has efficiencies typically below 20−30%, while the exclusive 8j selection below 10−15%. Table 4 gives the selection efficiencies at selected $(m_{\rm H^\pm}, m_{\rm A})$ points.

The composition of the background depends on the targeted Higgs-boson mass region. In the low-mass selection ($\sqrt{s}$=189 GeV) that is optimized for $m_{\rm H^\pm}$=40−50 GeV, the Higgs bosons are boosted and therefore the final state is two-jet-like with the largest background contribution coming from two-fermion processes: they account for 52% in the exclusive 8j, 80% in the exclusive 6j + ℓ and 76% in the overlap channel. On the other hand, in the high-mass analysis ($\sqrt{s} = 192 - 209$ GeV) the four-fermion fraction is dominant: it is 69% in the 8j, 56% in the 6j + ℓ and 70% in the overlap channel.

Although our studies show that the observed excess does not lie preferentially in the phase space region where the Higgs-boson signal is expected and that it probably originates from deficiencies of the Monte Carlo description of the jet-resolution parameters y_{ij} and the b-tagging variable $\mathcal{B}_{\rm evt}$, no further correction is applied to the estimated background in the background subtraction procedure of the statistical analysis to calculate exclusion limits. This leads to conservative limits on the production cross section. Therefore, no systematic uncertainty is assigned to the modeling of y_{34} and $\mathcal{B}_{\rm evt}$ at the preselection level. The systematic

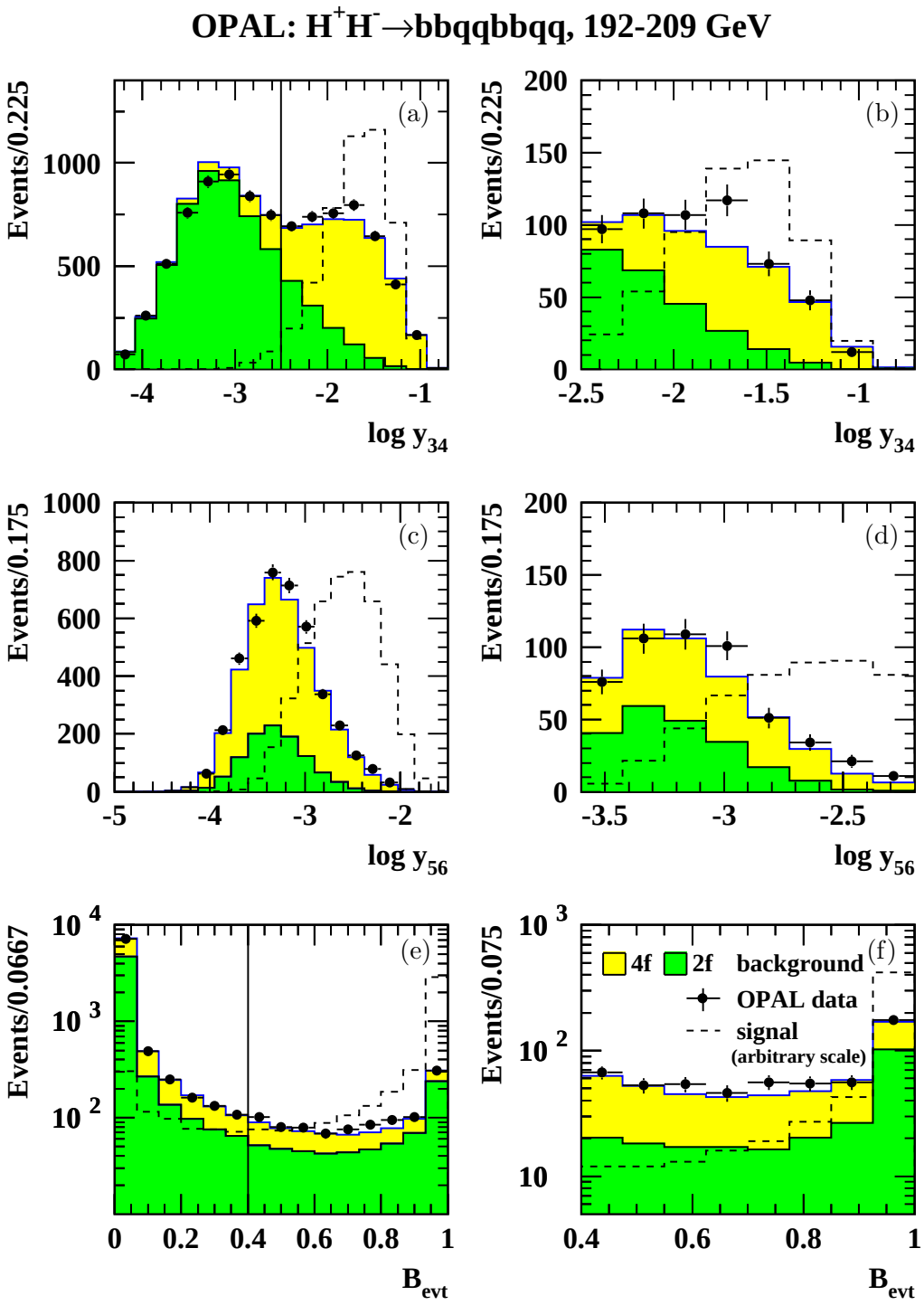

Figure 3: *Most important selection variables: (a-b)* $\log_{10} y_{34}$*, (c-d)* $\log_{10} y_{56}$ *and (e-f)* $\mathcal{B}_{\rm evt}$ *in the* 8j *channel at* $\sqrt{s} = 192 - 209$ *GeV. The distributions are shown (left) in a background-enriched data sample (see text for explanation) and (right) after the full preselection. To form the signal histograms, the Monte Carlo distributions are averaged for all simulated* $(m_{\rm H^{\pm}}, m_{\rm A})$ *mass combinations in the mass range of interest. The Monte Carlo reweighting to the measured gluon splitting rates is included. The expectations from SM processes are normalized to the data luminosity. The preselection cuts on* y_{34} *and* $\mathcal{B}_{\rm evt}$ *are indicated by vertical lines.*

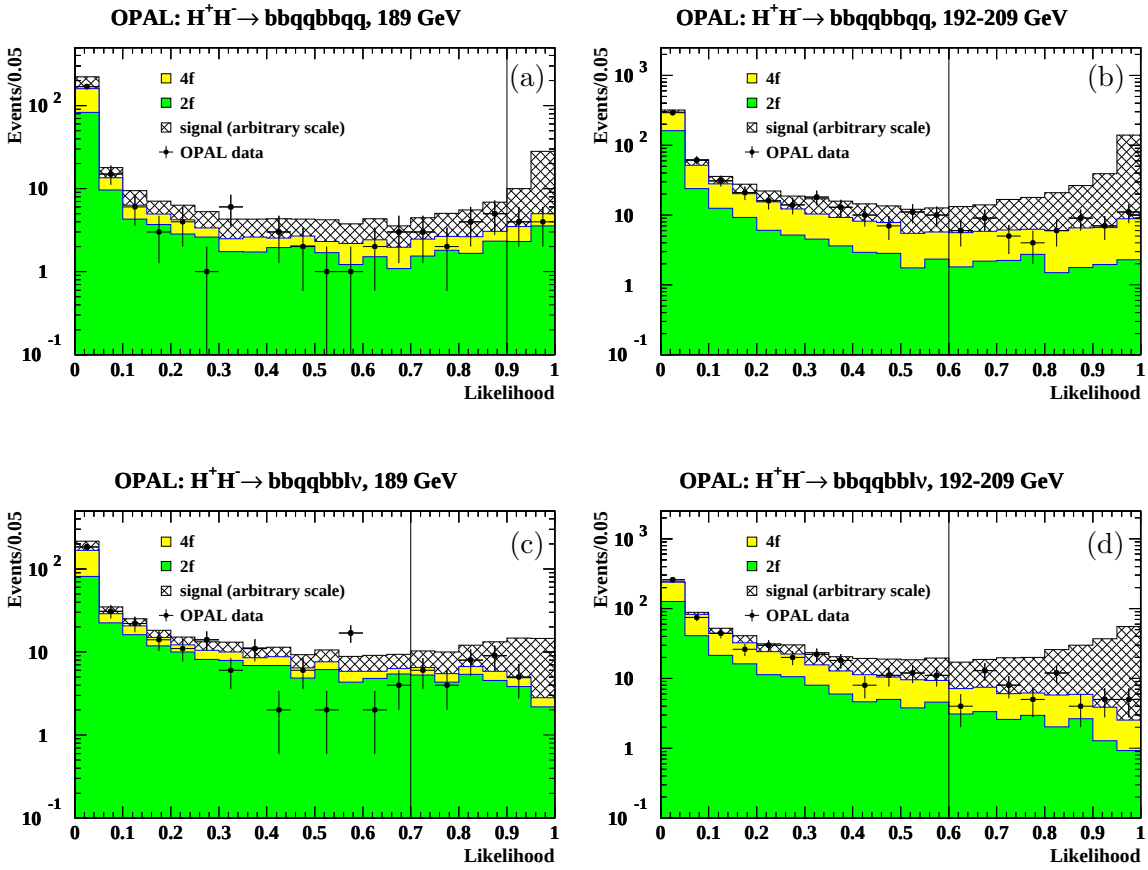

Figure 4: *Likelihood output distributions for the (a-b)* 8j *and (c-d)* $6\mathrm{j}+\ell$ *channels at* $\sqrt{s}$*=189 GeV and* $192-209$ *GeV. To form the signal histograms, the Monte Carlo distributions are averaged for all simulated* $(m_{\mathrm{H}^{\pm}}, m_{\mathrm{A}})$ *mass combinations in the mass range of interest. The Monte Carlo reweighting to the measured gluon splitting rates is included. The expectations from SM processes are normalized to the data luminosity. The lower cuts on the likelihood output are indicated by vertical lines.*

signal	selection	$(m_{\mathrm{H}^\pm}, m_{\mathrm{A}})$ (GeV, GeV)			
		(45,30)	(80,50)	(45,30)	(90,60)
		$\sqrt{s}$=189 GeV		$\sqrt{s}$=206 GeV	
$\mathrm{b\bar{b}q\bar{q}b\bar{b}q\bar{q}}$	8j	4.6	1.0	9.3	12.4
	overlap	41.0	2.8	14.9	69.6
	$6\mathrm{j}+\ell$	17.0	3.6	4.1	3.1
	total	62.6	7.4	28.3	85.0
$\mathrm{b\bar{b}q\bar{q}b\bar{b}}\ell\nu_\ell$	$6\mathrm{j}+\ell$	28.2	6.0	11.6	7.0
	overlap	31.8	3.6	14.2	62.2
	8j	1.8	0.1	2.2	6.1
	total	61.8	9.7	28.0	75.3
$\mathrm{b\bar{b}q\bar{q}}\tau\nu_\tau$	$4\mathrm{j}+\tau$	68.0	0.0	12.3	11.1

Table 4: *Signal selection efficiencies in percent for the* $\mathrm{H}^\pm\to\mathrm{AW}^{\pm *}$ *final states in the different search channels at* $\sqrt{s}$*=189 and 206 GeV at representative* $(m_{\mathrm{H}^\pm}, m_{\mathrm{A}})$ *points.*

uncertainties related to the other preselection variables, estimated from background-enriched data samples, are taken into account. The effect of mismodeling the shapes of the reference distributions in the likelihood selection is estimated for all variables, including y_{ij} and $\mathcal{B}_{\mathrm{evt}}$ and is accounted for in the statistical analysis.

Systematic uncertainties arise also due to the gluon splitting correction: the experimental uncertainty on the gluon splitting rate translates into uncertainties on the total background rates. Moreover, the weighted background counting introduces an uncertainty due to the Monte Carlo statistics of the $\mathrm{g}\to\mathrm{c\bar{c}}$ and $\mathrm{b\bar{b}}$ events.

In summary, the following sources of systematic uncertainties are considered: limited number of simulated signal and background events, modeling of the preselection variables (other than y_{ij} and $\mathcal{B}_{\mathrm{evt}}$), modeling of the shapes of the reference distributions in the likelihood selection and the gluon splitting correction. Uncertainties below the 1% level are neglected. The different contributions are summarized in Table 5.

5 Search for $\mathrm{AW}^{\pm *}\tau\nu_\tau$ events

In some parts of the 2HDM(I) parameter space, both the fermionic $\mathrm{H}^\pm\to\tau\nu_\tau$ and the bosonic $\mathrm{H}^\pm\to\mathrm{AW}^{\pm *}$ decay modes contribute. To cover this transition region parallel to the $(m_{\mathrm{H}^\pm}, m_{\mathrm{A}})$ diagonal, a search for the final state $\mathrm{H}^+\mathrm{H}^-\to\mathrm{AW}^{\pm *}\tau\nu_\tau$ is performed. The transition region is wide for small $\tan\beta$ and narrow for large $\tan\beta$; therefore, this analysis is more relevant for lower values of $\tan\beta$.

Only the hadronic decays of $\mathrm{W}^{\pm *}$ and the decay $\mathrm{A}\to\mathrm{b\bar{b}}$ are considered. Thus the events contain a tau lepton, four jets (two of which are b-flavored) and missing energy. Separating the signal from the $\mathrm{W}^+\mathrm{W}^-$ background becomes difficult close to $m_{\mathrm{H}^\pm}$=$m_{\mathrm{W}^\pm}$.

The preselection is designed to identify hadronic events containing a tau lepton plus significant missing energy and transverse momentum from the undetected neutrino. In most cases it is not practical to reconstruct the four jets originating from the $\mathrm{AW}^{\pm *}$ system. Instead, to suppress the main background from semi-leptonic $\mathrm{W}^+\mathrm{W}^-$ events, we remove the decay

Source	exclusive 8j		exclusive 6j + ℓ		overlap	
	signal	background	signal	background	signal	background
MC statistics	$\geq$15/$\geq$8.5	13.2/6.7	$\geq$5.7/$\geq$8.4	4.0/8.3	$\geq$4.0/$\geq$2.8	7.9/7.1
preselection	1.0	1.0	1.0	2.0	1.0	2.0/1.5
$\mathcal{L}$ selection						
y_{ij}	4.0/1.8	6.0/6.2	2.2/2.6	6.0/8.0	2.8/1.5	5.5/4.9
b-tag	0.0/1.8	4.7/7.0	2.9/1.4	4.4/7.1	1.0/1.3	4.0/5.1
other	1.8/0.7	3.9/3.2	1.0/1.6	3.7/3.5	1.2/0.7	3.4/2.4
gluon splitting						
g$\to$c$\bar{\text{c}}$, exp.	N.A.	0.6/2.5	N.A.	1.6	N.A.	1.4/2.3
g$\to$c$\bar{\text{c}}$, MC	N.A.	0.2/0.8	N.A.	0.6	N.A.	0.5/0.8
g$\to$b$\bar{\text{b}}$, exp.	N.A.	1.4/4.2	N.A.	3.8/4.3	N.A.	5.5/5.4
g$\to$b$\bar{\text{b}}$, MC	N.A.	0.5/1.7	N.A.	1.5/1.7	N.A.	2.2
gluon splitting correction factor	N.A.	1.05/1.18	N.A.	1.13/1.15	N.A.	1.15/1.22

Table 5: *Relative systematic uncertainties in percent for the* $\mathrm{AW}^{+*}\mathrm{AW}^{-*}$ *searches. Where two values are given separated by a "/", the first belongs to the 189 GeV selection and the second to the* $192-209$ *GeV selections. For the signal, the uncertainties due to the limited Monte Carlo statistics are calculated by binomial statistics for a sample size of 500 events and they also depend, via the selection efficiency, on the assumed Higgs-boson masses. N.A. stands for not applicable. The multiplicative gluon splitting correction factors, used to obtain the background-rate estimates as explained in the text, are given in the last line.*

products of the tau candidate and force the remaining hadronic system into two jets by the Durham algorithm. The requirements are then based on the preselection of Section 3.1 with additional preselection cuts on the effective center-of-mass energy, $\log_{10} y_{12}$ and $\log_{10} y_{23}$ of the hadronic system, and the charge-signed $\mathrm{W}^{\pm}$ production angle.

The likelihood selection uses seven variables: the momentum of the tau candidate, the cosine of the angle between the tau momentum and the nearest jet, $\log_{10} y_{12}$ of the hadronic system, the cosine of the angle between the two hadronic jets, the charge-signed cosine of the $\mathrm{W}^{\pm}$ production angle, the invariant mass of the hadronic system, and the b-tagging variable $\mathcal{B}_{\mathrm{evt}}$. Here, $\mathcal{B}_{\mathrm{evt}}$ is defined using the two jets of the hadronic system using Eq. (1) of Section 4, with $i = 1, 2$ and $\alpha = \beta = 1$. To form the signal reference distributions, all simulated $\mathrm{H}^{+}\mathrm{H}^{-}$ samples in the $(m_{\mathrm{H}^{\pm}}, m_{\mathrm{A}})$ mass range of interest are summed up. Since the search at $\sqrt{s} = 192-209$ GeV targets intermediate charged Higgs-boson masses (60−80 GeV), all masses up to the kinematic limit are included. At $\sqrt{s}$=189 GeV, only charged Higgs-boson masses up to 50 GeV are included since the selection is optimized for low charged Higgs-boson masses (40−50 GeV).

The likelihood output distributions are shown in Figure 5. There is an overall agreement between data and background distributions, apart from a small discrepancy at 189 GeV. Events are selected if their likelihood output is larger than 0.9. In total, 15 data events survive the selection at $\sqrt{s} = 192 - 209$ GeV, to be compared with 14.8 ± 0.6 (stat.) ± 1.9 (syst.) events expected from background sources. At $\sqrt{s}$=189 GeV, where the selection is optimized for low Higgs-boson masses, 13 data events are selected with 6.1 ± 0.5 (stat.) ± 1.3 (syst.) events expected. The contribution of four-fermion events, predominantly from semi-leptonic $\mathrm{W}^{+}\mathrm{W}^{-}$ production, amounts to 33% at $\sqrt{s}$=189 GeV and to 90% at $\sqrt{s} = 192 - 209$ GeV.

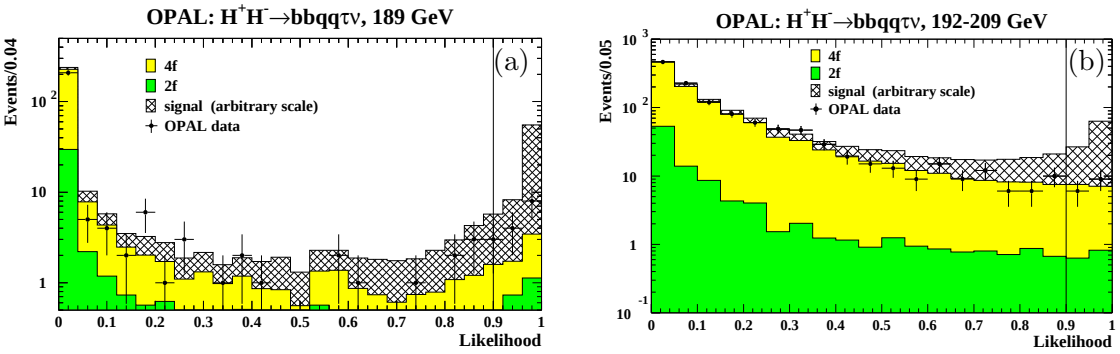

Figure 5: *Likelihood output distribution for the* $4\mathrm{j}+\tau$ *channel at (a)* $\sqrt{s}$*=189 GeV and (b)* $\sqrt{s}$*=*$192-209$ *GeV. To form the signal histograms, the Monte Carlo distributions are averaged for all simulated* $(m_{\mathrm{H}^\pm}, m_{\mathrm{A}})$ *mass combinations in the mass range of interest. The expectations from SM processes are normalized to the data luminosity. The lower cuts on the likelihood output are indicated by vertical line.*

At $\sqrt{s} = 192-209$ GeV, the signal selection efficiency starts at about 5% at $m_{\mathrm{H}^\pm}$=40 GeV, reaches its maximum of about 40% (depending on the mass difference $\Delta m = m_{\mathrm{H}^\pm} - m_{\mathrm{A}}$) at $m_{\mathrm{H}^\pm}$=60 GeV, then decreases to 12% at $m_{\mathrm{H}^\pm}$=90 GeV. In the low-mass selection at $\sqrt{s}$=189 GeV, the efficiency depends strongly on the mass difference: at $m_{\mathrm{H}^\pm}$=40 GeV, it is 22% for $\Delta m = 2$ GeV and 60% for $\Delta m = 10$ GeV. The selection efficiency approaches its maximum at $m_{\mathrm{H}^\pm}$=50 GeV (70% for $\Delta m = 10$ GeV) and then drops to zero at $m_{\mathrm{H}^\pm}$=80 GeV. Table 4 gives selection efficiencies at representative $(m_{\mathrm{H}^\pm}, m_{\mathrm{A}})$ points.

The systematic uncertainties due to the modeling of selection variables are evaluated with the method developed for the $\mathrm{AW}^{+*}\mathrm{AW}^{-*}$ channels and summarized in Table 6.

Source		$4\mathrm{j}+\tau$	
		signal	background
MC statistics		$\geq$2.7/$\geq$4.5	8.2/7.0
preselection: tau ID		0.0	2.3/5.0
	other	0.0/1.0	9.5/7.9
likelihood selection: b-tag		0.3/1.4	2.4/3.0
	other	3.2/2.1	18.4/11.2

Table 6: *Systematic uncertainties in percent for the* $4\mathrm{j}+\tau$ *channel. Where two values are given separated by a "/", the first one belongs to the 189 GeV selection and the second to the* $192-209$ *GeV selections. For the signal, the uncertainties due to the limited Monte Carlo statistics are calculated by binomial statistics for a sample size of 500 events and they also depend, via the selection efficiency, on the assumed Higgs-boson masses.*

6 Interpretation

None of the searches has revealed a signal-like excess over the SM expectation. The results presented here and those published previously [10, 31] by the OPAL Collaboration are combined using the method of [39] to study the compatibility of the observed events with "background-only" and "signal plus background" hypotheses and to derive limits on charged Higgs-boson production. The statistical analysis is based on weighted event counting, with the weights computed from physical observables, also called discriminating variables of the candidate events (see Table 7). Systematic uncertainties with correlations are taken into account in the confidence level (p-value) calculations. To improve the sensitivity of the analysis, they are also incorporated into the weight definition [39].

Channel	$\sqrt{s}$ (GeV)	Discriminant
2τ	183	simple event counting
2τ	189-209	likelihood output
$2\mathrm{j}+\tau$	183-209	reconstructed di-jet mass
4j	183-209	reconstructed di-jet mass
8j	189	simple event counting
8j	192-209	likelihood output
$6\mathrm{j}+\ell$	189	simple event counting
$6\mathrm{j}+\ell$	192-209	likelihood output
$4\mathrm{j}+\tau$	189-209	simple event counting

Table 7: *Discriminating variables entering the statistical analysis for each search topology. Previously published results are also included.*

The results are interpreted in two different scenarios: in the traditional, supersymmetry-favored 2HDM(II) (assuming that there are no new additional light particles other than the Higgs bosons) and in the 2HDM(I) where under certain conditions fermionic couplings are suppressed.

First, we calculate $1-CL_b$, the confidence [39] under the background-only hypothesis, and then proceed to calculate limits on the charged Higgs-boson production cross section in the signal + background hypothesis. These results are used to provide exclusions in the model parameter space, and in particular, on the charged Higgs-boson mass.

2HDM Type II

First a general 2HDM(II) is considered, where $\mathrm{BR}(\mathrm{H}^{\pm}\to\tau\nu_\tau)+\mathrm{BR}(\mathrm{H}^{\pm}\to\mathrm{q\bar{q}})=1$. This model was thoroughly studied at LEP. It is realized in supersymmetric extensions of the SM if no new additional light particles other than the Higgs bosons are present. As our previously published mass limit in such a model is $m_{\mathrm{H}^{\pm}} > 59.5$ GeV [10], only charged Higgs-boson masses above 50 GeV are tested. Cross-section limits for lower masses can be found in [9]. In this model, the results of the 2τ, $2\mathrm{j}+\tau$ and 4j searches enter the statistical combination.

The confidence $1-CL_b$ is plotted for each channel separately in Figure 6(a) and combined in Figure 6(b). Note that $1-CL_b < 0.5$ translates to negative values of sigma (as indicated by the dual y-axis scales in Figure 6(a)) and indicates an excess of events. The largest deviation, a 2.8σ excess observed in the $2\mathrm{j}+\tau$ channel at $m_{\mathrm{H}^{\pm}}$=88 GeV, comes

from a known deficiency [40] of the Monte Carlo simulation of isolated tracks from the fragmentation and hadronization process. When the three final states are combined assuming $\mathrm{BR}(\mathrm{H}^{\pm}\to\tau\nu_\tau) + \mathrm{BR}(\mathrm{H}^{\pm}\to\mathrm{q\bar{q}}) = 1$, no deviation reaches the 2σ level.

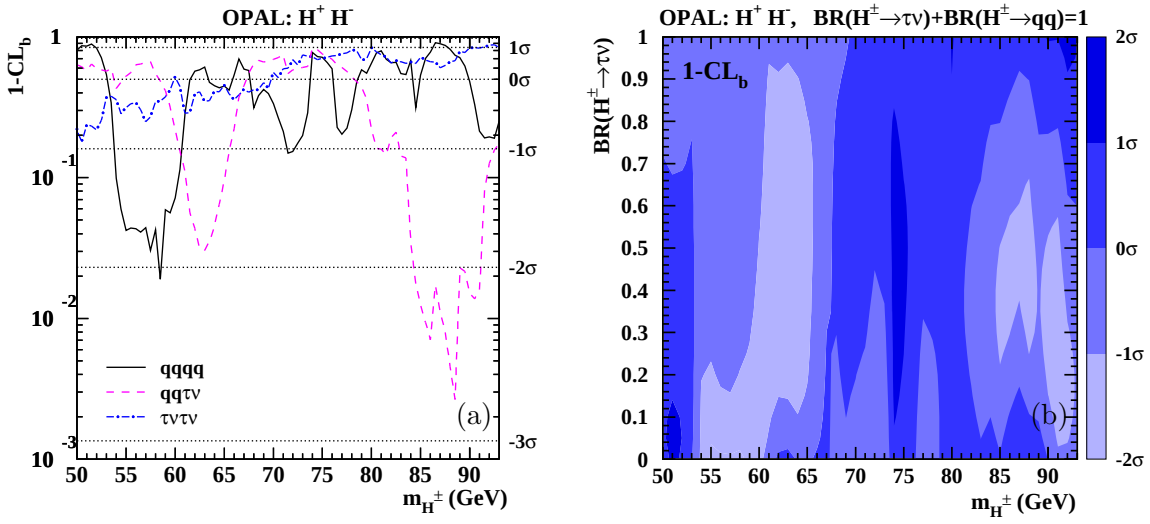

Figure 6: *The observed confidence levels for the background interpretation of the data,* $1 - CL_b$*, (a) for the three different final states as a function of the charged Higgs-boson mass, and (b) for the combined result in 2HDM(II) assuming* $\mathrm{BR}(\mathrm{H}^{\pm}\to\tau\nu_\tau) + \mathrm{BR}(\mathrm{H}^{\pm}\to\mathrm{q\bar{q}}) = 1$ *on the* $[m_{\mathrm{H}^{\pm}}, \mathrm{BR}(\mathrm{H}^{\pm}\to\tau\nu_\tau)]$ *plane. The significance values corresponding to the different shadings are shown by the bar at the right.*

The results are used to set upper bounds on the charged Higgs-boson pair production cross section relative to the 2HDM prediction as calculated by HZHA. The limits obtained are shown for each channel separately in Figures 7(a-c) and combined in Figure 7(d). The combined results are shown by "isolines" along which $\sigma_{95}(\mathrm{H}^{+}\mathrm{H}^{-})/\sigma_{\mathrm{2HDM}}$, the ratio of the limit on the production cross section and the 2HDM cross-section prediction, is equal to the number indicated next to the curves.

Excluded areas on the $[m_{\mathrm{H}^{\pm}}, \mathrm{BR}(\mathrm{H}^{\pm}\to\tau\nu_\tau)]$ plane are presented for each channel separately in Figure 8(a) and combined in Figure 8(b). The expected mass limit from simulated background experiments, assuming no signal, is also shown. For the combined results, the 90% and 99% CL contours are also given. Charged Higgs bosons are excluded up to a mass of 76.6 GeV at 95% CL, independent of $\mathrm{BR}(\mathrm{H}^{\pm}\to\tau\nu_\tau)$. Lower mass limits for different values of $\mathrm{BR}(\mathrm{H}^{\pm}\to\tau\nu_\tau)$ are presented in Table 8.

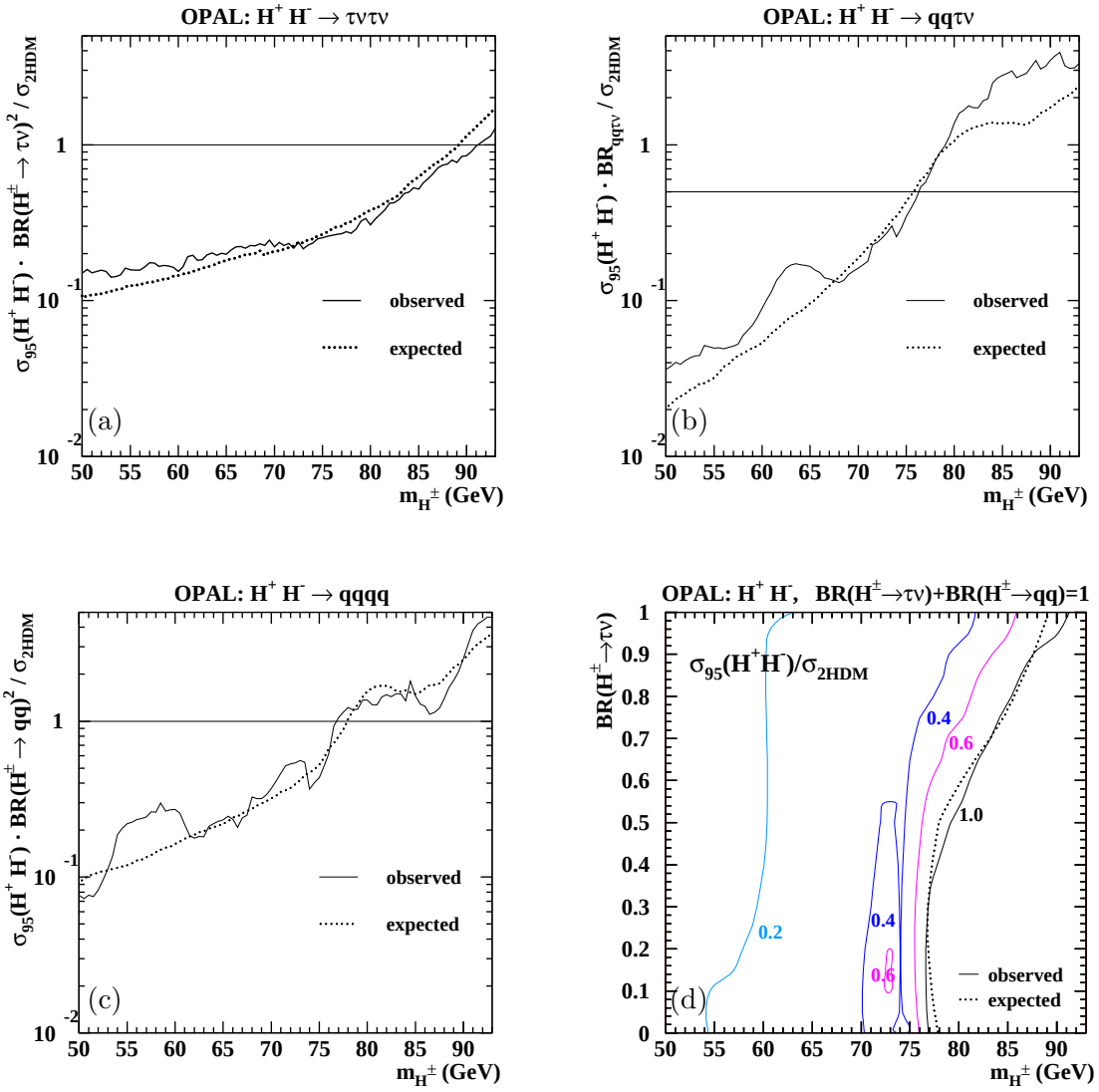

Figure 7: *Observed and expected 95% CL upper limits on the* $\mathrm{H^+H^-}$ *production cross section times the relevant* $\mathrm{H^\pm}$ *decay branching ratios relative to the theoretical prediction for the (a)* $\tau\nu_\tau\tau\nu_\tau$ *(b)* $\mathrm{q\bar{q}}\tau\nu_\tau$ *and (c)* $\mathrm{q\bar{q}q\bar{q}}$ *channels. The horizontal lines indicate the maximum possible branching ratios for a given channel. In (b),* $\mathrm{BR_{qq\tau\nu}} = 2 \cdot \mathrm{BR(H^\pm\to\tau\nu_\tau)} \cdot \mathrm{BR(H^\pm\to q\bar{q})}$. *(d) Upper limits on the production cross section relative to the 2HDM prediction on the* $[m_{\mathrm{H^\pm}}, \mathrm{BR(H^\pm\to\tau\nu_\tau)}]$ *plane in 2HDM(II) assuming* $\mathrm{BR(H^\pm\to\tau\nu_\tau)} + \mathrm{BR(H^\pm\to q\bar{q})} = 1$. *The plotted curves are isolines along which the limit is equal to the number indicated.*

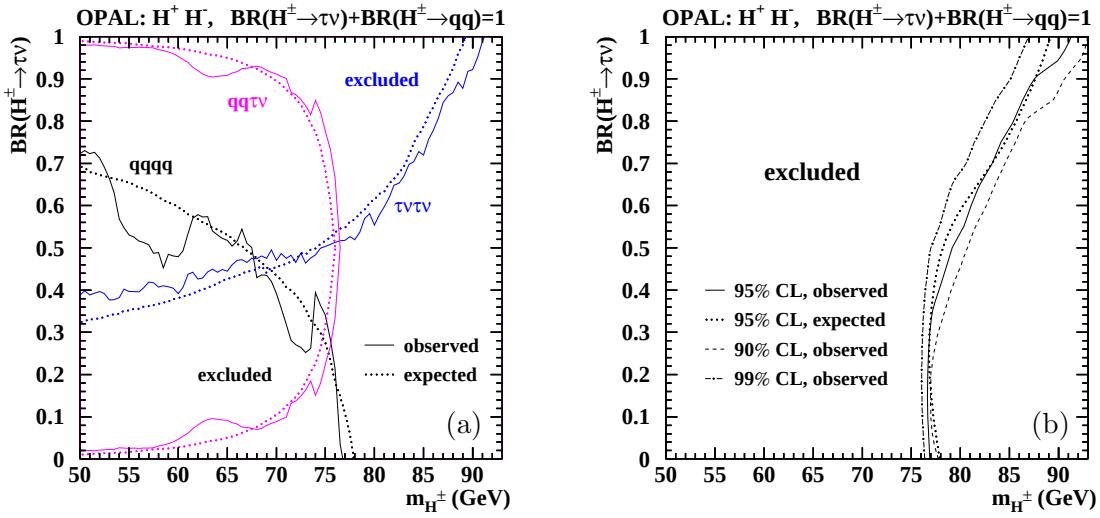

Figure 8: *Observed and expected excluded areas at 95% CL on the* $[m_{\mathrm{H}^\pm}, \mathrm{BR}(\mathrm{H}^\pm \to \tau\nu_\tau)]$ *plane (a) for each search channel separately and (b) combined in 2HDM(II) assuming* $\mathrm{BR}(\mathrm{H}^\pm \to \tau\nu_\tau) + \mathrm{BR}(\mathrm{H}^\pm \to \mathrm{q\bar{q}}) = 1$. *For the combined result, the 90% and 99% CL observed limits are also shown. See Table 8 for numerical values of the combined limit.*

$\mathrm{BR}(\mathrm{H}^\pm \to \tau\nu_\tau)$	Lower mass limit (GeV)	
	Observed	Expected
0	76.9	77.9
0.5	79.2	78.0
0.65	82.0	81.7
1	91.2	89.2
any	76.6 (0.15)	76.8 (0.27)

Table 8: *Observed and expected lower limits at 95% CL on the mass of the charged Higgs boson in 2HDM(II) assuming* $\mathrm{BR}(\mathrm{H}^\pm \to \tau\nu_\tau) + \mathrm{BR}(\mathrm{H}^\pm \to \mathrm{q\bar{q}}) = 1$. *For the results independent of the branching ratio (last line), the* $\mathrm{BR}(\mathrm{H}^\pm \to \tau\nu_\tau)$ *value at which the limit is set, is given in parenthesis.*

2HDM Type I

We present here for the first time an interpretation of the OPAL charged Higgs-boson searches in an alternative theoretical scenario, a 2HDM(I). The novel feature of this model with respect to the more frequently studied 2HDM(II) is that the fermionic decays of the charged Higgs boson can be suppressed. If the A boson is light, the $H^{\pm}\to AW^{\pm *}$ decay may play a crucial role.

The charged Higgs-boson sector in these models is described by three parameters: $m_{H^{\pm}}$, m_A and $\tan\beta$. To test this scenario, the charged Higgs-boson decay branching ratios are calculated by the program of Akeroyd et al. [8], and the model parameters are scanned in the range: 40 GeV $\leq m_{H^{\pm}} \leq$ 94 GeV, 12 GeV $\leq m_A < m_{H^{\pm}}$, $0.1 \leq \tan\beta \leq 100$. Charged Higgs-boson pair production is excluded below 40 GeV by the measurement of the Z boson width [41]. As the A boson detection is based on the identification of b-quark jets, no limits are derived for $m_A < 2m_b$. Below $\tan\beta$=0.1, BR($H^{\pm}\to AW^{\pm *}$) vanishes and the limit is no longer sensitive to m_A.

Both the fermionic (2τ, $2j+\tau$ and 4j) and the bosonic ($4j+\tau$, $6j+\ell$ and 8j) final states play an important role and therefore their results are combined. There is, however, a significant overlap between the events selected by the $H^+H^-\to q\bar{q}q\bar{q}$ and $H^+H^-\to AW^{+*}AW^{-*}$ selections, and the events selected by the $H^+H^-\to q\bar{q}\tau\nu_\tau$ and $H^+H^-\to AW^{\pm *}\tau\nu_\tau$ selections. Therefore, an automatic procedure is implemented to switch off the less sensitive of the overlapping channels, based on the calculation of the expected limit assuming no signal. In general the fermionic channels are used close to the $[m_{H^{\pm}}, m_A]$ diagonal and for low $\tan\beta$, and the searches for $H^{\pm}\to AW^{\pm *}$ are crucial for low values of m_A and high values of $\tan\beta$.

The confidence $1-CL_b$ is calculated combining the $6j+\ell$ and 8j searches assuming SM branching ratios [42] for the $W^{\pm *}$ decay and is shown on Figure 9(a). The largest deviation $1-CL_b = 0.0009$ corresponding to 3.1σ is reached at $m_{H^{\pm}}$=45 GeV and m_A=44.9 GeV (in the middle of the very narrow lightest strip from $m_{H^{\pm}}$=40 GeV to 50 GeV at the $(m_{H^{\pm}}, m_A)$ diagonal). However, the mean background shift on the $[m_{H^{\pm}}, m_A]$ plane amounts only to 1.1σ. $1-CL_b$ for the $4j+\tau$ channel is shown in Figure 9(b). The largest deviation $1-CL_b = 0.013$ corresponding to 2.2σ appears for low charged Higgs-boson masses ($m_{H^{\pm}}$=40 GeV, m_A=21 GeV), reflecting the excess of events in the $\sqrt{s}$=189 GeV search. The mean background shift for this channel is 0.8σ. Note that the results shown in Figures 9(a-b) are model-independent.

When all channels are combined within 2HDM(I), a few hot spots with a significance above 2σ survive. This is illustrated in Figures 9(c-d), where the combined results are plotted for $\tan\beta$=10 and 100. For $\tan\beta$=10, the largest excess $1-CL_b = 0.01$ corresponding to 2.3σ is found at $m_{H^{\pm}}$=55 GeV and m_A=35 GeV (just before switching from the bosonic to the fermionic channels).

As mentioned previously, the $H^{\pm}\to AW^{\pm *}$ decay becomes dominant if the A boson is sufficiently light. The smaller $\tan\beta$ is, the smaller m_A should be. This is clearly seen from the structure of the result on Figures 9(c-d): for $\tan\beta$=10, the bosonic decay becomes dominant at $m_A \lessapprox m_{H^{\pm}} - 18$ GeV, while for $\tan\beta$=100, it dominates already at $m_A \lessapprox m_{H^{\pm}} - 6$ GeV.

The model-independent limits on the charged Higgs-boson production cross section relative to the 2HDM prediction are presented in Figure 10(a) for the $H^+H^-\to AW^{+*}AW^{-*}$ and in Figure 10(b) for $H^+H^-\to AW^{\pm *}\tau\nu_\tau$ searches, with the only assumption that $W^{\pm *}$ decays with SM branching ratios. The results combining all channels using 2HDM(I) branching ratios are shown on Figure 11 for different choices of $\tan\beta$.

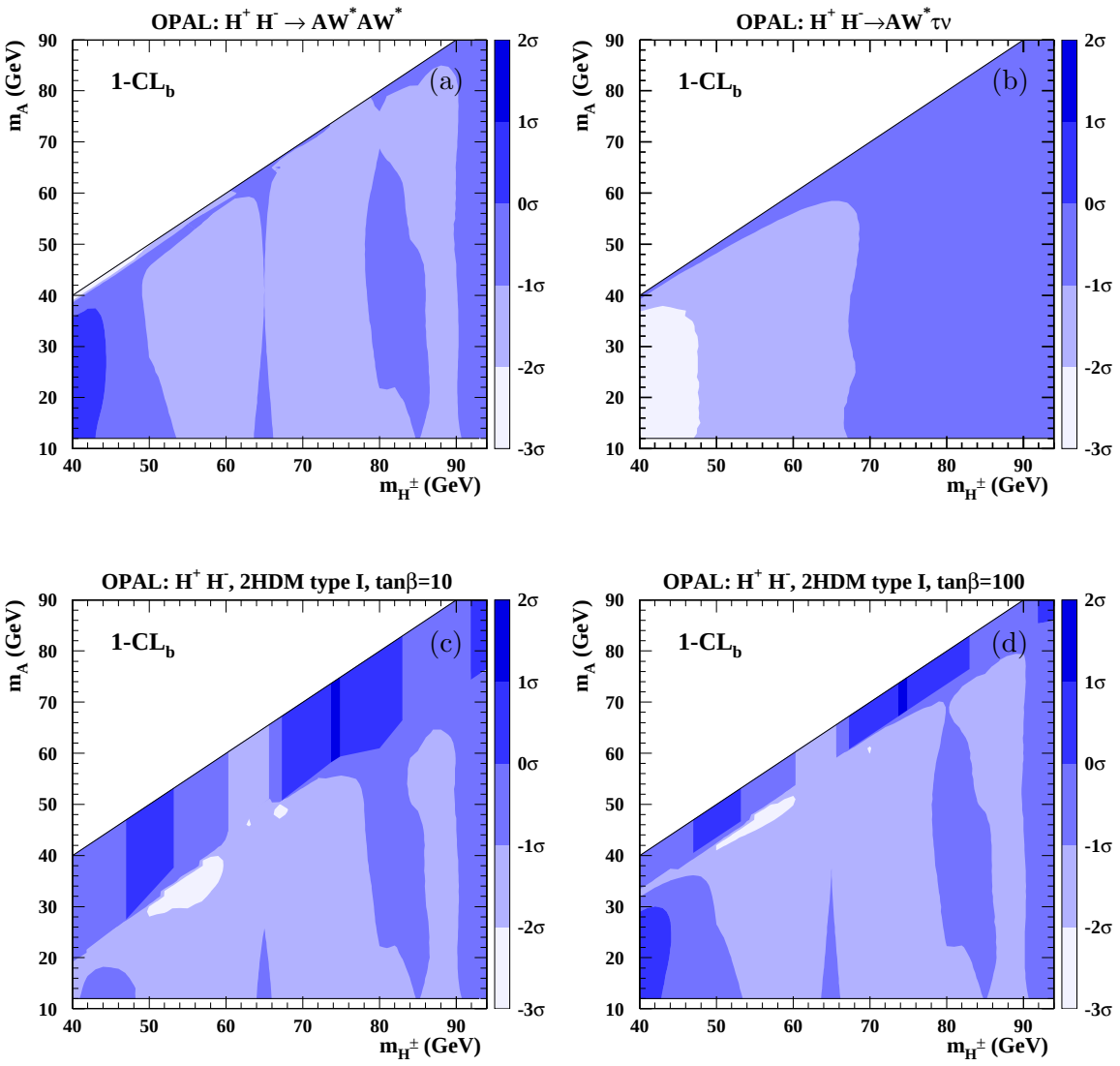

Figure 9: *The confidence* $1 - CL_b$ *on the* $[m_{\mathrm{H}^\pm}, m_{\mathrm{A}}]$ *plane (a) for* $\mathrm{H}^+\mathrm{H}^- \to \mathrm{AW}^{+*}\mathrm{AW}^{-*}$ *combining the results of the* $6\mathrm{j} + \ell$ *and* $8\mathrm{j}$ *searches, and (b) for* $\mathrm{H}^+\mathrm{H}^- \to \mathrm{AW}^{\pm *}\tau\nu_\tau$ *from the* $4\mathrm{j} + \tau$ *search. The combined results in 2HDM(I) for (c)* $\tan\beta$*=10 and (d)* $\tan\beta$*=100 are also shown. The significance values corresponding to the different shadings are shown by the bars at the right.*

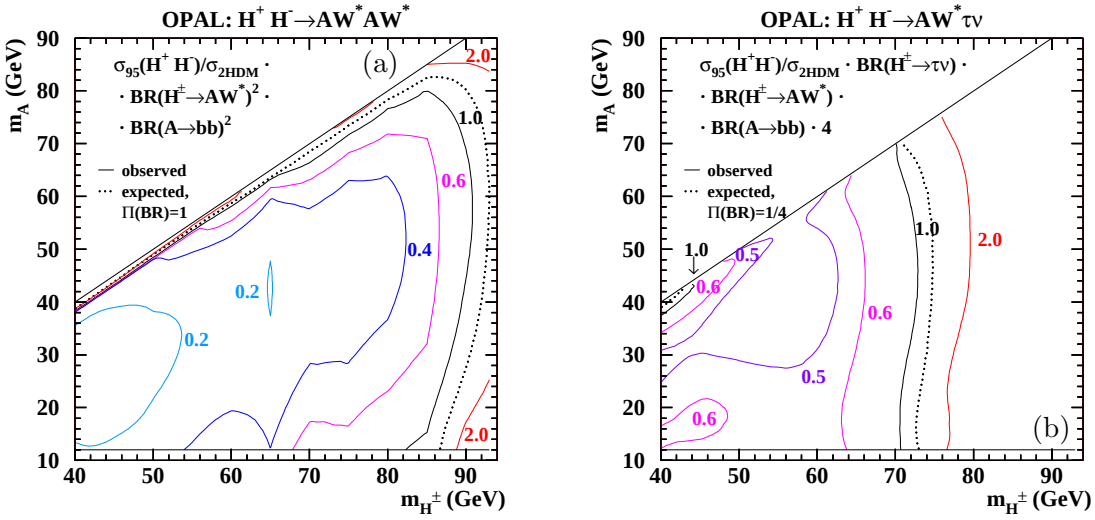

Figure 10: *The 95% CL upper limits on the production cross section times relevant* $\mathrm{H}^{\pm}$ *and A boson decay branching ratios relative to the 2HDM prediction on the* $[m_{\mathrm{H}^{\pm}}, m_{\mathrm{A}}]$ *plane for the process (a)* $\mathrm{H}^{+}\mathrm{H}^{-}\to\mathrm{AW}^{+*}\mathrm{AW}^{-*}$ *and (b)* $\mathrm{H}^{+}\mathrm{H}^{-}\to\mathrm{AW}^{\pm *}\tau\nu_{\tau}$. *The plotted curves are isolines along which the limit is equal to the number indicated. The expected limits are given for (a)* $\mathrm{BR}(\mathrm{H}^{\pm}\to\mathrm{AW}^{\pm *})^{2}\cdot\mathrm{BR}(A\to\mathrm{b\bar{b}})^{2}=1$ *and (b)* $\mathrm{BR}(\mathrm{H}^{\pm}\to\tau\nu_{\tau})\cdot\mathrm{BR}(\mathrm{H}^{\pm}\to\mathrm{AW}^{\pm *})\cdot\mathrm{BR}(A\to\mathrm{b\bar{b}})=0.25$ *corresponding to the maximal value in 2HDM(I).*

For intermediate and large values of $\tan\beta$, an unexcluded region appears parallel to the $[m_{\mathrm{H}^{\pm}}, m_{\mathrm{A}}]$ diagonal both in the observed and expected limits in Figure 11 (see the full and dotted black curves corresponding to a cross-section ratio of 1.0). This can be understood by making two observations: Close to the diagonal, the eight- or six-jet structure of the $\mathrm{H}^{\pm}\to\mathrm{AW}^{\pm *}$ signal events becomes less pronounced and the final state turns four-jet-like. As the selection variables for the signal and the background become similar, the likelihood cut removes more signal events resulting in a drop in efficiency and therefore in sensitivity. This decreased sensitivity at the $[m_{\mathrm{H}^{\pm}}, m_{\mathrm{A}}]$ diagonal is clearly visible in Figure 10(a). On the other hand, the rate of the fermionic events decreases in 2HDM(I) by the distance from the diagonal and by $\tan\beta$, so the fermionic searches also lose their sensitivity.

To further study the behavior of the unexcluded regions, 90%, 95% and 99% CL excluded areas are shown in Figure 12 for different choices of $\tan\beta$. At the 90% CL, the small unexcluded islands at m_{A}=12−15 GeV disappear and the observed limit (as expected) is set at the transition region discussed in the previous paragraph.

Due to the excess of events in the $\mathrm{H}^{+}\mathrm{H}^{-}\to\mathrm{AW}^{+*}\mathrm{AW}^{-*}$ searches in the year 1999 data, the observed limit is lower than the expectation in all regions where the $\mathrm{H}^{\pm}\to\mathrm{AW}^{\pm *}$ decay dominates.

Finally our results are presented independent of $\tan\beta$ in Figure 13, and the limits on the charged Higgs-boson mass are summarized in Table 9. The absolute lower limit on the charged Higgs-boson mass is 56.5 GeV for $\tan\beta\leq 100$ and 12 GeV $\leq m_{\mathrm{A}}\leq m_{\mathrm{H}^{\pm}}$, which should be compared to an expectation of 71.0 GeV. The observed limit is set by $\tan\beta$=3.5,

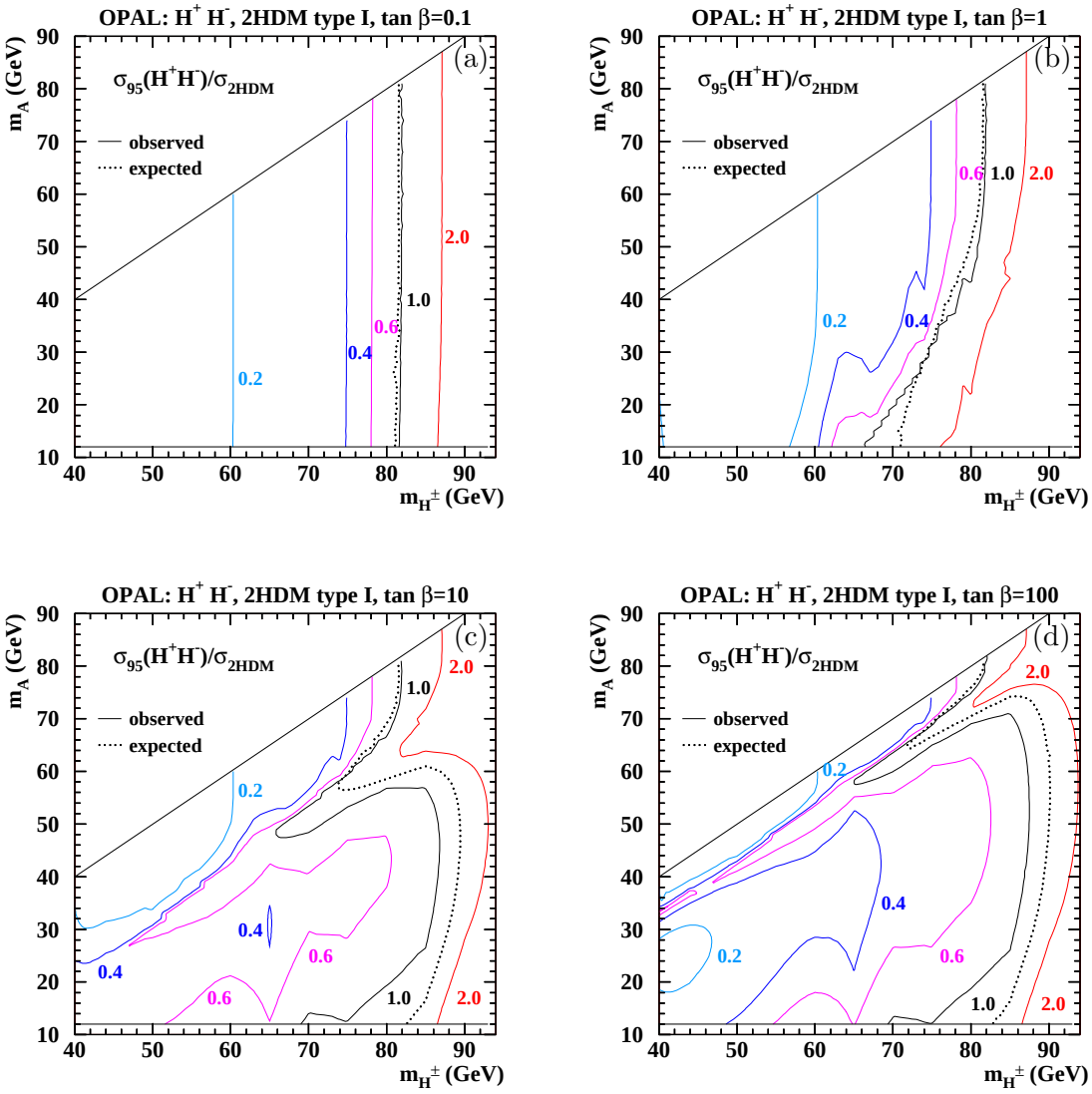

Figure 11: *The 95% CL upper limits on the production cross section in 2HDM(I) relative to the theoretical prediction on the* $[m_{\mathrm{H}^\pm}, m_{\mathrm{A}}]$ *plane for different choices of* $\tan\beta$*: (a) 0.1, (b) 1.0, (c) 10.0 and (d) 100.0. The plotted curves are isolines along which the limit is equal to the number indicated.*

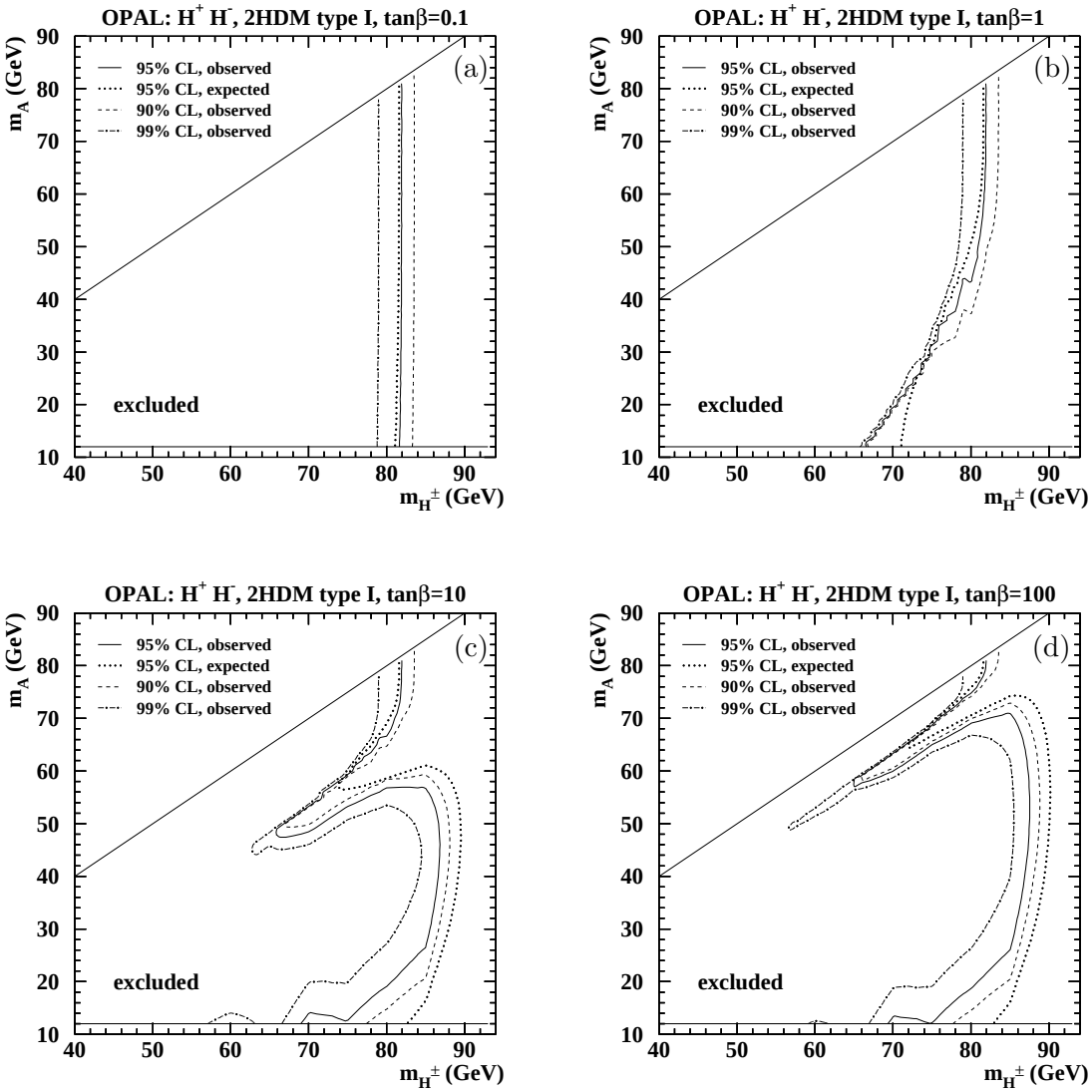

Figure 12: *Excluded areas at 90%, 95% and 99% CL on the* $[m_{\mathrm{H}^\pm}, m_{\mathrm{A}}]$ *plane in 2HDM(I) for different choices of* $\tan\beta$*: (a) 0.1, (b) 1.0, (c) 10.0 and (d) 100.0.*

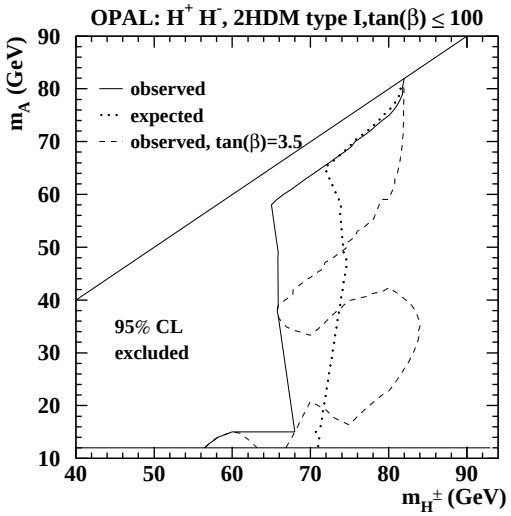

Figure 13: *Excluded areas in 2HDM(I) on the* $[m_{\mathrm{H}^\pm}, m_{\mathrm{A}}]$ *plane independent of* $\tan\beta$ *at 95% CL. The weakest overall mass limit is defined by the* $\tan\beta$*=3.5 exclusion, which is also shown.*

where a small unexcluded island is present around $m_{\mathrm{H}^\pm}\approx$60 GeV and $m_{\mathrm{A}}\approx$12 GeV (also shown on Figure 13). This unexcluded island is no longer present at 90% CL where the mass limit improves to 66.8 GeV.

For $m_{\mathrm{A}}>$15 GeV, the $\tan\beta$-independent lower limit on the charged Higgs-boson mass at 95% CL is 64.8 GeV with 71.0 GeV expected. Both the observed and expected limits are found in the transition region where the bosonic and fermionic channels have comparable sensitivities. The 6 GeV difference is due to the excess observed in the $\mathrm{H}^+\mathrm{H}^-\to\mathrm{AW}^{+*}\mathrm{AW}^{-*}$ search. On the $(m_{\mathrm{H}^\pm}, m_{\mathrm{A}})$ diagonal, the $\mathrm{H}^\pm\to\mathrm{AW}^{\pm*}$ decay becomes kinematically suppressed, and the 2HDM(II) result for $\mathrm{BR}(\mathrm{H}^\pm\to\tau\nu_\tau)$=0.65 of 81.6 GeV (see Figure 8 and Table 8) is reproduced.

7 Summary

A search is performed for the pair production of charged Higgs bosons in electron-positron collisions at LEP2, considering the decays $\mathrm{H}^\pm\to\tau\nu_\tau$, $\mathrm{q\bar{q}}$ and $\mathrm{AW}^{\pm*}$. No signal is observed. The results are interpreted in the framework of Two-Higgs-Doublet Models.

In 2HDM(II), required by the minimal supersymmetric extension of the SM, charged Higgs bosons are excluded up to a mass of 76.6 GeV (with an expected limit of 76.8 GeV) when $\mathrm{BR}(\mathrm{H}^\pm\to\tau\nu_\tau) + \mathrm{BR}(\mathrm{H}^\pm\to\mathrm{q\bar{q}}) = 1$ is assumed. See Figure 8 and Table 8 for $\mathrm{BR}(\mathrm{H}^\pm\to\tau\nu_\tau)$-dependent limits.

In the more exotic 2HDM(I), where fermionic decays can be suppressed and $\mathrm{H}^\pm\to\mathrm{AW}^{\pm*}$ can become dominant, a $\tan\beta$-independent lower mass limit of 56.5 GeV is observed for $m_{\mathrm{A}}>$ 12 GeV (with an expected limit of 71.0 GeV) due to a non-signal-like excess observed at $\sqrt{s}$=192−202 GeV in the $\mathrm{H}^+\mathrm{H}^-\to\mathrm{AW}^{+*}\mathrm{AW}^{-*}$ search, discussed in Section 4. For $m_{\mathrm{A}}>$ 15 GeV, the observed limit improves to $m_{\mathrm{H}^\pm}>$ 64.8 GeV (with an expected limit of 71.0 GeV). Figure 13 shows the excluded areas in the $[m_{\mathrm{H}^\pm}, m_{\mathrm{A}}]$ plane and Table 9 reports selected numerical results.

$\tan\beta$	m_{A}	limit on $m_{\mathrm{H}^{\pm}}$ (GeV)	
		observed	expected
≤ 100	12 GeV$\leq m_{\mathrm{A}} \leq m_{\mathrm{H}^{\pm}}$	56.5 (3.5)	71.0 (1.0)
	m_{A}=12 GeV	56.5 (3.5)	71.0 (1.0)
	$m_{\mathrm{A}}=m_{\mathrm{H}^{\pm}}/2$	66.0 (3.5)	73.5 (1.5)
	$m_{\mathrm{A}} \geq m_{\mathrm{H}^{\pm}} - 10$ GeV	64.8 (100)	71.7 (100)
	$m_{\mathrm{A}} \geq m_{\mathrm{H}^{\pm}} - 5$ GeV	80.5 (100)	78.0 (100)
0.1	12 GeV$\leq m_{\mathrm{A}} \leq m_{\mathrm{H}^{\pm}}$	81.6	81.1
	m_{A}=12 GeV	81.6	81.1
	$m_{\mathrm{A}}=m_{\mathrm{H}^{\pm}}/2$	81.8	81.5
	$m_{\mathrm{A}} \geq m_{\mathrm{H}^{\pm}} - 10$ GeV	81.9	81.6
	$m_{\mathrm{A}} \geq m_{\mathrm{H}^{\pm}} - 5$ GeV	81.9	81.6
1	12 GeV$\leq m_{\mathrm{A}} \leq m_{\mathrm{H}^{\pm}}$	66.4	71.0
	m_{A}=12 GeV	66.4	71.0
	$m_{\mathrm{A}}=m_{\mathrm{H}^{\pm}}/2$	78.3	76.6
	$m_{\mathrm{A}} \geq m_{\mathrm{H}^{\pm}} - 10$ GeV	81.9	81.5
	$m_{\mathrm{A}} \geq m_{\mathrm{H}^{\pm}} - 5$ GeV	81.9	81.6
10	12 GeV$\leq m_{\mathrm{A}} \leq m_{\mathrm{H}^{\pm}}$	65.8	73.9
	m_{A}=12 GeV	69.0	82.5
	$m_{\mathrm{A}}=m_{\mathrm{H}^{\pm}}/2$	86.7	89.8
	$m_{\mathrm{A}} \geq m_{\mathrm{H}^{\pm}} - 10$ GeV	81.5	80.4
	$m_{\mathrm{A}} \geq m_{\mathrm{H}^{\pm}} - 5$ GeV	81.9	81.5
100	12 GeV$\leq m_{\mathrm{A}} \leq m_{\mathrm{H}^{\pm}}$	64.8	71.7
	m_{A}=12 GeV	69.3	82.7
	$m_{\mathrm{A}}=m_{\mathrm{H}^{\pm}}/2$	87.1	89.9
	$m_{\mathrm{A}} \geq m_{\mathrm{H}^{\pm}} - 10$ GeV	64.8	71.7
	$m_{\mathrm{A}} \geq m_{\mathrm{H}^{\pm}} - 5$ GeV	80.5	78.0

Table 9: *Lower mass limits for the charged Higgs boson in 2HDM(I). For the* $\tan\beta \leq 100$ *results, the* $\tan\beta$ *value at which the limit is set is indicated in parenthesis. For any* $\tan\beta$ *value, an extrapolation of the exclusion limits to* $m_{\mathrm{H}^{\pm}}=m_{\mathrm{A}}$ *gives the result quoted in Table 8 for* $\mathrm{BR}(\mathrm{H}^{\pm}\rightarrow\tau\nu_{\tau})=0.65$.

Acknowledgements

We particularly wish to thank the SL Division for the efficient operation of the LEP accelerator at all energies and for their close cooperation with our experimental group. In addition to the support staff at our own institutions we are pleased to acknowledge the
Department of Energy, USA,
National Science Foundation, USA,
Particle Physics and Astronomy Research Council, UK,
Natural Sciences and Engineering Research Council, Canada,
Israel Science Foundation, administered by the Israel Academy of Science and Humanities,
Benoziyo Center for High Energy Physics,
Japanese Ministry of Education, Culture, Sports, Science and Technology (MEXT) and a grant under the MEXT International Science Research Program,
Japanese Society for the Promotion of Science (JSPS),
German Israeli Bi-national Science Foundation (GIF),
Bundesministerium für Bildung und Forschung, Germany,
National Research Council of Canada,
Hungarian Foundation for Scientific Research, OTKA T-038240, and T-042864,
The NWO/NATO Fund for Scientific Research, the Netherlands.

References

[1] S. L. Glashow, Nucl. Phys. **22** (1961) 579;
S. Weinberg, Phys. Rev. Lett. **19** (1967) 1264;
A. Salam, *Elementary Particle Theory*, ed. N. Svartholm (Almquist and Wiksells, Stockholm, 1968), 367.

[2] P.W. Higgs, Phys. Lett. **12** (1964) 132;
F. Englert and R. Brout, Phys. Rev. Lett. **13** (1964) 321;
G.S. Guralnik, C.R. Hagen and T.W.B. Kibble, Phys. Rev. Lett. **13** (1964) 585.

[3] J.F. Gunion, H.E. Haber, G.L. Kane and S. Dawson, *The Higgs Hunter's Guide*, Addison–Wesley Publishing Company, Reading, MA, 1990; and references therein.

[4] S.L. Glashow and S. Weinberg, Phys. Rev. **D15** (1977) 1958;
E.A. Paschos, Phys. Rev. **D15** (1977) 1966.

[5] H.E. Haber *et al.*, Nucl. Phys. **B161** (1979) 493.

[6] S. Kanemura, Eur. Phys. J. **C17** (2000) 473.

[7] A. Djouadi, J. Kalinowski and P.M. Zerwas, Z. Phys. **C57** (1993) 569.

[8] A.G. Akeroyd, Nucl. Phys. **B544** (1999) 557;
A.G. Akeroyd, A. Arhrib, E. Naimi, Eur. Phys. J. **C20** (2001) 51.

[9] OPAL Collaboration, K. Ackerstaff *et al.*, Phys. Lett. **B426** (1998) 180.

[10] OPAL Collaboration, G. Abbiendi *et al.*, Eur. Phys. J. **C7** (1999) 407.

[11] ALEPH Collaboration, A. Heister *et al.*, Phys. Lett. **B543** (2002) 1.

[12] DELPHI Collaboration, J. Abdallah *et al.*, Eur. Phys. J. **C34** (2004) 399.

[13] L3 Collaboration, P. Achard *et al.*, Phys. Lett. **B575** (2003) 208.

[14] OPAL Collaboration, K. Ahmet *et al.*, Nucl. Inst. and Meth. **A305** (1991) 275;
B.E. Anderson *et al.*, IEEE Transactions on Nuclear Science **41** (1994) 845;
S. Anderson *et al.*, Nucl. Inst. and Meth. **A403** (1998) 326;
G. Aguillion *et al.*, Nucl. Inst. and Meth. **A417** (1998) 266.

[15] OPAL Collaboration, G. Abbiendi *et al.*, Eur. Phys. J. **C26** (2003) 479.

[16] The HZHA generator: G. Ganis and P. Janot, in *Physics at LEP2*, CERN 96–01, Vol.2, p. 309.

[17] The PYTHIA 5.721 and JETSET 7.408 generators: T. Sjöstrand, Comp. Phys. Comm. **82** (1994) 74; T. Sjöstrand, LU TP 95–20.

[18] The KK2F generator: S. Jadach, B.F.L. Ward and Z. Wąs, Comp. Phys. Comm. **130** (2000) 260;
S. Jadach, B.F. Ward and Z. Wąs, Phys. Lett. **B449** (1999) 97.

[19] The grc4f 1.1 generator: J. Fujimoto *et al.*, Comp. Phys. Comm. **100** (1997) 128;
J. Fujimoto *et al.*, in *Physics at LEP2*, CERN 96–01, Vol.2, p. 30.

[20] The BHWIDE generator: S. Jadach, W. Płaczek and B.F.L. Ward, in *Physics at LEP2*, CERN 96–01, Vol.2, p. 286; UTHEP–95–1001.

[21] The TEEGG generator: D. Karlen, Nucl. Phys. **B289** (1987) 23.

[22] The KORALZ 4.0 generator: S. Jadach, B.F.L. Ward and Z. Wąs, Comp. Phys. Comm. **79** (1994) 503.

[23] The PHOJET 1.05 generator: E. Budinov *et al.*, in *Physics at LEP2*, CERN 96–01, Vol.2, p. 216;
R. Engel and J. Ranft, Phys. Rev. **D54** (1996) 4244.

[24] The HERWIG generator: G. Marchesini *et al.*, Comp. Phys. Comm. **67** (1992) 465.

[25] The Vermaseren generator: J.A.M. Vermaseren, Nucl. Phys. **B229** (1983) 347.

[26] OPAL Collaboration, G. Alexander *et al.*, Z. Phys **C69** (1996) 543.

[27] The EXCALIBUR generator: F.A. Berends, R. Pittau and R. Kleiss, Comp. Phys. Comm. **85** (1995) 437.

[28] S. Jadach, W. Płaczek, M. Skrzypek, B.F.L. Ward and Z. Wąs, Comp. Phys. Comm. **119** (1999) 272.

[29] The KandY generator: S. Jadach, W. Płaczek, M. Skrzypek, B.F.L. Ward, Z. Wąs, Comp. Phys. Comm. **140** (2001) 475.

[30] J. Allison *et al.*, Nucl. Inst. and Meth. **A317** (1992) 47.

[31] OPAL Collaboration, G. Abbiendi *et al.*, Eur. Phys. J. **C32** (2004) 453.

[32] OPAL Collaboration, G. Abbiendi *et al.*, Eur. Phys. J. C **18** (2001) 425.

[33] N. Brown and W.J. Stirling, Phys. Lett. **B252** (1990) 657;
S. Bethke, Z. Kunszt, D. Soper and W.J. Stirling, Nucl. Phys. **B370** (1992) 310;
S. Catani *et al.*, Phys. Lett. **B269** (1991) 432;
N. Brown and W.J. Stirling, Z. Phys. **C53** (1992) 629.

[34] OPAL Collaboration, G. Abbiendi *et al.*, Eur. Phys. J. **C13** (2000) 1.

[35] OPAL Collaboration, G. Abbiendi *et al.*, Eur. Phys. J. **C18** (2001) 447.

[36] M.H. Seymour, Nucl.Phys. **B436** (1995) 163.

[37] Mark J Collaboration, D.P. Barber *et al.*, Phys. Rev. Lett. 43 (1979) 830.

[38] G. Hanson *et al.*, Phys. Rev. Lett. **35** (1975) 1609.

[39] P. Bock, JHEP **01** (2007) 080.
For the weight definition, we use criteria (i) and (ii) in the 2HDM parameter scans and criterion (vii) in calculating model independent results. The generalized version of Eq. (2.9), given in Eq. (6.1), is used to include systematic errors in the event weights. The treatment of correlations between systematic errors is discussed in section 5.1.

[40] OPAL Collaboration, G. Abbiendi *et al.*, Eur. Phys. J. **C52** (2007) 767 (section 3.2.2, point iii).

[41] ALEPH, DELPHI, L3, OPAL and SLD Collborations, LEP Electroweak Working Group, SLD Electroweak and Heavy Flavour Groups, S. Schael *et al.*, Phys. Rep. **427** (2006) 257.

[42] Particle Data Group, C. Amsler *et al.*, Phys. Lett. **B667** (2008) 1.

EUROPEAN ORGANIZATION FOR NUCLEAR RESEARCH

CERN-PH-EP/2008-xxx
September 15, 2008

Search for Charged Higgs Bosons in e^+e^- Collisions at $\sqrt{s} = 189 - 209$ GeV

The OPAL Collaboration

Abstract

A search is made for charged Higgs bosons predicted by Two-Higgs-Doublet extensions of the Standard Model (2HDM) using electron-positron collision data collected by the OPAL experiment at $\sqrt{s} = 189 - 209$ GeV, corresponding to an integrated luminosity of approximately 600 pb^{-1}. Charged Higgs bosons are assumed to be pair-produced and to decay into $q\bar{q}$, $\tau\nu_\tau$ or $AW^{\pm *}$. No signal is observed. Model-independent limits on the charged Higgs-boson production cross section are derived by combining these results with previous searches at lower energies. Excluded areas on the $[m_{H^\pm}, BR(H^\pm \to \tau\nu_\tau)]$ plane are presented assuming $BR(H^\pm \to \tau\nu_\tau) + BR(H^\pm \to q\bar{q}) = 1$. Under the above assumption, motivated by general 2HDM type II models, charged Higgs bosons are excluded up to a mass of 76.6 GeV at 95% confidence level, independent of the branching ratio $BR(H^\pm \to \tau\nu_\tau)$. A scan of the 2HDM type I model parameter space is performed and limits on the Higgs-boson masses $m_{H^\pm}$ and m_A are presented for different choices of $\tan\beta$.

Submitted to Eur. Phys. J. C

The OPAL Collaboration

G. Abbiendi[2], C. Ainsley[5], P.F. Åkesson[7], G. Alexander[21], G. Anagnostou[1], K.J. Anderson[8], S. Asai[22], D. Axen[26], I. Bailey[25], E. Barberio[7,p], T. Barillari[31], R.J. Barlow[15], R.J. Batley[5], P. Bechtle[24], T. Behnke[24], K.W. Bell[19], P.J. Bell[1], G. Bella[21], A. Bellerive[6], G. Benelli[4], S. Bethke[31], O. Biebel[30], O. Boeriu[9], P. Bock[10], M. Boutemeur[30], S. Braibant[2], R.M. Brown[19], H.J. Burckhart[7], S. Campana[4], P. Capiluppi[2], R.K. Carnegie[6], A.A. Carter[12], J.R. Carter[5], C.Y. Chang[16], D.G. Charlton[1], C. Ciocca[2], A. Csilling[28], M. Cuffiani[2], S. Dado[20], M. Dallavalle[2], A. De Roeck[7], E.A. De Wolf[7,s], K. Desch[24], B. Dienes[29], J. Dubbert[30], E. Duchovni[23], G. Duckeck[30], I.P. Duerdoth[15], E. Etzion[21], F. Fabbri[2], P. Ferrari[7], F. Fiedler[30], I. Fleck[9], M. Ford[15], A. Frey[7], P. Gagnon[11], J.W. Gary[4], C. Geich-Gimbel[3], G. Giacomelli[2], P. Giacomelli[2], M. Giunta[4], J. Goldberg[20], E. Gross[23], J. Grunhaus[21], M. Gruwé[7], A. Gupta[8], C. Hajdu[28], M. Hamann[24], G.G. Hanson[4], A. Harel[20], M. Hauschild[7], C.M. Hawkes[1], R. Hawkings[7], G. Herten[9], R.D. Heuer[24], J.C. Hill[5], D. Horváth[28,c], P. Igo-Kemenes[10], K. Ishii[22], H. Jeremie[17], P. Jovanovic[1], T.R. Junk[6,i], J. Kanzaki[22,u], D. Karlen[25], K. Kawagoe[22], T. Kawamoto[22], R.K. Keeler[25], R.G. Kellogg[16], B.W. Kennedy[19], S. Kluth[31], T. Kobayashi[22], M. Kobel[3,t], S. Komamiya[22], T. Krämer[24], A. Krasznahorkay Jr.[29,e], P. Krieger[6,l], J. von Krogh[10], T. Kuhl[24], M. Kupper[23], G.D. Lafferty[15], H. Landsman[20], D. Lanske[13], D. Lellouch[23], J. Letts[o], L. Levinson[23], J. Lillich[9], S.L. Lloyd[12], F.K. Loebinger[15], J. Lu[26,b], A. Ludwig[3,t], J. Ludwig[9], W. Mader[3,t], S. Marcellini[2], A.J. Martin[12], T. Mashimo[22], P. Mättig[m], J. McKenna[26], R.A. McPherson[25], F. Meijers[7], W. Menges[24], F.S. Merritt[8], H. Mes[6,a], N. Meyer[24], A. Michelini[2], S. Mihara[22], G. Mikenberg[23], D.J. Miller[14], W. Mohr[9], T. Mori[22], A. Mutter[9], K. Nagai[12], I. Nakamura[22,v], H. Nanjo[22], H.A. Neal[32], S.W. O'Neale[1,*], A. Oh[7], A. Okpara[10], M.J. Oreglia[8], S. Orito[22,*], C. Pahl[31], G. Pásztor[4,g], J.R. Pater[15], J.E. Pilcher[8], J. Pinfold[27], D.E. Plane[7], O. Pooth[13], M. Przybycień[7,n], A. Quadt[31], K. Rabbertz[7,r], C. Rembser[7], P. Renkel[23], J.M. Roney[25], A.M. Rossi[2], Y. Rozen[20], K. Runge[9], K. Sachs[6], T. Saeki[22], E.K.G. Sarkisyan[7,j], A.D. Schaile[30], O. Schaile[30], P. Scharff-Hansen[7], J. Schieck[31], T. Schörner-Sadenius[7,z], M. Schröder[7], M. Schumacher[3], R. Seuster[13,f], T.G. Shears[7,h], B.C. Shen[4], P. Sherwood[14], A. Skuja[16], A.M. Smith[7], R. Sobie[25], S. Söldner-Rembold[15], F. Spano[8,x], A. Stahl[13], D. Strom[18], R. Ströhmer[30], S. Tarem[20], M. Tasevsky[7,d], R. Teuscher[8], M.A. Thomson[5], E. Torrence[18], D. Toya[22], I. Trigger[7,w], Z. Trócsányi[29,e], E. Tsur[21], M.F. Turner-Watson[1], I. Ueda[22], B. Ujvári[29,e], C.F. Vollmer[30], P. Vannerem[9], R. Vértesi[29,e], M. Verzocchi[16], H. Voss[7,q], J. Vossebeld[7,h], C.P. Ward[5], D.R. Ward[5], P.M. Watkins[1], A.T. Watson[1], N.K. Watson[1], P.S. Wells[7], T. Wengler[7], N. Wermes[3], G.W. Wilson[15,k], J.A. Wilson[1], G. Wolf[23], T.R. Wyatt[15], S. Yamashita[22], D. Zer-Zion[4], L. Zivkovic[20]

[1]School of Physics and Astronomy, University of Birmingham, Birmingham B15 2TT, UK
[2]Dipartimento di Fisica dell' Università di Bologna and INFN, I-40126 Bologna, Italy
[3]Physikalisches Institut, Universität Bonn, D-53115 Bonn, Germany
[4]Department of Physics, University of California, Riverside CA 92521, USA
[5]Cavendish Laboratory, Cambridge CB3 0HE, UK
[6]Ottawa-Carleton Institute for Physics, Department of Physics, Carleton University, Ottawa, Ontario K1S 5B6, Canada

[7]CERN, European Organisation for Nuclear Research, CH-1211 Geneva 23, Switzerland
[8]Enrico Fermi Institute and Department of Physics, University of Chicago, Chicago IL 60637, USA
[9]Fakultät für Physik, Albert-Ludwigs-Universität Freiburg, D-79104 Freiburg, Germany
[10]Physikalisches Institut, Universität Heidelberg, D-69120 Heidelberg, Germany
[11]Indiana University, Department of Physics, Bloomington IN 47405, USA
[12]Queen Mary and Westfield College, University of London, London E1 4NS, UK
[13]Technische Hochschule Aachen, III Physikalisches Institut, Sommerfeldstrasse 26-28, D-52056 Aachen, Germany
[14]University College London, London WC1E 6BT, UK
[15]School of Physics and Astronomy, Schuster Laboratory, The University of Manchester M13 9PL, UK
[16]Department of Physics, University of Maryland, College Park, MD 20742, USA
[17]Laboratoire de Physique Nucléaire, Université de Montréal, Montréal, Québec H3C 3J7, Canada
[18]University of Oregon, Department of Physics, Eugene OR 97403, USA
[19]Rutherford Appleton Laboratory, Chilton, Didcot, Oxfordshire OX11 0QX, UK
[20]Department of Physics, Technion-Israel Institute of Technology, Haifa 32000, Israel
[21]Department of Physics and Astronomy, Tel Aviv University, Tel Aviv 69978, Israel
[22]International Centre for Elementary Particle Physics and Department of Physics, University of Tokyo, Tokyo 113-0033, and Kobe University, Kobe 657-8501, Japan
[23]Particle Physics Department, Weizmann Institute of Science, Rehovot 76100, Israel
[24]Universität Hamburg/DESY, Institut für Experimentalphysik, Notkestrasse 85, D-22607 Hamburg, Germany
[25]University of Victoria, Department of Physics, P O Box 3055, Victoria BC V8W 3P6, Canada
[26]University of British Columbia, Department of Physics, Vancouver BC V6T 1Z1, Canada
[27]University of Alberta, Department of Physics, Edmonton AB T6G 2J1, Canada
[28]Research Institute for Particle and Nuclear Physics, H-1525 Budapest, P O Box 49, Hungary
[29]Institute of Nuclear Research, H-4001 Debrecen, P O Box 51, Hungary
[30]Ludwig-Maximilians-Universität München, Sektion Physik, Am Coulombwall 1, D-85748 Garching, Germany
[31]Max-Planck-Institute für Physik, Föhringer Ring 6, D-80805 München, Germany
[32]Yale University, Department of Physics, New Haven, CT 06520, USA

[a] and at TRIUMF, Vancouver, Canada V6T 2A3
[b] now at University of Alberta
[c] and Institute of Nuclear Research, Debrecen, Hungary
[d] now at Institute of Physics, Academy of Sciences of the Czech Republic 18221 Prague, Czech Republic
[e] and Department of Experimental Physics, University of Debrecen, Hungary
[f] and MPI München
[g] and Research Institute for Particle and Nuclear Physics, Budapest, Hungary
[h] now at University of Liverpool, Dept of Physics, Liverpool L69 3BX, U.K.
[i] now at Dept. Physics, University of Illinois at Urbana-Champaign, U.S.A.

[j] now at University of Texas at Arlington, Department of Physics, Arlington TX, 76019, U.S.A.
[k] now at University of Kansas, Dept of Physics and Astronomy, Lawrence, KS 66045, U.S.A.
[l] now at University of Toronto, Dept of Physics, Toronto, Canada
[m] current address Bergische Universität, Wuppertal, Germany
[n] now at University of Mining and Metallurgy, Cracow, Poland
[o] now at University of California, San Diego, U.S.A.
[p] now at The University of Melbourne, Victoria, Australia
[q] now at IPHE Université de Lausanne, CH-1015 Lausanne, Switzerland
[r] now at IEKP Universität Karlsruhe, Germany
[s] now at University of Antwerpen, Physics Department,B-2610 Antwerpen, Belgium; supported by Interuniversity Attraction Poles Programme – Belgian Science Policy
[t] now at Technische Universität, Dresden, Germany
[u] and High Energy Accelerator Research Organisation (KEK), Tsukuba, Ibaraki, Japan
[v] now at University of Pennsylvania, Philadelphia, Pennsylvania, USA
[w] now at TRIUMF, Vancouver, Canada
[x] now at Columbia University
[y] now at CERN
[z] now at DESY
[*] Deceased

1 Introduction

In the Standard Model (SM) [1], the electroweak symmetry is broken via the Higgs mechanism [2] generating the masses of elementary particles. This requires the introduction of a complex scalar Higgs-field doublet and implies the existence of a single neutral scalar particle, the Higgs boson. While the SM accurately describes the interactions between elementary particles, it leaves several fundamental questions unanswered. Therefore, it is of great interest to study extended models.

The minimal extension of the SM Higgs sector required, for example, by supersymmetric models contains two Higgs-field doublets [3] resulting in five Higgs bosons: two charged ($H^{\pm}$) and three neutral. If CP-conservation is assumed, the three neutral Higgs bosons are CP-eigenstates: h and H are CP-even and A is CP-odd. Two-Higgs-Doublet Models (2HDMs) are classified according to the Higgs-fermion coupling structure. In type I models (2HDM(I)) [4], all quarks and leptons couple to the same Higgs doublet, while in type II models (2HDM(II)) [5], down-type fermions couple to the first Higgs doublet, and up-type fermions to the second.

Charged Higgs bosons are expected to be pair-produced in the process $e^+e^- \to H^+H^-$ at LEP, the reaction $e^+e^- \to H^{\pm}W^{\mp}$ having a much lower cross section [6]. In 2HDMs, the tree-level cross section [7] for pair production is completely determined by the charged Higgs-boson mass and known SM parameters.

The $H^{\pm}$ branching ratios are model-dependent. In most of the 2HDM(II) parameter space, charged Higgs bosons decay into the heaviest kinematically allowed fermions, namely $\tau\nu_\tau$ and quark pairs[1]. The situation changes in 2HDM(I), where the decay $H^{\pm} \to AW^{\pm *}$ can become

[1] Throughout this paper charge conjugation is implied. For simplicity, the notation $\tau\nu_\tau$ stands for $\tau^+\nu_\tau$ and $\tau^-\bar{\nu}_\tau$ and $q\bar{q}$ for a quark and anti-quark of any flavor.

dominant if the ratio of the vacuum expectation values of the two Higgs-field doublets $\tan\beta \gtrapprox 1$ and the A boson is sufficiently light [8].

In this paper we search for charged Higgs bosons decaying into $q\bar{q}$, $\tau\nu_\tau$ and $AW^{\pm *}$ using the data collected by the OPAL Collaboration in 1998−2000. The results are interpreted within general 2HDM(II) assuming $BR(H^\pm \to \tau\nu_\tau) + BR(H^\pm \to q\bar{q}) = 1$ for the branching ratios and in 2HDM(I) taking into account decays of charged Higgs bosons via $AW^{\pm *}$, as well. Our result is not confined to $q\bar{q}$=$\{c\bar{s}, \bar{c}s\}$ although that is the dominant hadronic decay channel in most of the parameter space.

The previously published OPAL lower limit on the charged Higgs-boson mass, under the assumption of $BR(H^\pm \to \tau\nu_\tau) + BR(H^\pm \to q\bar{q}) = 1$, is $m_{H^\pm} > 59.5$ GeV at 95% confidence level (CL) using data collected at $\sqrt{s} \leq 183$ GeV [9, 10]. Lower bounds of $74.4 - 79.3$ GeV have been reported by the other LEP collaborations [11–13] based on the full LEP2 data set. The DELPHI Collaboration also performed a search for $H^\pm \to AW^{\pm *}$ decay and constrained the charged Higgs-boson mass in 2HDM(I) [12] to be $m_{H^\pm} \geq 76.7$ GeV at 95%CL.

2 Experimental considerations

The OPAL detector is described in [14]. The events are reconstructed from charged-particle tracks and energy deposits (*clusters*) in the electromagnetic and hadron calorimeters. The tracks and clusters must pass a set of quality requirements similar to those used in previous OPAL Higgs-boson searches [15]. In calculating the total visible energies and momenta of events and individual jets, corrections are applied to prevent double-counting of energy in the case of tracks and associated clusters [15].

The data analyzed in this paper were collected in 1998−2000 at center-of-mass energies of $189 - 209$ GeV as given in Table 1. Due to different requirements on the operational state of the OPAL subdetectors, the integrated luminosity of about 600 pb^{-1} differs slightly among search channels.

Year	1998	1999				2000
E_{cm} (GeV)	186−190	190−194	194−198	198−201	201−203	200−209
$<E_{cm}>$ (GeV)	188.6	191.6	195.5	199.5	201.9	206.0
E_{cm}^{MC} (GeV)	189	192	196	200	202	206
$\int \mathcal{L}dt$ (pb^{-1}) (2τ)	183.5	29.3	76.4	76.6	45.5	212.6
$\int \mathcal{L}dt$ (pb^{-1}) ($2j + \tau$, $4j$)	179.6	29.3	76.3	75.9	36.6	217.4
$\int \mathcal{L}dt$ (pb^{-1}) ($8j$, $6j + \ell$, $4j + \tau$)	175.0	28.9	74.8	77.2	36.1	211.1

Table 1: *Data-taking year, center-of-mass energy bins, luminosity-weighted average center-of-mass energies, the energies of signal and background Monte Carlo simulations, and integrated luminosities of the data. The data correspond to total integrated luminosities of 623.9* pb^{-1} *for the two-tau, 615.1* pb^{-1} *for the two-jet plus tau and the four-jet channels and 603.1* pb^{-1} *for the* $H^\pm \to AW^{\pm *}$ *selections.*

In this paper the following final states are sought:
- $H^+H^- \to \tau^+\nu_\tau\tau^-\bar{\nu}_\tau$ (*two-tau final state,* 2τ),
- $H^+H^- \to q\bar{q}\tau\nu_\tau$ (*two-jet plus tau final state,* $2j + \tau$),
- $H^+H^- \to q\bar{q}q\bar{q}$ (*four-jet final state,* $4j$),
- $H^+H^- \to AW^{+*}AW^{-*} \to b\bar{b}q\bar{q}b\bar{b}q\bar{q}$ (*eight-jet final state,* $8j$),

- $H^+H^- \to AW^{+*}AW^{-*} \to b\bar{b}q\bar{q}b\bar{b}\ell\nu_\ell$ (*six-jet plus lepton final state,* $6j + \ell$),
- $H^+H^- \to AW^{\pm *}\tau\nu_\tau \to b\bar{b}q\bar{q}\tau\nu_\tau$ (*four-jet plus tau final state,* $4j + \tau$).

The signal detection efficiencies and accepted background cross sections are estimated using a variety of Monte Carlo samples. The HZHA generator [16] is used to simulate H^+H^- production at fixed values of the charged Higgs-boson mass in steps of $1 - 5$ GeV from the kinematic limit down to 50 GeV for fermionic decays and 40 GeV for bosonic decays.

The background processes are simulated primarily by the following event generators: PYTHIA [17] and KK2F [18] ($Z/\gamma^* \to q\bar{q}(\gamma)$), grc4f [19] (four-fermion processes, 4f), BHWIDE [20] and TEEGG [21] ($e^+e^-(\gamma)$), KORALZ [22] and KK2F ($\mu^+\mu^-(\gamma)$ and $\tau^+\tau^-(\gamma)$), PHOJET [23], HERWIG [24], Vermaseren [25] (hadronic and leptonic two-photon processes).

The generated partons, both for the signal and the SM Monte Carlo simulations, are hadronized using JETSET [17], with parameters described in [26]. For systematic studies, cluster fragmentation implemented in HERWIG for the process $Z/\gamma^* \to q\bar{q}(\gamma)$ is used. The predictions of 4f processes are cross-checked using EXCALIBUR [27], KoralW [28] and KandY [29].

The obtained Monte Carlo samples are processed through a full simulation of the OPAL detector [30]. The event selection is described below.

3 Search for four-fermion final states

In most of the parameter space of 2HDM(II) and with a sufficiently heavy A boson in 2HDM(I), the fermionic decays of the charged Higgs boson dominate and lead to four-fermion final states. The most important decay mode is typically $H^\pm \to \tau\nu_\tau$, with the hadronic mode $H^\pm \to q\bar{q}$ reaching about 40% branching ratio at maximum.

The search for the fully leptonic final state $H^+H^- \to \tau^+\nu_\tau\tau^-\bar{\nu}_\tau$ is described in [31]. The searches for the $H^+H^- \to q\bar{q}\tau\nu_\tau$ and the $H^+H^- \to q\bar{q}q\bar{q}$ events are optimized using Monte Carlo simulation of $H^+ \to c\bar{s}$ decays. The sensitivities to other quark flavors are similar and the possible differences are taken into account as systematic uncertainties. Therefore, our results are valid for any hadronic decay of the charged Higgs boson.

Four-fermion final states originating from H^+H^- production would have very similar kinematic properties to W^+W^- production, which therefore constitutes an irreducible background to our searches, especially when $m_{H^\pm}$ is close to $m_{W^\pm}$. To suppress this difficult SM background, a mass-dependent likelihood selection (similar to the technique described in [32]) is introduced. For each charged Higgs-boson mass tested ($m_{\rm test}$), a specific analysis optimized for a reference mass ($m_{\rm ref}$) close to the hypothesized value is used.

We have chosen a set of reference charged Higgs-boson masses at which signal samples are generated. Around these reference points, mass regions (labeled by $m_{\rm ref}$) are defined with the borders centered between the neighboring points. For each individual mass region, at each center-of-mass energy, we create a separate likelihood selection with the signal histograms built using events generated at $m_{\rm ref}$. The background histograms are composed of the SM processes and are identical for all mass regions.

When testing the hypothesis of a signal with mass $m_{\rm test}$, the background and data rate and discriminant (i.e. the reconstructed Higgs-boson mass) distribution depend on the mass region to which $m_{\rm test}$ belongs. The signal quantities depend on the value of $m_{\rm test}$ itself and are determined as follows. The signal rate and discriminant distribution are computed, with the likelihood selection optimized for $m_{\rm ref}$, for three simulated signal samples with masses $m_{\rm low}$,

$m_{\rm ref}$ and $m_{\rm high}$. Here, $m_{\rm low}$ and $m_{\rm high}$ are the closest mass points to $m_{\rm ref}$ at which signal Monte Carlo samples are generated, with $m_{\rm low} < m_{\rm ref} < m_{\rm high}$. The signal rate and discriminant distribution for $m_{\rm test}$ are then calculated by linear interpolation from the quantities for $m_{\rm low}$ and $m_{\rm ref}$ if $m_{\rm test} < m_{\rm ref}$, or for $m_{\rm ref}$ and $m_{\rm high}$ if $m_{\rm test} > m_{\rm ref}$.

When building the likelihood function three event classes are considered: signal, four-fermion background and two-fermion background. The likelihood output gives the probability that a given event belongs to the signal rather than to one of the two background sources.

3.1 The two-jet plus tau final state

The analysis closely follows our published one at $\sqrt{s}$ = 183 GeV [10]. It proceeds in two steps. First, events consistent with the final state topology of an isolated tau lepton, a pair of hadronic jets and sizable missing energy are preselected and are then processed by a likelihood selection. The sensitivity of the likelihood selection is improved by building mass-dependent discriminant functions as explained above.

Events are selected if their likelihood output ($\mathcal{L}$) is greater than a cut value chosen to maximize the sensitivity of the selection at each simulated charged Higgs-boson mass. Apart from the neighborhood of the $\mathrm{W^+W^-}$ peak, the optimal cut does not depend significantly on the simulated mass and is chosen to be $\mathcal{L} > 0.85$. Around the $\mathrm{W^+W^-}$ peak, it is gradually reduced to 0.6 at the lowest.

At the end of the selection, 331 events are selected in the data sample with 316.9 $\pm$ 3.2 (stat.) $\pm$38.4 (syst.) events expected from SM processes for a test mass of $m_{\mathrm{H^\pm}}$=75 GeV. The sources of systematic uncertainties are discussed below. Four-fermion processes account for more than 99% of the SM background and result in a large peak in the reconstructed mass centered at the $\mathrm{W^\pm}$ mass (with a second peak at the Z mass for test masses of $m_{\mathrm{H^\pm}} > 85$ GeV). The signal detection efficiencies for the various LEP energies are between 25% and 53% for any charged Higgs-boson mass.

The likelihood output and reconstructed di-jet mass distributions for simulated Higgs-boson masses of 60 GeV and 75 GeV are presented in Figures 1(a-d). The reconstructed Higgs-boson mass resolution is $2.0 - 2.5$ GeV [10]. Figure 2(a) gives the mass dependence of the expected number of background and signal events and compares them to the observed number of events at each test mass.

The systematic uncertainties are estimated for several choices of the charged Higgs-boson mass from 50 GeV to 90 GeV at center-of-mass energies of $\sqrt{s}$=189 GeV, 200 GeV and 206 GeV to cover the full LEP2 range. The following sources of uncertainties are considered: limited number of generated Monte Carlo events, statistical and systematic uncertainty on the luminosity measurement, modeling of kinematic variables in the pre- and likelihood selections, tau lepton identification, dependence of the signal detection efficiency on final-state quark flavor, signal selection efficiency interpolation between generated Monte Carlo points, background hadronization model, and four-fermion background model. The contributions from the different sources are summarized in Table 2.

In the limit calculation, the efficiency and background estimates of the $2\mathrm{j} + \tau$ channel are reduced by $0.8-1.7\%$ (depending on the center-of-mass energy) in order to account for accidental vetoes due to accelerator-related backgrounds in the forward detectors.

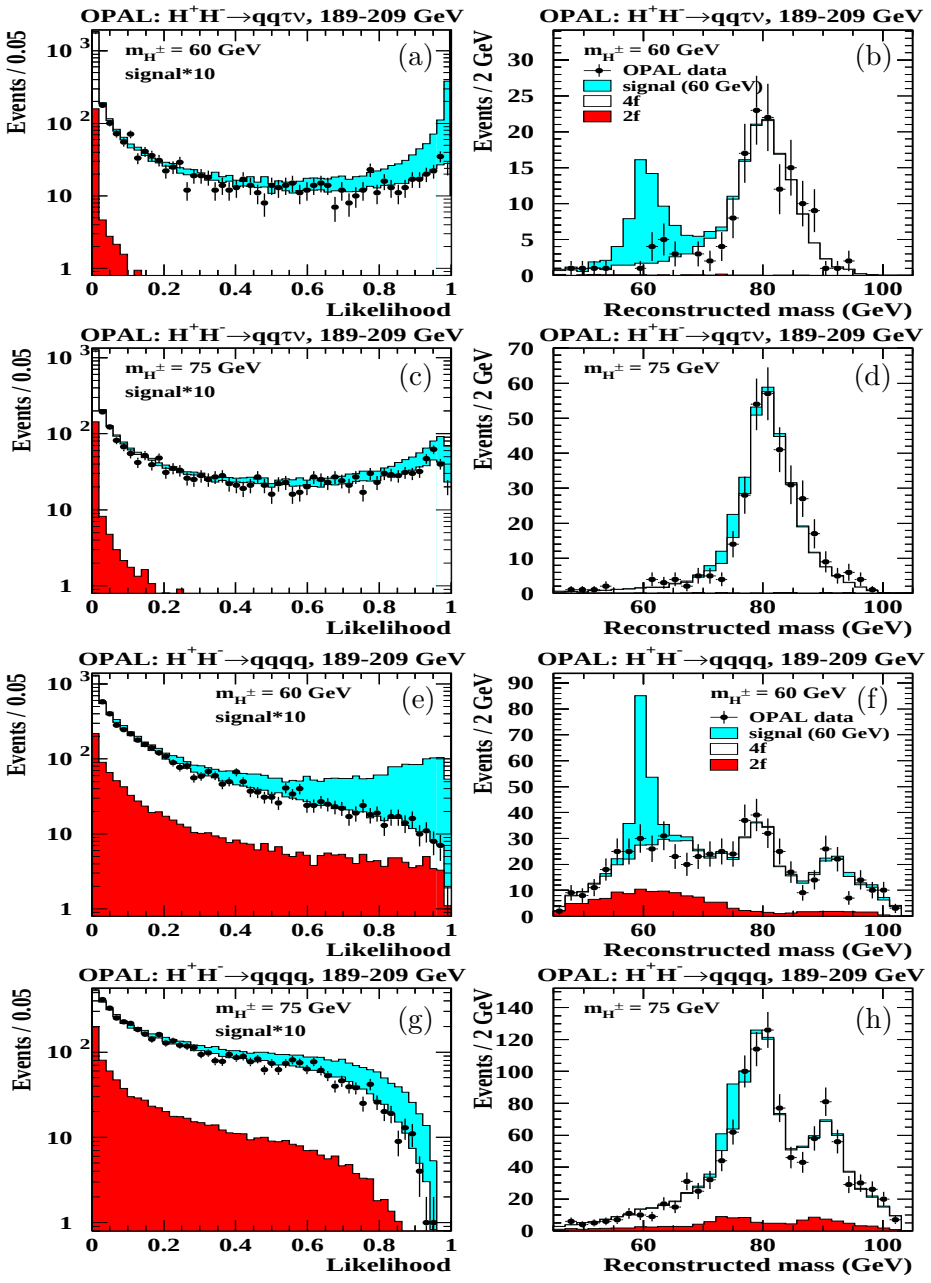

Figure 1: *Likelihood output and reconstructed di-jet mass distributions for the (a-d)* $2\mathrm{j}+\tau$ *and (e-h)* $4\mathrm{j}$ *channels. The distributions are summed up for all center-of-mass energies and correspond to 60 GeV and 75 GeV simulated charged Higgs-boson masses. All Monte Carlo distributions are normalized to the integrated luminosity of the data. When plotting the likelihood output, the signal expectation is scaled up by a factor of 10 for better visibility. A hadronic branching ratio of 0.5 is assumed for the* $2\mathrm{j}+\tau$ *signal, and 1.0 for the* $4\mathrm{j}$ *signal. The reconstructed mass distributions are shown after the likelihood selection.*

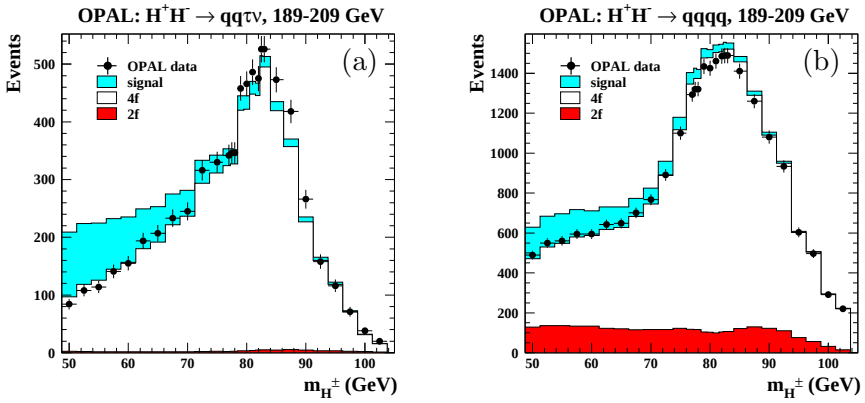

Figure 2: *The number of observed data, expected background and signal events for the (a)* $2\mathrm{j}+\tau$ *and (b)* 4j *channels. The numbers are summed up for all center-of-mass energies and shown as a function of the reference charged Higgs-boson mass. A hadronic branching ratio of 0.5 is assumed for the* $2\mathrm{j}+\tau$ *signal, and 1.0 for the* 4j *signal. Each bin corresponds to a different likelihood selection optimized for the mass at which the dot is centered. Since the same background simulations are used to form the reference histograms and the same data enter the selection, the neighboring points are strongly correlated.*

Source	$2\mathrm{j}+\tau$		4j	
	signal	background	signal	background
MC statistics	3.1−4.6	1.4−4.3	1.6−2.4	0.9−1.9
luminosity	0.3	0.3	0.3	0.3
preselection	1.5−4.7	1.8−7.6	0.3−1.1	0.5−2.2
likelihood selection	0.9−6.5	5.8−22.7	0.7−2.4	2.1−7.5
tau identification	3.0	3.0	N.A.	N.A.
quark flavor	2.7−3.8	N.A.	1.2−6.4	N.A.
interpolation	0.2−0.4	N.A.	0.7−3.7	N.A.
hadronization model	N.A.	1.0−2.7	N.A.	0.7−4.1
4f background model	N.A.	0.3−3.3	N.A.	1.7−3.7

Table 2: *Relative systematic uncertainties on the expected background and signal rates for the* $2\mathrm{j}+\tau$ *and* 4j *final states. The numbers are given in % and depend on the centre-of-mass energy and the reference charged Higgs-boson mass. N.A. stands for not applicable.*

3.2 The four-jet final state

The event selection follows our published analysis at $\sqrt{s}$=183 GeV [10]: first, well-separated four-jet events with large visible energy are preselected; then a set of variables is combined using a likelihood technique. To improve the discriminating power of the likelihood selection, a new reference variable is introduced: the logarithm of the matrix element probability for W^+W^- production averaged over all possible jet-parton assignments computed by EXCALIBUR [27]. Moreover, we introduce mass-dependent likelihood functions as explained above. As the optimal cut value on the likelihood output is not that sensitive to the charged Higgs-boson mass in this search channel, we use the condition $\mathcal{L} > 0.45$ at all center-of-mass energies and for all test masses.

There is a good agreement between the observed data and the SM Monte Carlo expectations at all stages of the selection. After all cuts, 1100 events are selected in the data, while 1117.8 $\pm$ 5.9 (stat.) $\pm$74.4 (syst.) events are expected from SM processes for a test mass of $m_{H^\pm}$=75 GeV. The four-fermion processes account for about 90% of the expected background and result in a large peak centered at the $W^\pm$ mass and a smaller one at the Z boson mass. The signal detection efficiencies are between 41% and 59% for any test mass and center-of-mass energy.

Typical likelihood output and reconstructed di-jet mass distributions of the selected events together with the SM background expectation and signal shapes for simulated charged Higgs-boson masses of 60 GeV and 75 GeV are plotted in Figures 1(e-h). The Higgs-boson mass can be reconstructed with a resolution of $1 - 1.5$ GeV [10]. Figure 2(b) shows the mass dependence of the expected number of background and signal events and compares them to the observed number of events at each test mass. Systematic uncertainties are estimated in the same manner as for the $2j + \tau$ search and are given in Table 2.

4 Search for $AW^{+*}AW^{-*}$ events

In a large part of the 2HDM(I) parameter space, the branching ratio of $H^\pm \to AW^{\pm *}$ dominates. The possible decay modes of the A boson and the $W^{\pm *}$ lead to many possible $H^+H^- \to AW^{+*}AW^{-*}$ event topologies. Above $m_A \approx 12$ GeV, the A boson decays predominantly into a $b\bar{b}$ pair, and thus its detection is based on b-flavor identification. Two possibilities, covering 90% of the decays of two $W^{\pm *}$, are considered: quark pairs from both $W^{\pm *}$ bosons or a quark pair from one and a leptonic final state from the other. The event topologies are therefore "eight jets" or "six jets and a lepton with missing energy", with four jets containing b-flavor in both cases.

The background comes from several Standard Model processes. ZZ and W^+W^- production can result in multi-jet events. While ZZ events can contain true b-flavored jets, W^+W^- events are selected as candidates when c-flavored jets fake b-jets. Radiative QCD corrections to $e^+e^- \to q\bar{q}$ also give a significant contribution to the expected background.

Due to the complexity of the eight-parton final state, it is more efficient to use general event properties and variables designed specifically to discriminate against the main background than a full reconstruction of the event. As a consequence, no attempt is made to reconstruct the charged Higgs-boson mass.

The analysis proceeds in two steps. First a preselection is applied to select b-tagged multi-jet events compatible with the signal hypothesis. Then a likelihood selection (with three event classes: signal, four-fermion background and two-fermion background) is applied.

The preselection of multi-jet events uses the same variables as the search for the hadronic final state in [10] with optimized cut positions. However, it introduces a very powerful new criterion, especially against the W^+W^- background, on a combined b-tagging variable ($\mathcal{B}_{\rm evt}$) requiring the consistency of the event with the presence of b-quark jets.

The neural network method used for b-tagging in the OPAL SM Higgs-boson search [15] is used to calculate on a jet-by-jet basis the discriminating variables $f^i_{\rm c/b}$ and $f^i_{\rm uds/b}$. These are constructed for each jet i as the ratios of probabilities for the jet to be c- or uds-like versus the probability to be b-like. The inputs to the neural network include information about the presence of secondary vertices in a jet, the jet shape, and the presence of leptons with large transverse momentum. The Monte Carlo description of the neural network output was checked with LEP1 data with a jet energy of about 46 GeV. The main background in this search at LEP2 comes from four-fermion processes, in which the mean jet energy is about 50 GeV, very close to the LEP1 jet energy; therefore, an adequate modeling of the data is expected with an event reconstruction assuming four jets.

The $AW^{+*}AW^{-*}$ signal topology depends on the Higgs-boson masses. At $m_{\rm A}{\approx}12$ GeV or $m_{\rm A}{\approx}m_{\rm H^\pm}$, the available energy in the A or $W^{\pm *}$ system is too low to form two clean, collimated jets. At high $m_{\rm H^\pm}$, the boost of the A and $W^{\pm *}$ bosons is small in the laboratory frame and the original eight partons cannot be identified. At low $m_{\rm H^\pm}$, the A and $W^{\pm *}$ bosons might have a boost, but it is still not possible to resolve correctly the two partons from their decay. From these considerations, one can conclude that it is not useful to require eight (or even six) jets in the event, as these jets will not correspond to the original partons. Consequently, to get the best possible modeling of the data, four jets are reconstructed with the Durham jet-finding algorithm [33] before the b-tagger is run.

The flavor-discriminating variables are combined for the four reconstructed jets by

$$\mathcal{B}_{\rm evt} = \frac{1}{1 + \alpha \cdot \prod_i f^i_{\rm c/b} + \beta \cdot \prod_i f^i_{\rm uds/b}} \tag{1}$$

The index i runs over the reconstructed jets ($i = 1, ...4$) and the parameters α and β are numerical coefficients whose optimal values depend on the flavor composition of the signal and background final states. However, since the expected sensitivity of the search is only slightly dependent on the values of α and β, they are fixed at $\alpha = 0.1$ and $\beta = 0.7$. Events are retained if $\mathcal{B}_{\rm evt} > 0.4$.

The preselections of the two event topologies (8j and $6j + \ell$) are very similar. However, in the $6j + \ell$ channel, no kinematic fit is made to the $W^+W^-{\to}q\bar{q}q\bar{q}$ hypothesis and, therefore, no cuts are made on the fit probabilities. No lepton identification is applied; instead the search is based on indirect detection of the associated neutrino by measuring the missing energy.

After the preselection the observed data show an excess over the predicted Monte Carlo background. This can partly be explained by the apparent difference between the gluon splitting rate into $c\bar{c}$ and $b\bar{b}$ pairs in the data and in the background Monte Carlo simulation. The measured rates are $g_{c\bar{c}} = 3.2 \pm 0.21 \pm 0.38\%$ [34] and $g_{b\bar{b}} = 0.307 \pm 0.053 \pm 0.097\%$ [35] from the LEP1 OPAL data. The gluon splitting rates in the Monte Carlo are extracted from $e^+e^-{\to}ZZ{\to}\ell^+\ell^-q\bar{q}$ events and are found to be $g^{\rm MC}_{c\bar{c}} = 1.33 \pm 0.06\%$ and $g^{\rm MC}_{b\bar{b}} = 0.116 \pm 0.0167\%$, averaged over all center-of-mass energies. This mismodeling can be compensated by reweighting the SM Monte Carlo events with gluon splitting to heavy quarks by universal reweighting factors [36] and at the same time deweighting the non-split events to keep the

total numbers of W^+W^-, ZZ and two-fermion background events fixed at generator level. The reweighting factor is 2.41 for $g \to c\bar{c}$ and 2.65 for $g \to b\bar{b}$. This correction results in a background enhancement factor of 1.08 to 1.1 after the preselection, depending on the search channel and the center-of-mass energy, but it does not affect the shape of the background distributions. The numbers of preselected events after the reweighting are given in Table 3.

LEP energy (year)		preselection 8j	preselection 6j + ℓ	exclusive 8j	exclusive 6j + ℓ	overlap
189 GeV	data	238	358	3	24	5
(1998)	background	231.2±2.9	342.2±3.6	2.1±0.3	24.4±1.0	6.3±0.5
192 − 202 GeV	data	297	310	16	16	17
(1999)	background	270.4±2.9	285.0±3.0	13.3±0.7	10.4±0.6	13.4±0.7
200 − 209 GeV	data	265	281	9	8	15
(2000)	background	252.5±3.7	270.5±5.0	13.0±0.9	9.3±0.8	12.9±0.9

Table 3: *Observed data and expected SM background events for each year in the* $AW^{+*}AW^{-*}$ *searches. The* 8j *and* 6j + ℓ *event samples after the preselection step (2nd and 3rd columns) are highly overlapping. After the likelihood selection, the overlapping events are removed from the* 8j *and* 6j + ℓ *samples and form a separate search channel (last three columns). The uncertainty on the background prediction due to the limited number of simulated events is given. The Monte Carlo reweighting to the measured gluon splitting rates is included.*

As a final selection, likelihood functions are built to identify signal events. The reference distributions depend on the LEP energy, but they are constructed to be independent of the considered $(m_{H^\pm}, m_A)$ combination. To this end, we form the signal reference distributions by averaging all simulated H^+H^- samples in the $(m_{H^\pm}, m_A)$ mass range of interest.

Since the selections at $\sqrt{s} = 192 - 209$ GeV are aimed at charged Higgs-boson masses around the expected sensitivity reach of about 80−90 GeV, all masses up to the kinematic limit are included. On the other hand, at $\sqrt{s}$=189 GeV only charged Higgs-boson masses up to 50 GeV are included since the selections at this energy are optimized to reach down to as low as a charged Higgs-boson mass of 40 GeV where the LEP1 exclusion limit lies. The input variables for the 8j final state are: the Durham jet-resolution parameters[2] $\log_{10} y_{34}$ and $\log_{10} y_{56}$, the oblateness [37] event shape variable, the opening angle of the widest jet defined by the size of the cone containing 68% of the total jet energy, the charge-signed cosine of the production angle in the $W^+W^- \to q\bar{q}q\bar{q}$ hypothesis, and the b-tagging variable $\mathcal{B}_{evt}$. At $\sqrt{s}$=189 GeV, $\log_{10} y_{23}$, $\log_{10} y_{45}$, $\log_{10} y_{67}$, and the maximum jet energy are also used. Moreover, the sphericity [38] event shape variable has more discriminating power and thus replaces oblateness. Although the y_{ij} variables are somewhat correlated, they contain additional information: their differences reflect the kinematics of the initial partons.

The input variables for the 6j + ℓ selection are: $\log_{10} y_{34}$, $\log_{10} y_{56}$, the oblateness, the missing energy of the event, and $\mathcal{B}_{evt}$. At $\sqrt{s}$=189 GeV, $\log_{10} y_{23}$, the maximum jet energy and the sphericity are also included.

Events are selected if they pass a lower cut on the likelihood output. This final cut does not remove (especially in the year 1999 data) all the excess events observed after the

[2]Throughout this paper y_{ij} denotes the parameter of the Durham jet finder at which the event classification changes from i-jet to j-jet, where $j = i + 1$.

preselection. The distributions of the critical selection variables, y_{34}, y_{56} and $\mathcal{B}_{\rm evt}$, are plotted on Figure 3 both in background-enriched data samples and after the preselection. To prepare these background-enriched data samples, the preselection cuts on y_{34} and $\mathcal{B}_{\rm evt}$ are dropped, except for the study of the y_{56} variable where we keep the cut on y_{34} in order to select multi-jet events. The resulting samples are completely dominated by background processes. We find systematic differences between the data samples and the equivalent background Monte Carlo simulations at both stages. The observed excess cannot be attributed to a Higgs-boson signal whose contribution is expected to be at most 0.5% in the background-enriched data samples. The interpretation of the excess in terms of a systematic uncertainty on the background prediction will be discussed later.

The non-signal nature of the excess is also demonstrated by Figure 4, which shows the distributions of the likelihood output. The positions of the likelihood cut are indicated by vertical lines.

Because the 8j and the 6j + ℓ selections have several discriminating variables in common, a major overlap between these selections exists. To assure that every event is counted only once, the two samples are redistributed into three: (*i*) events exclusively classified as 8j candidates, (*ii*) events exclusively classified as 6j + ℓ candidates and (*iii*) events accepted by both selections. If an event falls into class (*iii*), the larger likelihood output of the two selections is kept for further processing. The final results using the above classification are quoted in Table 3.

This modified channel definition not only removes the overlap but also increases the efficiency for detecting signal events by considering the cross-channel efficiencies (e.g. the efficiency to select $\rm H^+H^-\to b\bar{b}q\bar{q}b\bar{b}q\bar{q}$ signal by the exclusive 6j + ℓ selection can be as high as 18%, though it is typically only a few %). The efficiencies are determined independently for all simulated $(m_{\rm H^\pm}, m_{\rm A})$ combinations and interpolated to arbitrary $(m_{\rm H^\pm}, m_{\rm A})$ by two-dimensional spline interpolation. The behavior of the selection efficiencies depends strongly on the targeted charged Higgs-boson mass range and also varies with the mass difference $\Delta m = m_{\rm H^\pm} - m_{\rm A}$. In most cases the overlap channel has the highest efficiency. At $\sqrt{s}$=189 GeV and $m_{\rm H^\pm}$=45 GeV, it reaches 32% for the $\rm b\bar{b}q\bar{q}b\bar{b}\ell\nu_\ell$ and 44% for the $\rm H^+H^-\to b\bar{b}q\bar{q}b\bar{b}q\bar{q}$ signal close to the $m_{\rm H^\pm}$=$m_{\rm A}$ diagonal. At $\sqrt{s}$=206 GeV and $m_{\rm H^\pm}$=90 GeV, the overlap efficiency can be as high as 62% for the $\rm b\bar{b}q\bar{q}b\bar{b}\ell\nu_\ell$ and 71% for the $\rm H^+H^-\to b\bar{b}q\bar{q}b\bar{b}q\bar{q}$ signal. The exclusive 6j + ℓ selection has efficiencies typically below 20−30%, while the exclusive 8j selection below 10−15%. Table 4 gives the selection efficiencies at selected $(m_{\rm H^\pm}, m_{\rm A})$ points.

The composition of the background depends on the targeted Higgs-boson mass region. In the low-mass selection ($\sqrt{s}$=189 GeV) that is optimized for $m_{\rm H^\pm}$=40−50 GeV, the Higgs bosons are boosted and therefore the final state is two-jet-like with the largest background contribution coming from two-fermion processes: they account for 52% in the exclusive 8j, 80% in the exclusive 6j + ℓ and 76% in the overlap channel. On the other hand, in the high-mass analysis ($\sqrt{s} = 192 - 209$ GeV) the four-fermion fraction is dominant: it is 69% in the 8j, 56% in the 6j + ℓ and 70% in the overlap channel.

Although our studies show that the observed excess does not lie preferentially in the phase space region where the Higgs-boson signal is expected and that it probably originates from deficiencies of the Monte Carlo description of the jet-resolution parameters y_{ij} and the b-tagging variable $\mathcal{B}_{\rm evt}$, no further correction is applied to the estimated background in the background subtraction procedure of the statistical analysis to calculate exclusion limits. This leads to conservative limits on the production cross section. Therefore, no systematic uncertainty is assigned to the modeling of y_{34} and $\mathcal{B}_{\rm evt}$ at the preselection level. The systematic

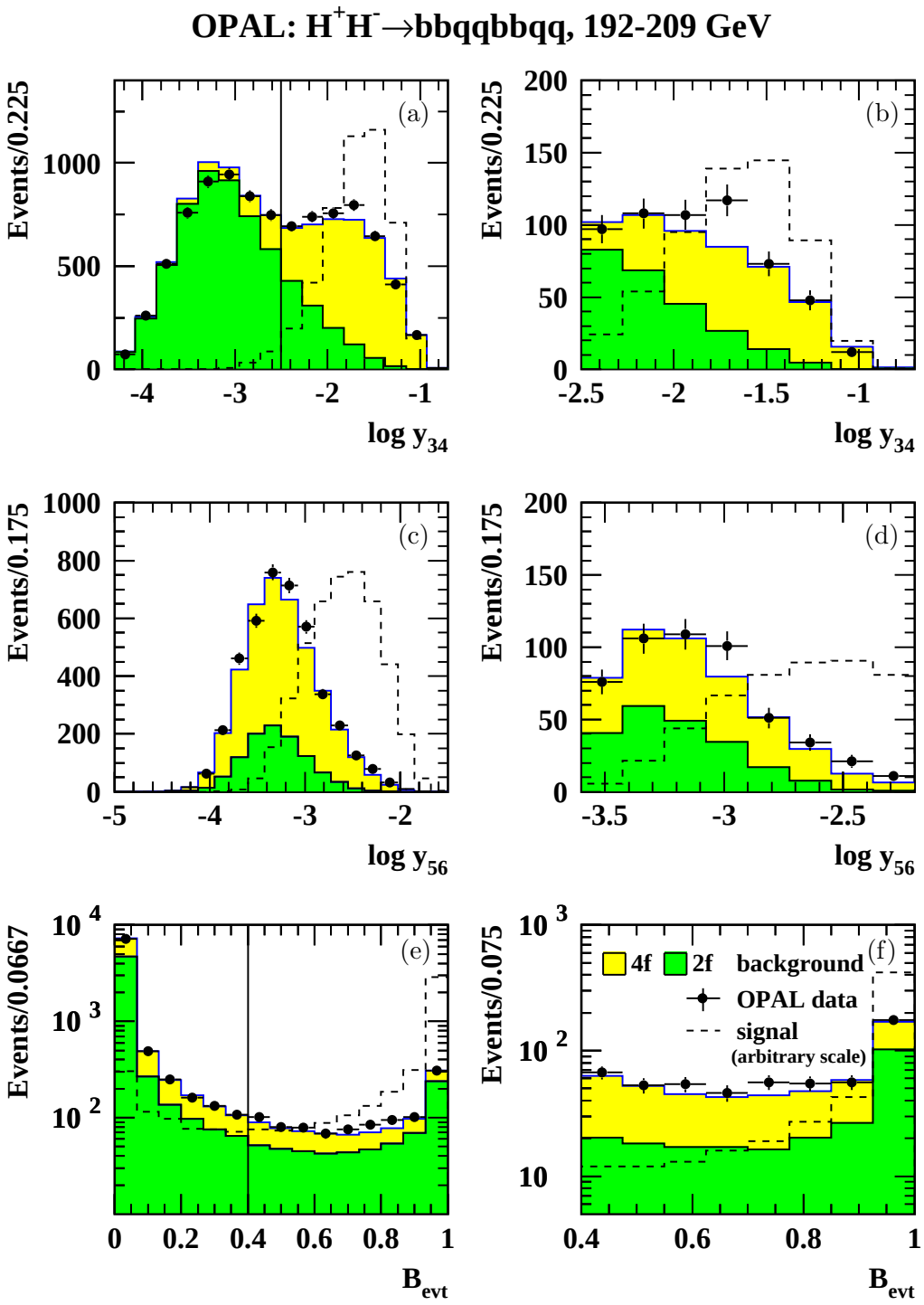

Figure 3: *Most important selection variables: (a-b)* $\log_{10} y_{34}$*, (c-d)* $\log_{10} y_{56}$ *and (e-f)* $\mathcal{B}_{\rm evt}$ *in the* 8j *channel at* $\sqrt{s} = 192 - 209$ *GeV. The distributions are shown (left) in a background-enriched data sample (see text for explanation) and (right) after the full preselection. To form the signal histograms, the Monte Carlo distributions are averaged for all simulated* $(m_{\rm H^{\pm}}, m_{\rm A})$ *mass combinations in the mass range of interest. The Monte Carlo reweighting to the measured gluon splitting rates is included. The expectations from SM processes are normalized to the data luminosity. The preselection cuts on* y_{34} *and* $\mathcal{B}_{\rm evt}$ *are indicated by vertical lines.*

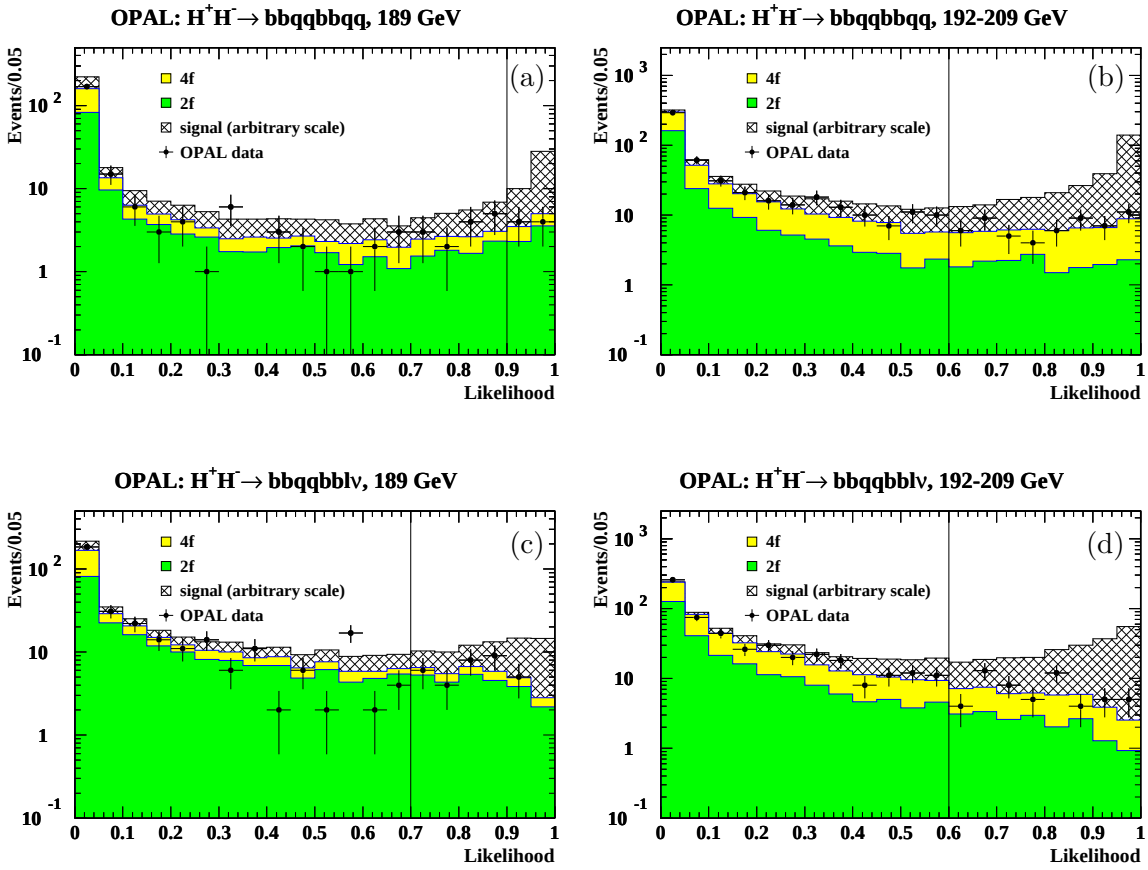

Figure 4: *Likelihood output distributions for the (a-b)* 8j *and (c-d)* $6\mathrm{j}+\ell$ *channels at* $\sqrt{s}$*=189 GeV and* $192-209$ *GeV. To form the signal histograms, the Monte Carlo distributions are averaged for all simulated* $(m_{\mathrm{H}^{\pm}}, m_{\mathrm{A}})$ *mass combinations in the mass range of interest. The Monte Carlo reweighting to the measured gluon splitting rates is included. The expectations from SM processes are normalized to the data luminosity. The lower cuts on the likelihood output are indicated by vertical lines.*

signal	selection	$(m_{\mathrm{H}^\pm}, m_{\mathrm{A}})$ (GeV, GeV)			
		(45,30)	(80,50)	(45,30)	(90,60)
		$\sqrt{s}$=189 GeV		$\sqrt{s}$=206 GeV	
$\mathrm{b\bar{b}q\bar{q}b\bar{b}q\bar{q}}$	8j	4.6	1.0	9.3	12.4
	overlap	41.0	2.8	14.9	69.6
	$6\mathrm{j}+\ell$	17.0	3.6	4.1	3.1
	total	62.6	7.4	28.3	85.0
$\mathrm{b\bar{b}q\bar{q}b\bar{b}}\ell\nu_\ell$	$6\mathrm{j}+\ell$	28.2	6.0	11.6	7.0
	overlap	31.8	3.6	14.2	62.2
	8j	1.8	0.1	2.2	6.1
	total	61.8	9.7	28.0	75.3
$\mathrm{b\bar{b}q\bar{q}}\tau\nu_\tau$	$4\mathrm{j}+\tau$	68.0	0.0	12.3	11.1

Table 4: *Signal selection efficiencies in percent for the* $\mathrm{H}^\pm\to\mathrm{AW}^{\pm *}$ *final states in the different search channels at* $\sqrt{s}$*=189 and 206 GeV at representative* $(m_{\mathrm{H}^\pm}, m_{\mathrm{A}})$ *points.*

uncertainties related to the other preselection variables, estimated from background-enriched data samples, are taken into account. The effect of mismodeling the shapes of the reference distributions in the likelihood selection is estimated for all variables, including y_{ij} and $\mathcal{B}_{\mathrm{evt}}$ and is accounted for in the statistical analysis.

Systematic uncertainties arise also due to the gluon splitting correction: the experimental uncertainty on the gluon splitting rate translates into uncertainties on the total background rates. Moreover, the weighted background counting introduces an uncertainty due to the Monte Carlo statistics of the $\mathrm{g}\to\mathrm{c\bar{c}}$ and $\mathrm{b\bar{b}}$ events.

In summary, the following sources of systematic uncertainties are considered: limited number of simulated signal and background events, modeling of the preselection variables (other than y_{ij} and $\mathcal{B}_{\mathrm{evt}}$), modeling of the shapes of the reference distributions in the likelihood selection and the gluon splitting correction. Uncertainties below the 1% level are neglected. The different contributions are summarized in Table 5.

5 Search for $\mathrm{AW}^{\pm *}\tau\nu_\tau$ events

In some parts of the 2HDM(I) parameter space, both the fermionic $\mathrm{H}^\pm\to\tau\nu_\tau$ and the bosonic $\mathrm{H}^\pm\to\mathrm{AW}^{\pm *}$ decay modes contribute. To cover this transition region parallel to the $(m_{\mathrm{H}^\pm}, m_{\mathrm{A}})$ diagonal, a search for the final state $\mathrm{H}^+\mathrm{H}^-\to\mathrm{AW}^{\pm *}\tau\nu_\tau$ is performed. The transition region is wide for small $\tan\beta$ and narrow for large $\tan\beta$; therefore, this analysis is more relevant for lower values of $\tan\beta$.

Only the hadronic decays of $\mathrm{W}^{\pm *}$ and the decay $\mathrm{A}\to\mathrm{b\bar{b}}$ are considered. Thus the events contain a tau lepton, four jets (two of which are b-flavored) and missing energy. Separating the signal from the $\mathrm{W}^+\mathrm{W}^-$ background becomes difficult close to $m_{\mathrm{H}^\pm}$=$m_{\mathrm{W}^\pm}$.

The preselection is designed to identify hadronic events containing a tau lepton plus significant missing energy and transverse momentum from the undetected neutrino. In most cases it is not practical to reconstruct the four jets originating from the $\mathrm{AW}^{\pm *}$ system. Instead, to suppress the main background from semi-leptonic $\mathrm{W}^+\mathrm{W}^-$ events, we remove the decay

Source	exclusive 8j		exclusive 6j + ℓ		overlap	
	signal	background	signal	background	signal	background
MC statistics	$\geq$15/$\geq$8.5	13.2/6.7	$\geq$5.7/$\geq$8.4	4.0/8.3	$\geq$4.0/$\geq$2.8	7.9/7.1
preselection	1.0	1.0	1.0	2.0	1.0	2.0/1.5
$\mathcal{L}$ selection						
y_{ij}	4.0/1.8	6.0/6.2	2.2/2.6	6.0/8.0	2.8/1.5	5.5/4.9
b-tag	0.0/1.8	4.7/7.0	2.9/1.4	4.4/7.1	1.0/1.3	4.0/5.1
other	1.8/0.7	3.9/3.2	1.0/1.6	3.7/3.5	1.2/0.7	3.4/2.4
gluon splitting						
g$\to$c$\bar{\text{c}}$, exp.	N.A.	0.6/2.5	N.A.	1.6	N.A.	1.4/2.3
g$\to$c$\bar{\text{c}}$, MC	N.A.	0.2/0.8	N.A.	0.6	N.A.	0.5/0.8
g$\to$b$\bar{\text{b}}$, exp.	N.A.	1.4/4.2	N.A.	3.8/4.3	N.A.	5.5/5.4
g$\to$b$\bar{\text{b}}$, MC	N.A.	0.5/1.7	N.A.	1.5/1.7	N.A.	2.2
gluon splitting correction factor	N.A.	1.05/1.18	N.A.	1.13/1.15	N.A.	1.15/1.22

Table 5: *Relative systematic uncertainties in percent for the* $\mathrm{AW}^{+*}\mathrm{AW}^{-*}$ *searches. Where two values are given separated by a "/", the first belongs to the 189 GeV selection and the second to the* $192-209$ *GeV selections. For the signal, the uncertainties due to the limited Monte Carlo statistics are calculated by binomial statistics for a sample size of 500 events and they also depend, via the selection efficiency, on the assumed Higgs-boson masses. N.A. stands for not applicable. The multiplicative gluon splitting correction factors, used to obtain the background-rate estimates as explained in the text, are given in the last line.*

products of the tau candidate and force the remaining hadronic system into two jets by the Durham algorithm. The requirements are then based on the preselection of Section 3.1 with additional preselection cuts on the effective center-of-mass energy, $\log_{10} y_{12}$ and $\log_{10} y_{23}$ of the hadronic system, and the charge-signed $\mathrm{W}^{\pm}$ production angle.

The likelihood selection uses seven variables: the momentum of the tau candidate, the cosine of the angle between the tau momentum and the nearest jet, $\log_{10} y_{12}$ of the hadronic system, the cosine of the angle between the two hadronic jets, the charge-signed cosine of the $\mathrm{W}^{\pm}$ production angle, the invariant mass of the hadronic system, and the b-tagging variable $\mathcal{B}_{\mathrm{evt}}$. Here, $\mathcal{B}_{\mathrm{evt}}$ is defined using the two jets of the hadronic system using Eq. (1) of Section 4, with $i = 1, 2$ and $\alpha = \beta = 1$. To form the signal reference distributions, all simulated $\mathrm{H}^{+}\mathrm{H}^{-}$ samples in the $(m_{\mathrm{H}^{\pm}}, m_{\mathrm{A}})$ mass range of interest are summed up. Since the search at $\sqrt{s} = 192-209$ GeV targets intermediate charged Higgs-boson masses (60−80 GeV), all masses up to the kinematic limit are included. At $\sqrt{s}$=189 GeV, only charged Higgs-boson masses up to 50 GeV are included since the selection is optimized for low charged Higgs-boson masses (40−50 GeV).

The likelihood output distributions are shown in Figure 5. There is an overall agreement between data and background distributions, apart from a small discrepancy at 189 GeV. Events are selected if their likelihood output is larger than 0.9. In total, 15 data events survive the selection at $\sqrt{s} = 192 - 209$ GeV, to be compared with 14.8 ± 0.6 (stat.) ± 1.9 (syst.) events expected from background sources. At $\sqrt{s}$=189 GeV, where the selection is optimized for low Higgs-boson masses, 13 data events are selected with 6.1 ± 0.5 (stat.) ± 1.3 (syst.) events expected. The contribution of four-fermion events, predominantly from semi-leptonic $\mathrm{W}^{+}\mathrm{W}^{-}$ production, amounts to 33% at $\sqrt{s}$=189 GeV and to 90% at $\sqrt{s} = 192 - 209$ GeV.

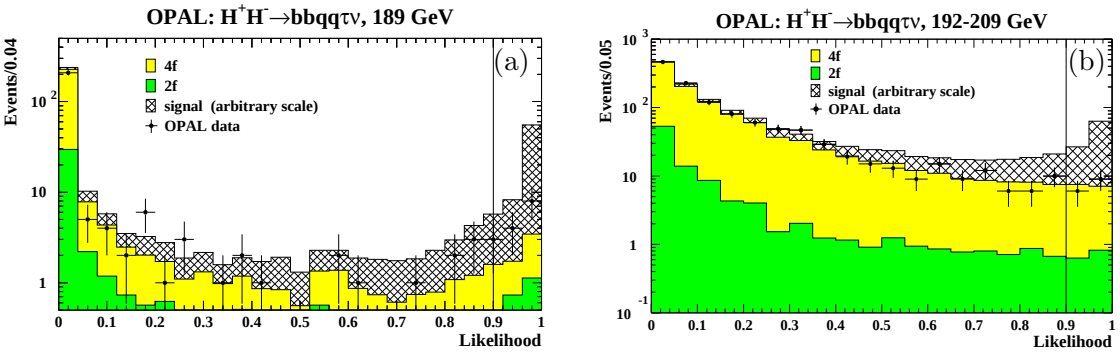

Figure 5: *Likelihood output distribution for the* $4\mathrm{j}+\tau$ *channel at (a)* $\sqrt{s}$*=189 GeV and (b)* $\sqrt{s}$*=*$192-209$ *GeV. To form the signal histograms, the Monte Carlo distributions are averaged for all simulated* $(m_{\mathrm{H}^\pm}, m_{\mathrm{A}})$ *mass combinations in the mass range of interest. The expectations from SM processes are normalized to the data luminosity. The lower cuts on the likelihood output are indicated by vertical line.*

At $\sqrt{s} = 192-209$ GeV, the signal selection efficiency starts at about 5% at $m_{\mathrm{H}^\pm}$=40 GeV, reaches its maximum of about 40% (depending on the mass difference $\Delta m = m_{\mathrm{H}^\pm} - m_{\mathrm{A}}$) at $m_{\mathrm{H}^\pm}$=60 GeV, then decreases to 12% at $m_{\mathrm{H}^\pm}$=90 GeV. In the low-mass selection at $\sqrt{s}$=189 GeV, the efficiency depends strongly on the mass difference: at $m_{\mathrm{H}^\pm}$=40 GeV, it is 22% for $\Delta m = 2$ GeV and 60% for $\Delta m = 10$ GeV. The selection efficiency approaches its maximum at $m_{\mathrm{H}^\pm}$=50 GeV (70% for $\Delta m = 10$ GeV) and then drops to zero at $m_{\mathrm{H}^\pm}$=80 GeV. Table 4 gives selection efficiencies at representative $(m_{\mathrm{H}^\pm}, m_{\mathrm{A}})$ points.

The systematic uncertainties due to the modeling of selection variables are evaluated with the method developed for the $\mathrm{AW}^{+*}\mathrm{AW}^{-*}$ channels and summarized in Table 6.

Source		$4\mathrm{j}+\tau$	
		signal	background
MC statistics		$\geq$2.7/$\geq$4.5	8.2/7.0
preselection: tau ID		0.0	2.3/5.0
	other	0.0/1.0	9.5/7.9
likelihood selection: b-tag		0.3/1.4	2.4/3.0
	other	3.2/2.1	18.4/11.2

Table 6: *Systematic uncertainties in percent for the* $4\mathrm{j}+\tau$ *channel. Where two values are given separated by a "/", the first one belongs to the 189 GeV selection and the second to the* $192-209$ *GeV selections. For the signal, the uncertainties due to the limited Monte Carlo statistics are calculated by binomial statistics for a sample size of 500 events and they also depend, via the selection efficiency, on the assumed Higgs-boson masses.*

6 Interpretation

None of the searches has revealed a signal-like excess over the SM expectation. The results presented here and those published previously [10, 31] by the OPAL Collaboration are combined using the method of [39] to study the compatibility of the observed events with "background-only" and "signal plus background" hypotheses and to derive limits on charged Higgs-boson production. The statistical analysis is based on weighted event counting, with the weights computed from physical observables, also called discriminating variables of the candidate events (see Table 7). Systematic uncertainties with correlations are taken into account in the confidence level (p-value) calculations. To improve the sensitivity of the analysis, they are also incorporated into the weight definition [39].

Channel	$\sqrt{s}$ (GeV)	Discriminant
2τ	183	simple event counting
2τ	189-209	likelihood output
$2\mathrm{j}+\tau$	183-209	reconstructed di-jet mass
4j	183-209	reconstructed di-jet mass
8j	189	simple event counting
8j	192-209	likelihood output
$6\mathrm{j}+\ell$	189	simple event counting
$6\mathrm{j}+\ell$	192-209	likelihood output
$4\mathrm{j}+\tau$	189-209	simple event counting

Table 7: *Discriminating variables entering the statistical analysis for each search topology. Previously published results are also included.*

The results are interpreted in two different scenarios: in the traditional, supersymmetry-favored 2HDM(II) (assuming that there are no new additional light particles other than the Higgs bosons) and in the 2HDM(I) where under certain conditions fermionic couplings are suppressed.

First, we calculate $1-CL_b$, the confidence [39] under the background-only hypothesis, and then proceed to calculate limits on the charged Higgs-boson production cross section in the signal + background hypothesis. These results are used to provide exclusions in the model parameter space, and in particular, on the charged Higgs-boson mass.

2HDM Type II

First a general 2HDM(II) is considered, where $\mathrm{BR}(\mathrm{H}^{\pm}\to\tau\nu_\tau)+\mathrm{BR}(\mathrm{H}^{\pm}\to\mathrm{q\bar{q}})=1$. This model was thoroughly studied at LEP. It is realized in supersymmetric extensions of the SM if no new additional light particles other than the Higgs bosons are present. As our previously published mass limit in such a model is $m_{\mathrm{H}^{\pm}} > 59.5$ GeV [10], only charged Higgs-boson masses above 50 GeV are tested. Cross-section limits for lower masses can be found in [9]. In this model, the results of the 2τ, $2\mathrm{j}+\tau$ and 4j searches enter the statistical combination.

The confidence $1-CL_b$ is plotted for each channel separately in Figure 6(a) and combined in Figure 6(b). Note that $1-CL_b < 0.5$ translates to negative values of sigma (as indicated by the dual y-axis scales in Figure 6(a)) and indicates an excess of events. The largest deviation, a 2.8σ excess observed in the $2\mathrm{j}+\tau$ channel at $m_{\mathrm{H}^{\pm}}$=88 GeV, comes

from a known deficiency [40] of the Monte Carlo simulation of isolated tracks from the fragmentation and hadronization process. When the three final states are combined assuming $\mathrm{BR}(\mathrm{H}^{\pm}\to\tau\nu_\tau) + \mathrm{BR}(\mathrm{H}^{\pm}\to\mathrm{q\bar{q}}) = 1$, no deviation reaches the 2σ level.

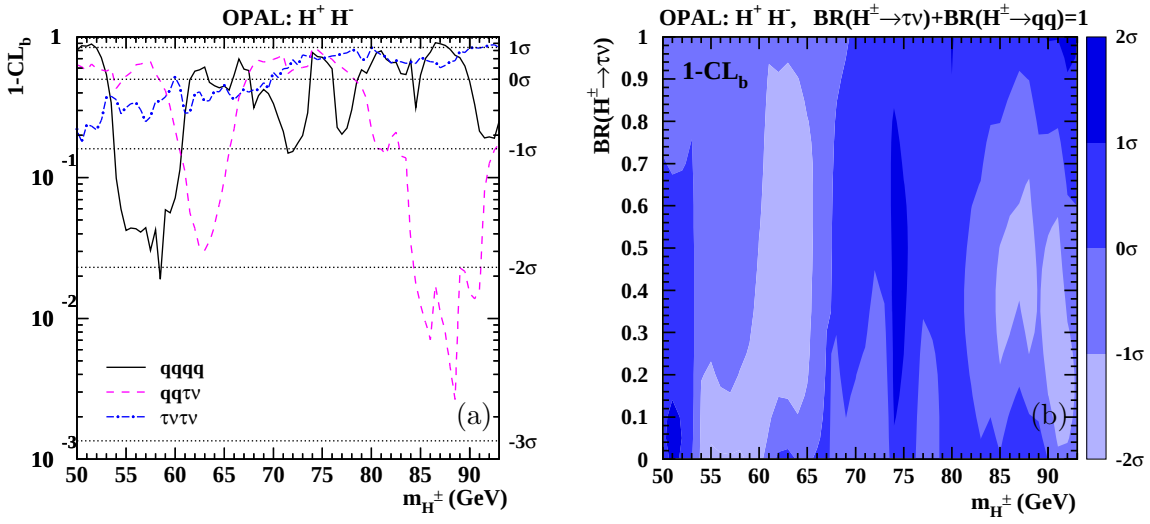

Figure 6: *The observed confidence levels for the background interpretation of the data,* $1 - CL_b$*, (a) for the three different final states as a function of the charged Higgs-boson mass, and (b) for the combined result in 2HDM(II) assuming* $\mathrm{BR}(\mathrm{H}^{\pm}\to\tau\nu_\tau) + \mathrm{BR}(\mathrm{H}^{\pm}\to\mathrm{q\bar{q}}) = 1$ *on the* $[m_{\mathrm{H}^{\pm}}, \mathrm{BR}(\mathrm{H}^{\pm}\to\tau\nu_\tau)]$ *plane. The significance values corresponding to the different shadings are shown by the bar at the right.*

The results are used to set upper bounds on the charged Higgs-boson pair production cross section relative to the 2HDM prediction as calculated by HZHA. The limits obtained are shown for each channel separately in Figures 7(a-c) and combined in Figure 7(d). The combined results are shown by "isolines" along which $\sigma_{95}(\mathrm{H}^{+}\mathrm{H}^{-})/\sigma_{\mathrm{2HDM}}$, the ratio of the limit on the production cross section and the 2HDM cross-section prediction, is equal to the number indicated next to the curves.

Excluded areas on the $[m_{\mathrm{H}^{\pm}}, \mathrm{BR}(\mathrm{H}^{\pm}\to\tau\nu_\tau)]$ plane are presented for each channel separately in Figure 8(a) and combined in Figure 8(b). The expected mass limit from simulated background experiments, assuming no signal, is also shown. For the combined results, the 90% and 99% CL contours are also given. Charged Higgs bosons are excluded up to a mass of 76.6 GeV at 95% CL, independent of $\mathrm{BR}(\mathrm{H}^{\pm}\to\tau\nu_\tau)$. Lower mass limits for different values of $\mathrm{BR}(\mathrm{H}^{\pm}\to\tau\nu_\tau)$ are presented in Table 8.

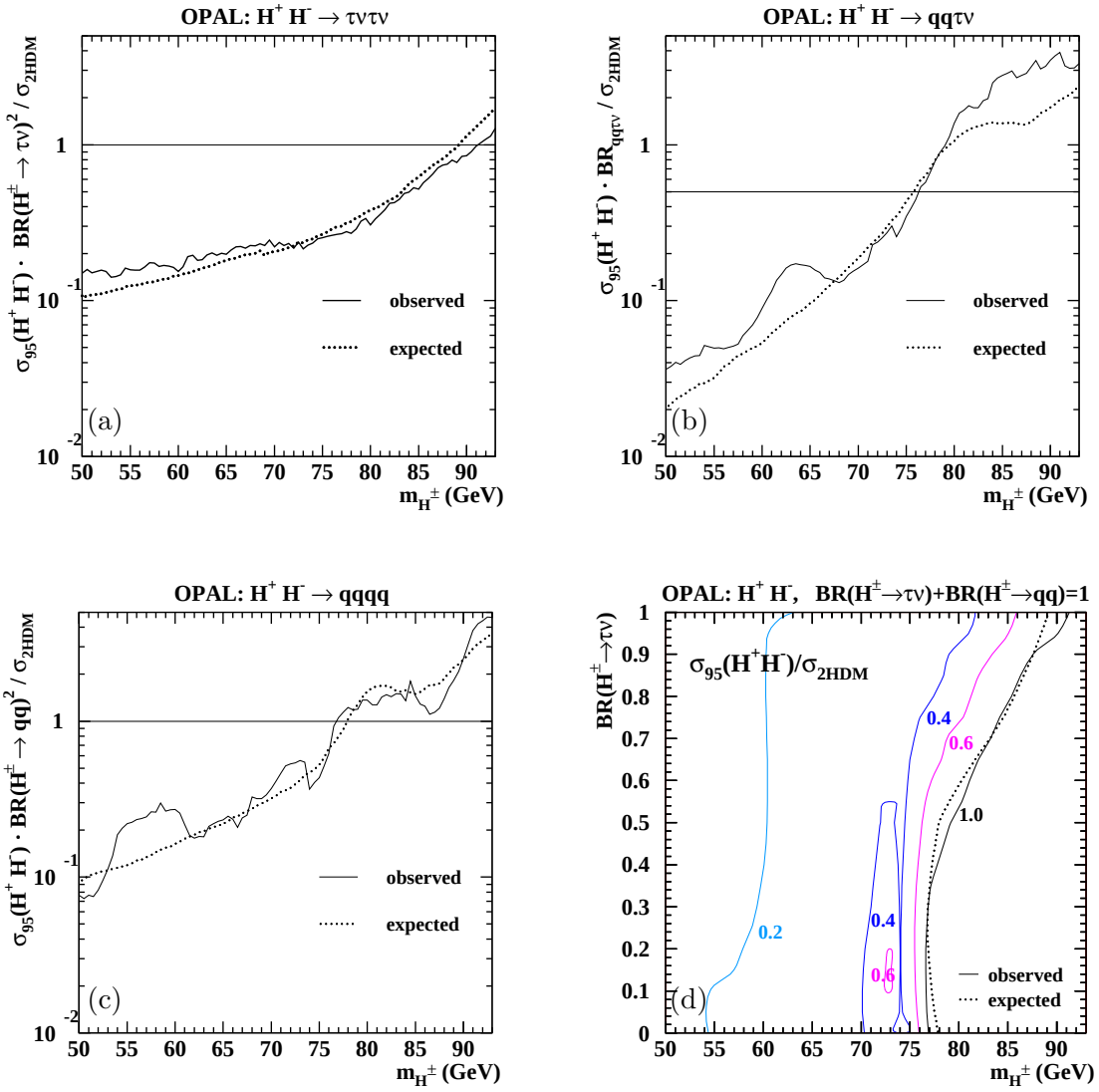

Figure 7: *Observed and expected 95% CL upper limits on the* $\mathrm{H^+H^-}$ *production cross section times the relevant* $\mathrm{H^\pm}$ *decay branching ratios relative to the theoretical prediction for the (a)* $\tau\nu_\tau\tau\nu_\tau$ *(b)* $\mathrm{q\bar{q}}\tau\nu_\tau$ *and (c)* $\mathrm{q\bar{q}q\bar{q}}$ *channels. The horizontal lines indicate the maximum possible branching ratios for a given channel. In (b),* $\mathrm{BR_{qq\tau\nu}} = 2 \cdot \mathrm{BR(H^\pm\to\tau\nu_\tau)} \cdot \mathrm{BR(H^\pm\to q\bar{q})}$. *(d) Upper limits on the production cross section relative to the 2HDM prediction on the* $[m_{\mathrm{H^\pm}}, \mathrm{BR(H^\pm\to\tau\nu_\tau)}]$ *plane in 2HDM(II) assuming* $\mathrm{BR(H^\pm\to\tau\nu_\tau)} + \mathrm{BR(H^\pm\to q\bar{q})} = 1$. *The plotted curves are isolines along which the limit is equal to the number indicated.*

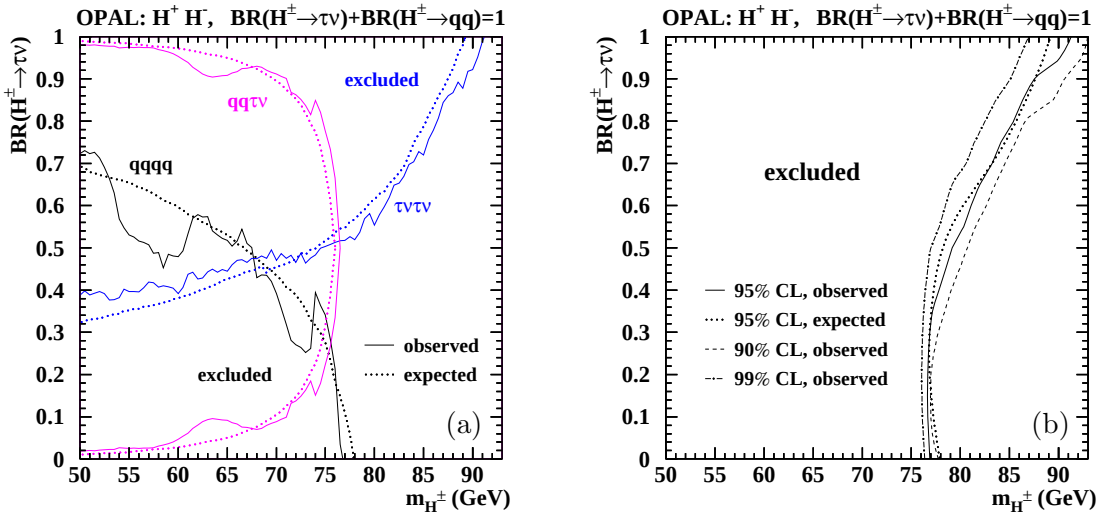

Figure 8: *Observed and expected excluded areas at 95% CL on the* $[m_{\mathrm{H}^\pm}, \mathrm{BR}(\mathrm{H}^\pm \to \tau\nu_\tau)]$ *plane (a) for each search channel separately and (b) combined in 2HDM(II) assuming* $\mathrm{BR}(\mathrm{H}^\pm \to \tau\nu_\tau) + \mathrm{BR}(\mathrm{H}^\pm \to \mathrm{q\bar{q}}) = 1$. *For the combined result, the 90% and 99% CL observed limits are also shown. See Table 8 for numerical values of the combined limit.*

$\mathrm{BR}(\mathrm{H}^\pm \to \tau\nu_\tau)$	Lower mass limit (GeV)	
	Observed	Expected
0	76.9	77.9
0.5	79.2	78.0
0.65	82.0	81.7
1	91.2	89.2
any	76.6 (0.15)	76.8 (0.27)

Table 8: *Observed and expected lower limits at 95% CL on the mass of the charged Higgs boson in 2HDM(II) assuming* $\mathrm{BR}(\mathrm{H}^\pm \to \tau\nu_\tau) + \mathrm{BR}(\mathrm{H}^\pm \to \mathrm{q\bar{q}}) = 1$. *For the results independent of the branching ratio (last line), the* $\mathrm{BR}(\mathrm{H}^\pm \to \tau\nu_\tau)$ *value at which the limit is set, is given in parenthesis.*

2HDM Type I

We present here for the first time an interpretation of the OPAL charged Higgs-boson searches in an alternative theoretical scenario, a 2HDM(I). The novel feature of this model with respect to the more frequently studied 2HDM(II) is that the fermionic decays of the charged Higgs boson can be suppressed. If the A boson is light, the $H^{\pm}\to AW^{\pm *}$ decay may play a crucial role.

The charged Higgs-boson sector in these models is described by three parameters: $m_{H^{\pm}}$, m_A and $\tan\beta$. To test this scenario, the charged Higgs-boson decay branching ratios are calculated by the program of Akeroyd et al. [8], and the model parameters are scanned in the range: 40 GeV $\leq m_{H^{\pm}} \leq$ 94 GeV, 12 GeV $\leq m_A < m_{H^{\pm}}$, $0.1 \leq \tan\beta \leq 100$. Charged Higgs-boson pair production is excluded below 40 GeV by the measurement of the Z boson width [41]. As the A boson detection is based on the identification of b-quark jets, no limits are derived for $m_A < 2m_b$. Below $\tan\beta$=0.1, BR($H^{\pm}\to AW^{\pm *}$) vanishes and the limit is no longer sensitive to m_A.

Both the fermionic (2τ, $2j+\tau$ and 4j) and the bosonic ($4j+\tau$, $6j+\ell$ and 8j) final states play an important role and therefore their results are combined. There is, however, a significant overlap between the events selected by the $H^+H^-\to q\bar{q}q\bar{q}$ and $H^+H^-\to AW^{+*}AW^{-*}$ selections, and the events selected by the $H^+H^-\to q\bar{q}\tau\nu_\tau$ and $H^+H^-\to AW^{\pm *}\tau\nu_\tau$ selections. Therefore, an automatic procedure is implemented to switch off the less sensitive of the overlapping channels, based on the calculation of the expected limit assuming no signal. In general the fermionic channels are used close to the $[m_{H^{\pm}}, m_A]$ diagonal and for low $\tan\beta$, and the searches for $H^{\pm}\to AW^{\pm *}$ are crucial for low values of m_A and high values of $\tan\beta$.

The confidence $1-CL_b$ is calculated combining the $6j+\ell$ and 8j searches assuming SM branching ratios [42] for the $W^{\pm *}$ decay and is shown on Figure 9(a). The largest deviation $1-CL_b = 0.0009$ corresponding to 3.1σ is reached at $m_{H^{\pm}}$=45 GeV and m_A=44.9 GeV (in the middle of the very narrow lightest strip from $m_{H^{\pm}}$=40 GeV to 50 GeV at the $(m_{H^{\pm}}, m_A)$ diagonal). However, the mean background shift on the $[m_{H^{\pm}}, m_A]$ plane amounts only to 1.1σ. $1-CL_b$ for the $4j+\tau$ channel is shown in Figure 9(b). The largest deviation $1-CL_b = 0.013$ corresponding to 2.2σ appears for low charged Higgs-boson masses ($m_{H^{\pm}}$=40 GeV, m_A=21 GeV), reflecting the excess of events in the $\sqrt{s}$=189 GeV search. The mean background shift for this channel is 0.8σ. Note that the results shown in Figures 9(a-b) are model-independent.

When all channels are combined within 2HDM(I), a few hot spots with a significance above 2σ survive. This is illustrated in Figures 9(c-d), where the combined results are plotted for $\tan\beta$=10 and 100. For $\tan\beta$=10, the largest excess $1-CL_b = 0.01$ corresponding to 2.3σ is found at $m_{H^{\pm}}$=55 GeV and m_A=35 GeV (just before switching from the bosonic to the fermionic channels).

As mentioned previously, the $H^{\pm}\to AW^{\pm *}$ decay becomes dominant if the A boson is sufficiently light. The smaller $\tan\beta$ is, the smaller m_A should be. This is clearly seen from the structure of the result on Figures 9(c-d): for $\tan\beta$=10, the bosonic decay becomes dominant at $m_A \lessapprox m_{H^{\pm}} - 18$ GeV, while for $\tan\beta$=100, it dominates already at $m_A \lessapprox m_{H^{\pm}} - 6$ GeV.

The model-independent limits on the charged Higgs-boson production cross section relative to the 2HDM prediction are presented in Figure 10(a) for the $H^+H^-\to AW^{+*}AW^{-*}$ and in Figure 10(b) for $H^+H^-\to AW^{\pm *}\tau\nu_\tau$ searches, with the only assumption that $W^{\pm *}$ decays with SM branching ratios. The results combining all channels using 2HDM(I) branching ratios are shown on Figure 11 for different choices of $\tan\beta$.

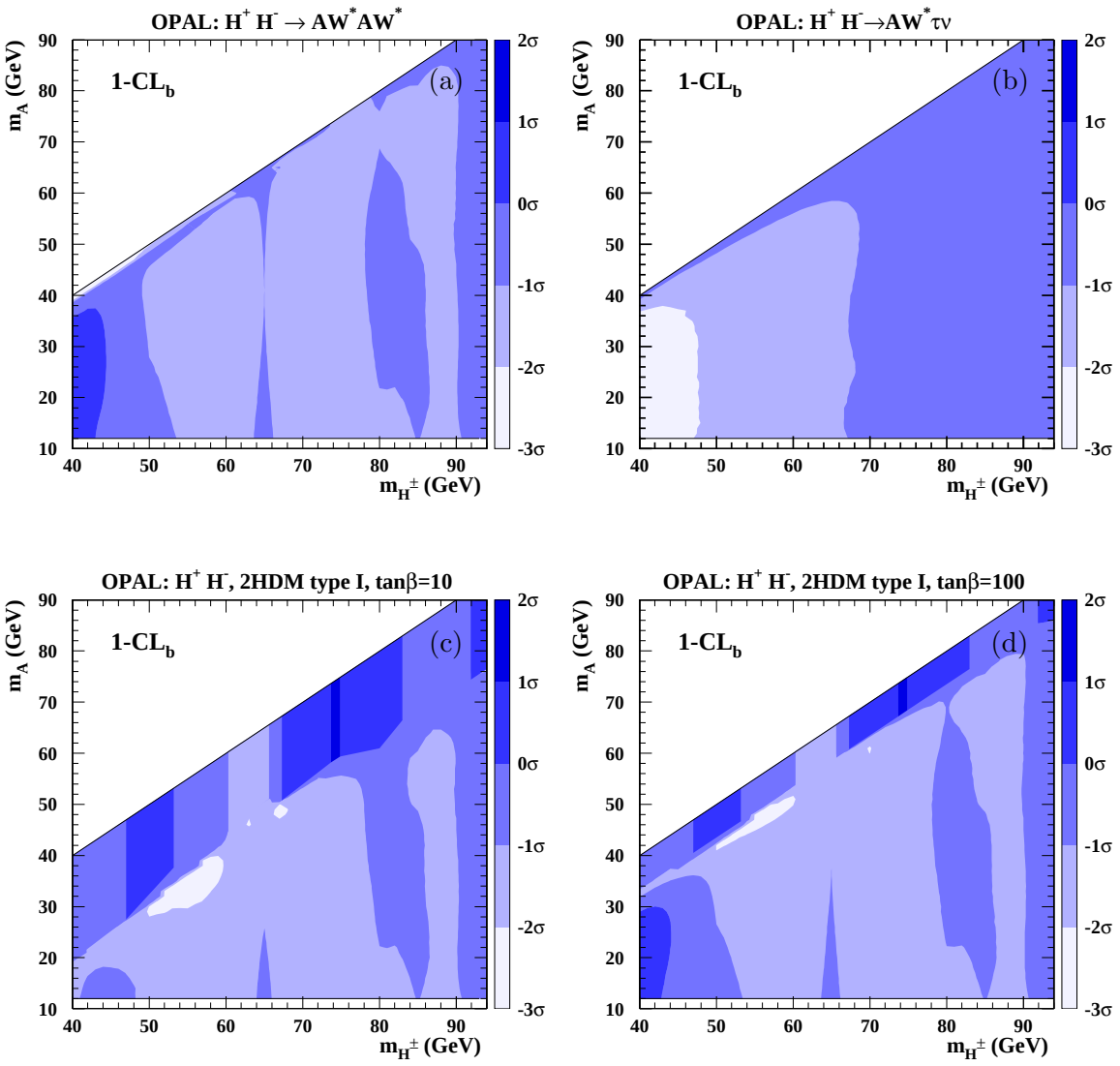

Figure 9: *The confidence* $1 - CL_b$ *on the* $[m_{\mathrm{H}^\pm}, m_{\mathrm{A}}]$ *plane (a) for* $\mathrm{H}^+\mathrm{H}^- \to \mathrm{AW}^{+*}\mathrm{AW}^{-*}$ *combining the results of the* $6\mathrm{j} + \ell$ *and* $8\mathrm{j}$ *searches, and (b) for* $\mathrm{H}^+\mathrm{H}^- \to \mathrm{AW}^{\pm *}\tau\nu_\tau$ *from the* $4\mathrm{j} + \tau$ *search. The combined results in 2HDM(I) for (c)* $\tan\beta$*=10 and (d)* $\tan\beta$*=100 are also shown. The significance values corresponding to the different shadings are shown by the bars at the right.*

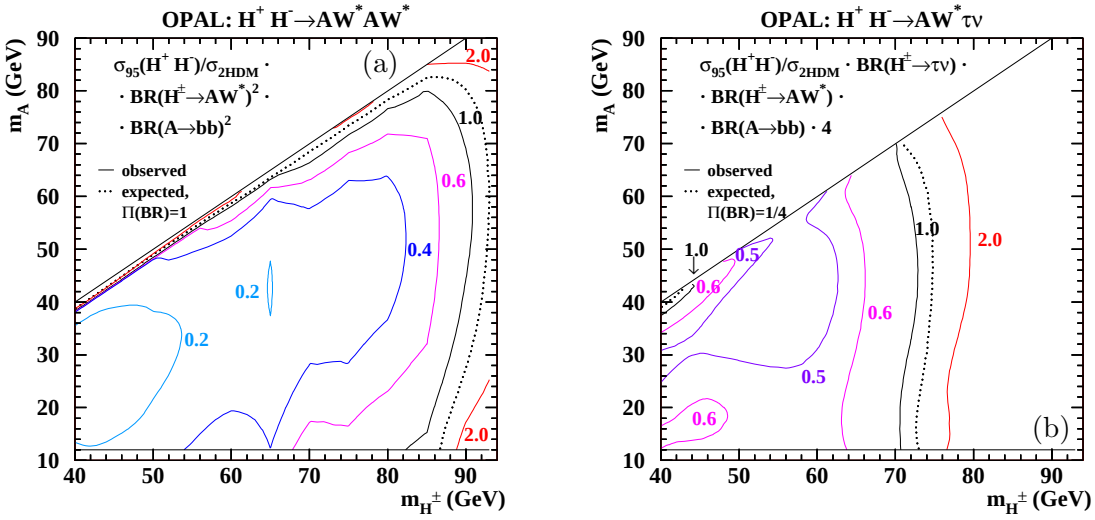

Figure 10: *The 95% CL upper limits on the production cross section times relevant* $\mathrm{H}^{\pm}$ *and A boson decay branching ratios relative to the 2HDM prediction on the* $[m_{\mathrm{H}^{\pm}}, m_{\mathrm{A}}]$ *plane for the process (a)* $\mathrm{H}^{+}\mathrm{H}^{-}\to\mathrm{AW}^{+*}\mathrm{AW}^{-*}$ *and (b)* $\mathrm{H}^{+}\mathrm{H}^{-}\to\mathrm{AW}^{\pm *}\tau\nu_{\tau}$. *The plotted curves are isolines along which the limit is equal to the number indicated. The expected limits are given for (a)* $\mathrm{BR}(\mathrm{H}^{\pm}\to\mathrm{AW}^{\pm *})^{2}\cdot\mathrm{BR}(A\to\mathrm{b\bar{b}})^{2}=1$ *and (b)* $\mathrm{BR}(\mathrm{H}^{\pm}\to\tau\nu_{\tau})\cdot\mathrm{BR}(\mathrm{H}^{\pm}\to\mathrm{AW}^{\pm *})\cdot\mathrm{BR}(A\to\mathrm{b\bar{b}})=0.25$ *corresponding to the maximal value in 2HDM(I).*

For intermediate and large values of $\tan\beta$, an unexcluded region appears parallel to the $[m_{\mathrm{H}^{\pm}}, m_{\mathrm{A}}]$ diagonal both in the observed and expected limits in Figure 11 (see the full and dotted black curves corresponding to a cross-section ratio of 1.0). This can be understood by making two observations: Close to the diagonal, the eight- or six-jet structure of the $\mathrm{H}^{\pm}\to\mathrm{AW}^{\pm *}$ signal events becomes less pronounced and the final state turns four-jet-like. As the selection variables for the signal and the background become similar, the likelihood cut removes more signal events resulting in a drop in efficiency and therefore in sensitivity. This decreased sensitivity at the $[m_{\mathrm{H}^{\pm}}, m_{\mathrm{A}}]$ diagonal is clearly visible in Figure 10(a). On the other hand, the rate of the fermionic events decreases in 2HDM(I) by the distance from the diagonal and by $\tan\beta$, so the fermionic searches also lose their sensitivity.

To further study the behavior of the unexcluded regions, 90%, 95% and 99% CL excluded areas are shown in Figure 12 for different choices of $\tan\beta$. At the 90% CL, the small unexcluded islands at m_{A}=12−15 GeV disappear and the observed limit (as expected) is set at the transition region discussed in the previous paragraph.

Due to the excess of events in the $\mathrm{H}^{+}\mathrm{H}^{-}\to\mathrm{AW}^{+*}\mathrm{AW}^{-*}$ searches in the year 1999 data, the observed limit is lower than the expectation in all regions where the $\mathrm{H}^{\pm}\to\mathrm{AW}^{\pm *}$ decay dominates.

Finally our results are presented independent of $\tan\beta$ in Figure 13, and the limits on the charged Higgs-boson mass are summarized in Table 9. The absolute lower limit on the charged Higgs-boson mass is 56.5 GeV for $\tan\beta\leq 100$ and 12 GeV $\leq m_{\mathrm{A}}\leq m_{\mathrm{H}^{\pm}}$, which should be compared to an expectation of 71.0 GeV. The observed limit is set by $\tan\beta$=3.5,

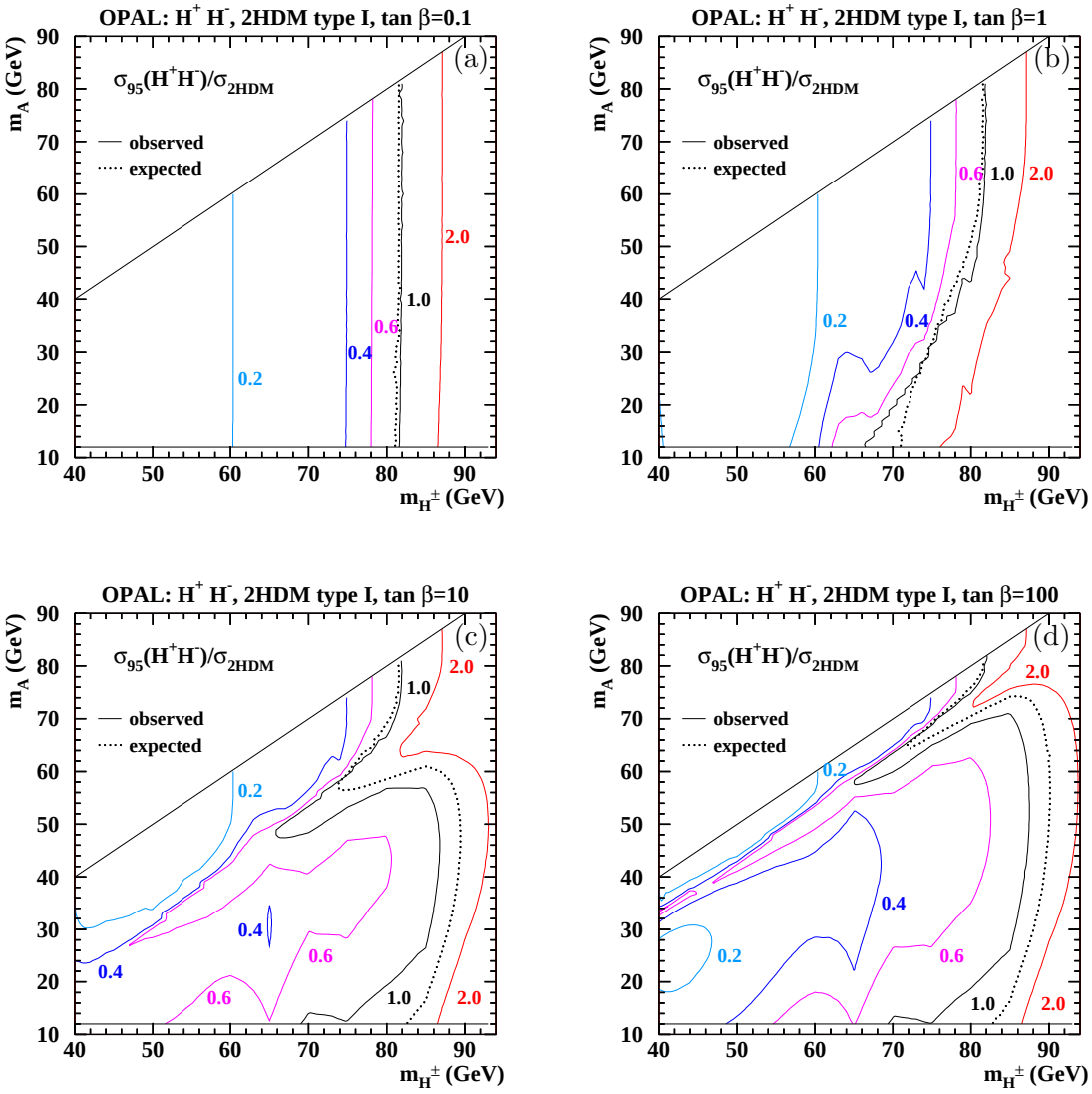

Figure 11: *The 95% CL upper limits on the production cross section in 2HDM(I) relative to the theoretical prediction on the* $[m_{\mathrm{H}^\pm}, m_{\mathrm{A}}]$ *plane for different choices of* $\tan\beta$*: (a) 0.1, (b) 1.0, (c) 10.0 and (d) 100.0. The plotted curves are isolines along which the limit is equal to the number indicated.*

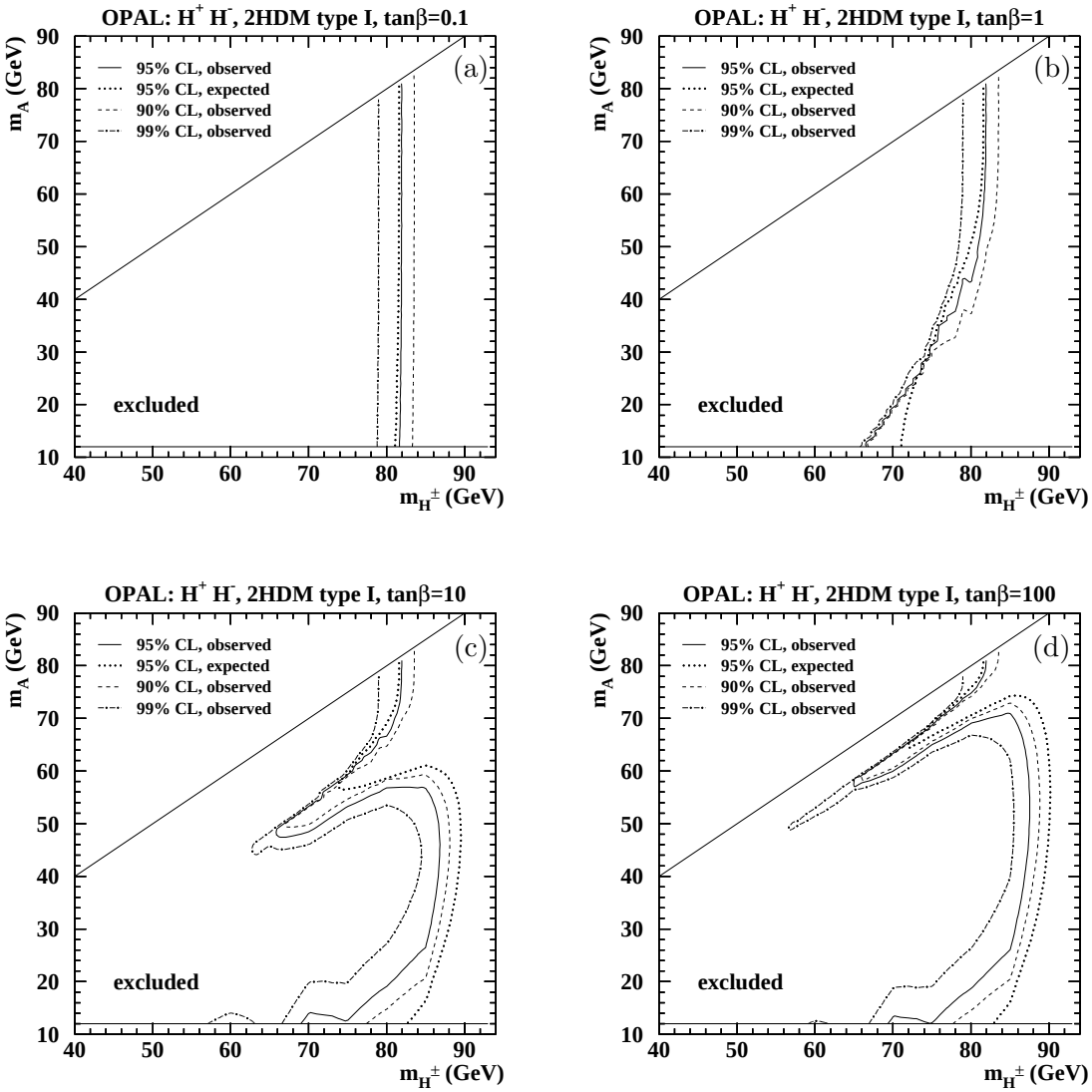

Figure 12: *Excluded areas at 90%, 95% and 99% CL on the* $[m_{\mathrm{H}^\pm}, m_{\mathrm{A}}]$ *plane in 2HDM(I) for different choices of* $\tan\beta$*: (a) 0.1, (b) 1.0, (c) 10.0 and (d) 100.0.*

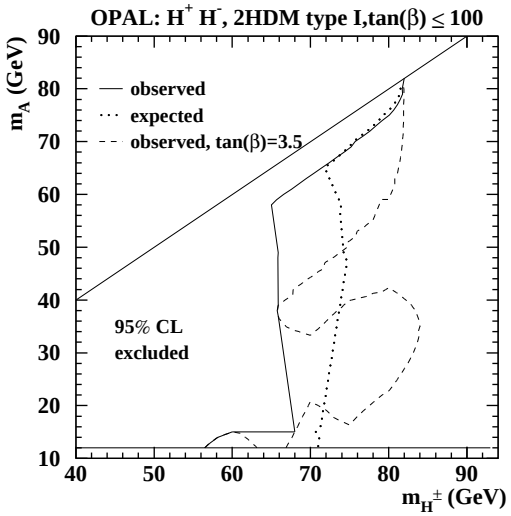

Figure 13: *Excluded areas in 2HDM(I) on the* $[m_{\mathrm{H}^\pm}, m_{\mathrm{A}}]$ *plane independent of* $\tan\beta$ *at 95% CL. The weakest overall mass limit is defined by the* $\tan\beta$*=3.5 exclusion, which is also shown.*

where a small unexcluded island is present around $m_{\mathrm{H}^\pm}\approx$60 GeV and $m_{\mathrm{A}}\approx$12 GeV (also shown on Figure 13). This unexcluded island is no longer present at 90% CL where the mass limit improves to 66.8 GeV.

For $m_{\mathrm{A}}>$15 GeV, the $\tan\beta$-independent lower limit on the charged Higgs-boson mass at 95% CL is 64.8 GeV with 71.0 GeV expected. Both the observed and expected limits are found in the transition region where the bosonic and fermionic channels have comparable sensitivities. The 6 GeV difference is due to the excess observed in the $\mathrm{H}^+\mathrm{H}^-\to\mathrm{AW}^{+*}\mathrm{AW}^{-*}$ search. On the $(m_{\mathrm{H}^\pm}, m_{\mathrm{A}})$ diagonal, the $\mathrm{H}^\pm\to\mathrm{AW}^{\pm*}$ decay becomes kinematically suppressed, and the 2HDM(II) result for $\mathrm{BR}(\mathrm{H}^\pm\to\tau\nu_\tau)$=0.65 of 81.6 GeV (see Figure 8 and Table 8) is reproduced.

7 Summary

A search is performed for the pair production of charged Higgs bosons in electron-positron collisions at LEP2, considering the decays $\mathrm{H}^\pm\to\tau\nu_\tau$, $\mathrm{q\bar{q}}$ and $\mathrm{AW}^{\pm*}$. No signal is observed. The results are interpreted in the framework of Two-Higgs-Doublet Models.

In 2HDM(II), required by the minimal supersymmetric extension of the SM, charged Higgs bosons are excluded up to a mass of 76.6 GeV (with an expected limit of 76.8 GeV) when $\mathrm{BR}(\mathrm{H}^\pm\to\tau\nu_\tau) + \mathrm{BR}(\mathrm{H}^\pm\to\mathrm{q\bar{q}}) = 1$ is assumed. See Figure 8 and Table 8 for $\mathrm{BR}(\mathrm{H}^\pm\to\tau\nu_\tau)$-dependent limits.

In the more exotic 2HDM(I), where fermionic decays can be suppressed and $\mathrm{H}^\pm\to\mathrm{AW}^{\pm*}$ can become dominant, a $\tan\beta$-independent lower mass limit of 56.5 GeV is observed for $m_{\mathrm{A}}>$ 12 GeV (with an expected limit of 71.0 GeV) due to a non-signal-like excess observed at $\sqrt{s}$=192−202 GeV in the $\mathrm{H}^+\mathrm{H}^-\to\mathrm{AW}^{+*}\mathrm{AW}^{-*}$ search, discussed in Section 4. For $m_{\mathrm{A}}>$ 15 GeV, the observed limit improves to $m_{\mathrm{H}^\pm}>$ 64.8 GeV (with an expected limit of 71.0 GeV). Figure 13 shows the excluded areas in the $[m_{\mathrm{H}^\pm}, m_{\mathrm{A}}]$ plane and Table 9 reports selected numerical results.

$\tan\beta$	m_{A}	limit on $m_{\mathrm{H}^{\pm}}$ (GeV)	
		observed	expected
≤ 100	12 GeV$\leq m_{\mathrm{A}} \leq m_{\mathrm{H}^{\pm}}$	56.5 (3.5)	71.0 (1.0)
	m_{A}=12 GeV	56.5 (3.5)	71.0 (1.0)
	$m_{\mathrm{A}}=m_{\mathrm{H}^{\pm}}/2$	66.0 (3.5)	73.5 (1.5)
	$m_{\mathrm{A}} \geq m_{\mathrm{H}^{\pm}} - 10$ GeV	64.8 (100)	71.7 (100)
	$m_{\mathrm{A}} \geq m_{\mathrm{H}^{\pm}} - 5$ GeV	80.5 (100)	78.0 (100)
0.1	12 GeV$\leq m_{\mathrm{A}} \leq m_{\mathrm{H}^{\pm}}$	81.6	81.1
	m_{A}=12 GeV	81.6	81.1
	$m_{\mathrm{A}}=m_{\mathrm{H}^{\pm}}/2$	81.8	81.5
	$m_{\mathrm{A}} \geq m_{\mathrm{H}^{\pm}} - 10$ GeV	81.9	81.6
	$m_{\mathrm{A}} \geq m_{\mathrm{H}^{\pm}} - 5$ GeV	81.9	81.6
1	12 GeV$\leq m_{\mathrm{A}} \leq m_{\mathrm{H}^{\pm}}$	66.4	71.0
	m_{A}=12 GeV	66.4	71.0
	$m_{\mathrm{A}}=m_{\mathrm{H}^{\pm}}/2$	78.3	76.6
	$m_{\mathrm{A}} \geq m_{\mathrm{H}^{\pm}} - 10$ GeV	81.9	81.5
	$m_{\mathrm{A}} \geq m_{\mathrm{H}^{\pm}} - 5$ GeV	81.9	81.6
10	12 GeV$\leq m_{\mathrm{A}} \leq m_{\mathrm{H}^{\pm}}$	65.8	73.9
	m_{A}=12 GeV	69.0	82.5
	$m_{\mathrm{A}}=m_{\mathrm{H}^{\pm}}/2$	86.7	89.8
	$m_{\mathrm{A}} \geq m_{\mathrm{H}^{\pm}} - 10$ GeV	81.5	80.4
	$m_{\mathrm{A}} \geq m_{\mathrm{H}^{\pm}} - 5$ GeV	81.9	81.5
100	12 GeV$\leq m_{\mathrm{A}} \leq m_{\mathrm{H}^{\pm}}$	64.8	71.7
	m_{A}=12 GeV	69.3	82.7
	$m_{\mathrm{A}}=m_{\mathrm{H}^{\pm}}/2$	87.1	89.9
	$m_{\mathrm{A}} \geq m_{\mathrm{H}^{\pm}} - 10$ GeV	64.8	71.7
	$m_{\mathrm{A}} \geq m_{\mathrm{H}^{\pm}} - 5$ GeV	80.5	78.0

Table 9: *Lower mass limits for the charged Higgs boson in 2HDM(I). For the* $\tan\beta \leq 100$ *results, the* $\tan\beta$ *value at which the limit is set is indicated in parenthesis. For any* $\tan\beta$ *value, an extrapolation of the exclusion limits to* $m_{\mathrm{H}^{\pm}}=m_{\mathrm{A}}$ *gives the result quoted in Table 8 for* $\mathrm{BR}(\mathrm{H}^{\pm}\rightarrow\tau\nu_{\tau})=0.65$.

Acknowledgements

We particularly wish to thank the SL Division for the efficient operation of the LEP accelerator at all energies and for their close cooperation with our experimental group. In addition to the support staff at our own institutions we are pleased to acknowledge the
Department of Energy, USA,
National Science Foundation, USA,
Particle Physics and Astronomy Research Council, UK,
Natural Sciences and Engineering Research Council, Canada,
Israel Science Foundation, administered by the Israel Academy of Science and Humanities,
Benoziyo Center for High Energy Physics,
Japanese Ministry of Education, Culture, Sports, Science and Technology (MEXT) and a grant under the MEXT International Science Research Program,
Japanese Society for the Promotion of Science (JSPS),
German Israeli Bi-national Science Foundation (GIF),
Bundesministerium für Bildung und Forschung, Germany,
National Research Council of Canada,
Hungarian Foundation for Scientific Research, OTKA T-038240, and T-042864,
The NWO/NATO Fund for Scientific Research, the Netherlands.

References

[1] S. L. Glashow, Nucl. Phys. **22** (1961) 579;
S. Weinberg, Phys. Rev. Lett. **19** (1967) 1264;
A. Salam, *Elementary Particle Theory*, ed. N. Svartholm (Almquist and Wiksells, Stockholm, 1968), 367.

[2] P.W. Higgs, Phys. Lett. **12** (1964) 132;
F. Englert and R. Brout, Phys. Rev. Lett. **13** (1964) 321;
G.S. Guralnik, C.R. Hagen and T.W.B. Kibble, Phys. Rev. Lett. **13** (1964) 585.

[3] J.F. Gunion, H.E. Haber, G.L. Kane and S. Dawson, *The Higgs Hunter's Guide*, Addison–Wesley Publishing Company, Reading, MA, 1990; and references therein.

[4] S.L. Glashow and S. Weinberg, Phys. Rev. **D15** (1977) 1958;
E.A. Paschos, Phys. Rev. **D15** (1977) 1966.

[5] H.E. Haber *et al.*, Nucl. Phys. **B161** (1979) 493.

[6] S. Kanemura, Eur. Phys. J. **C17** (2000) 473.

[7] A. Djouadi, J. Kalinowski and P.M. Zerwas, Z. Phys. **C57** (1993) 569.

[8] A.G. Akeroyd, Nucl. Phys. **B544** (1999) 557;
A.G. Akeroyd, A. Arhrib, E. Naimi, Eur. Phys. J. **C20** (2001) 51.

[9] OPAL Collaboration, K. Ackerstaff *et al.*, Phys. Lett. **B426** (1998) 180.

[10] OPAL Collaboration, G. Abbiendi *et al.*, Eur. Phys. J. **C7** (1999) 407.

[11] ALEPH Collaboration, A. Heister *et al.*, Phys. Lett. **B543** (2002) 1.

[12] DELPHI Collaboration, J. Abdallah *et al.*, Eur. Phys. J. **C34** (2004) 399.

[13] L3 Collaboration, P. Achard *et al.*, Phys. Lett. **B575** (2003) 208.

[14] OPAL Collaboration, K. Ahmet *et al.*, Nucl. Inst. and Meth. **A305** (1991) 275;
B.E. Anderson *et al.*, IEEE Transactions on Nuclear Science **41** (1994) 845;
S. Anderson *et al.*, Nucl. Inst. and Meth. **A403** (1998) 326;
G. Aguillion *et al.*, Nucl. Inst. and Meth. **A417** (1998) 266.

[15] OPAL Collaboration, G. Abbiendi *et al.*, Eur. Phys. J. **C26** (2003) 479.

[16] The HZHA generator: G. Ganis and P. Janot, in *Physics at LEP2*, CERN 96–01, Vol.2, p. 309.

[17] The PYTHIA 5.721 and JETSET 7.408 generators: T. Sjöstrand, Comp. Phys. Comm. **82** (1994) 74; T. Sjöstrand, LU TP 95–20.

[18] The KK2F generator: S. Jadach, B.F.L. Ward and Z. Wąs, Comp. Phys. Comm. **130** (2000) 260;
S. Jadach, B.F. Ward and Z. Wąs, Phys. Lett. **B449** (1999) 97.

[19] The grc4f 1.1 generator: J. Fujimoto *et al.*, Comp. Phys. Comm. **100** (1997) 128;
J. Fujimoto *et al.*, in *Physics at LEP2*, CERN 96–01, Vol.2, p. 30.

[20] The BHWIDE generator: S. Jadach, W. Płaczek and B.F.L. Ward, in *Physics at LEP2*, CERN 96–01, Vol.2, p. 286; UTHEP–95–1001.

[21] The TEEGG generator: D. Karlen, Nucl. Phys. **B289** (1987) 23.

[22] The KORALZ 4.0 generator: S. Jadach, B.F.L. Ward and Z. Wąs, Comp. Phys. Comm. **79** (1994) 503.

[23] The PHOJET 1.05 generator: E. Budinov *et al.*, in *Physics at LEP2*, CERN 96–01, Vol.2, p. 216;
R. Engel and J. Ranft, Phys. Rev. **D54** (1996) 4244.

[24] The HERWIG generator: G. Marchesini *et al.*, Comp. Phys. Comm. **67** (1992) 465.

[25] The Vermaseren generator: J.A.M. Vermaseren, Nucl. Phys. **B229** (1983) 347.

[26] OPAL Collaboration, G. Alexander *et al.*, Z. Phys **C69** (1996) 543.

[27] The EXCALIBUR generator: F.A. Berends, R. Pittau and R. Kleiss, Comp. Phys. Comm. **85** (1995) 437.

[28] S. Jadach, W. Płaczek, M. Skrzypek, B.F.L. Ward and Z. Wąs, Comp. Phys. Comm. **119** (1999) 272.

[29] The KandY generator: S. Jadach, W. Płaczek, M. Skrzypek, B.F.L. Ward, Z. Wąs, Comp. Phys. Comm. **140** (2001) 475.

[30] J. Allison *et al.*, Nucl. Inst. and Meth. **A317** (1992) 47.

[31] OPAL Collaboration, G. Abbiendi *et al.*, Eur. Phys. J. **C32** (2004) 453.

[32] OPAL Collaboration, G. Abbiendi *et al.*, Eur. Phys. J. C **18** (2001) 425.

[33] N. Brown and W.J. Stirling, Phys. Lett. **B252** (1990) 657;
S. Bethke, Z. Kunszt, D. Soper and W.J. Stirling, Nucl. Phys. **B370** (1992) 310;
S. Catani *et al.*, Phys. Lett. **B269** (1991) 432;
N. Brown and W.J. Stirling, Z. Phys. **C53** (1992) 629.

[34] OPAL Collaboration, G. Abbiendi *et al.*, Eur. Phys. J. **C13** (2000) 1.

[35] OPAL Collaboration, G. Abbiendi *et al.*, Eur. Phys. J. **C18** (2001) 447.

[36] M.H. Seymour, Nucl.Phys. **B436** (1995) 163.

[37] Mark J Collaboration, D.P. Barber *et al.*, Phys. Rev. Lett. 43 (1979) 830.

[38] G. Hanson *et al.*, Phys. Rev. Lett. **35** (1975) 1609.

[39] P. Bock, JHEP **01** (2007) 080.
For the weight definition, we use criteria (i) and (ii) in the 2HDM parameter scans and criterion (vii) in calculating model independent results. The generalized version of Eq. (2.9), given in Eq. (6.1), is used to include systematic errors in the event weights. The treatment of correlations between systematic errors is discussed in section 5.1.

[40] OPAL Collaboration, G. Abbiendi *et al.*, Eur. Phys. J. **C52** (2007) 767 (section 3.2.2, point iii).

[41] ALEPH, DELPHI, L3, OPAL and SLD Collborations, LEP Electroweak Working Group, SLD Electroweak and Heavy Flavour Groups, S. Schael *et al.*, Phys. Rep. **427** (2006) 257.

[42] Particle Data Group, C. Amsler *et al.*, Phys. Lett. **B667** (2008) 1.